

# 1 OpenPBTA: An Open Pediatric Brain Tumor 2 Atlas

3 This manuscript ([permalink](#)) was automatically generated from [AlexsLemonade/OpenPBTA-](#)  
4 [manuscript@6ebef2d](mailto:manuscript@6ebef2d) on September 12, 2022.

## 5 Authors

- 6 • **Joshua A. Shapiro**  [0000-0002-6224-0347](#) ·  [jashapiro](#) ·  [jashapiro](#) Childhood  
7 Cancer Data Lab, Alex's Lemonade Stand Foundation, Bala Cynwyd, PA, USA · Funded  
8 by Alex's Lemonade Stand Foundation Childhood Cancer Data Lab (CCDL)
- 9 • **Krutika S. Gaonkar**  [0000-0003-0838-2405](#) ·  [kgaonkar6](#) ·  [aggokittu](#) Center  
10 for Data-Driven Discovery in Biomedicine, Children's Hospital of Philadelphia; Division of  
11 Neurosurgery, Children's Hospital of Philadelphia; Department of Bioinformatics and  
12 Health Informatics, Children's Hospital of Philadelphia
- 13 • **Candace L. Savonen**  [0000-0001-6331-7070](#) ·  [cansavvy](#) ·  [cansavvy](#)  
14 Childhood Cancer Data Lab, Alex's Lemonade Stand Foundation, Bala Cynwyd, PA,  
15 USA; Fred Hutchinson Cancer Center, Seattle, WA, USA · Funded by Alex's Lemonade  
16 Stand Foundation Childhood Cancer Data Lab (CCDL)
- 17 • **Stephanie J. Spielman**  [0000-0002-9090-4788](#) ·  [sjspielman](#) ·  [stephspiel](#)  
18 Childhood Cancer Data Lab, Alex's Lemonade Stand Foundation, Bala Cynwyd, PA,  
19 USA+; Rowan University, Glassboro, NJ, USA · Funded by Alex's Lemonade Stand  
20 Foundation Childhood Cancer Data Lab (CCDL) +Current affiliation
- 21 • **Chante J. Bethell**  [0000-0001-9653-8128](#) ·  [cbethell](#) ·  [cjbethell](#) Childhood  
22 Cancer Data Lab, Alex's Lemonade Stand Foundation, Bala Cynwyd, PA, USA · Funded  
23 by Alex's Lemonade Stand Foundation Childhood Cancer Data Lab (CCDL)
- 24 • **Run Jin**  [0000-0002-8958-9266](#) ·  [runjin326](#) ·  [runjin](#) Center for Data-Driven  
25 Discovery in Biomedicine, Children's Hospital of Philadelphia; Division of Neurosurgery,  
26 Children's Hospital of Philadelphia
- 27 • **Komal S. Rathi**  [0000-0001-5534-6904](#) ·  [komalsrathi](#) ·  [komalsrathi](#) Center  
28 for Data-Driven Discovery in Biomedicine, Children's Hospital of Philadelphia;  
29 Department of Bioinformatics and Health Informatics, Children's Hospital of Philadelphia

30     • **Yuankun Zhu**  [0000-0002-2455-9525](#) ·  [yuankunzhu](#) ·  [zhuyuankun](#) Center for  
31     Data-Driven Discovery in Biomedicine, Children's Hospital of Philadelphia; Division of  
32     Neurosurgery, Children's Hospital of Philadelphia

33     • **Laura E. Egolf**  [0000-0002-7103-4801](#) ·  [LauraEgolf](#) ·  [LauraEgolf](#) Cell and  
34     Molecular Biology Graduate Group, Perelman School of Medicine at the University of  
35     Pennsylvania; Division of Oncology, Children's Hospital of Philadelphia

36     • **Bailey K. Farrow**  [0000-0001-6727-6333](#) ·  [baileyckelly](#) Center for Data-Driven  
37     Discovery in Biomedicine, Children's Hospital of Philadelphia; Division of Neurosurgery,  
38     Children's Hospital of Philadelphia

39     • **Daniel P. Miller**  [0000-0002-2032-4358](#) ·  [dmiller15](#) Center for Data-Driven  
40     Discovery in Biomedicine, Children's Hospital of Philadelphia; Division of Neurosurgery,  
41     Children's Hospital of Philadelphia

42     • **Yang Yang** ·  [yangyangclover](#) Ben May Department for Cancer Research, University  
43     of Chicago, Chicago IL, USA

44     • **Tejaswi Koganti**  [0000-0002-7733-6480](#) ·  [tkoganti](#) Center for Data-Driven  
45     Discovery in Biomedicine, Children's Hospital of Philadelphia; Division of Neurosurgery,  
46     Children's Hospital of Philadelphia

47     • **Nighat Noureen**  [0000-0001-7495-8201](#) ·  [NNoureen](#) Greehey Children's Cancer  
48     Research Institute, UT Health San Antonio

49     • **Mateusz P. Koptyra**  [0000-0002-3857-6633](#) ·  [mkoptyra](#) ·  [koptyram](#) Center  
50     for Data-Driven Discovery in Biomedicine, Children's Hospital of Philadelphia; Division of  
51     Neurosurgery, Children's Hospital of Philadelphia

52     • **Nhat Duong**  [0000-0003-2852-4263](#) ·  [fingerfen](#) ·  [asiannhat](#) Department of  
53     Bioinformatics and Health Informatics, Children's Hospital of Philadelphia

54     • **Adam A. Kraya**  [0000-0002-8526-5694](#) ·  [aadamk](#) Center for Data-Driven  
55     Discovery in Biomedicine, Children's Hospital of Philadelphia; Division of Neurosurgery,  
56     Children's Hospital of Philadelphia

57     • **Cassie Kline**  [0000-0001-7765-7690](#) ·  [cassiekmd](#) Division of Oncology,  
58     Children's Hospital of Philadelphia

59     • **Yiran Guo**  [0000-0002-6549-8589](#) ·  [Yiran-Guo](#) ·  [YiranGuo3](#) Center for Data-  
60     Driven Discovery in Biomedicine, Children's Hospital of Philadelphia

61     • **Phillip B. Storm**  [0000-0002-7964-2449](#) Center for Data-Driven Discovery in  
62        Biomedicine, Children's Hospital of Philadelphia; Division of Neurosurgery, Children's  
63        Hospital of Philadelphia · Funded by Alex's Lemonade Stand Foundation (Catalyst);  
64        Children's Hospital of Philadelphia Division of Neurosurgery

65     • **Javad Nazarian**  [0000-0002-1951-9828](#) Children's National Research Institute,  
66        Washington, D.C.; George Washington University School of Medicine and Health  
67        Sciences, Washington, D.C.

68     • **Stephen C. Mack**  [0000-0001-9620-4742](#) Department of Developmental  
69        Neurobiology, St. Jude Children's Research Hospital

70     • **Pichai Raman**  [0000-0001-6948-2157](#) ·  [pichairaman](#) ·  [PichaiRaman](#) Center  
71        for Data-Driven Discovery in Biomedicine, Children's Hospital of Philadelphia;  
72        Department of Bioinformatics and Health Informatics, Children's Hospital of Philadelphia

73     • **Siyuan Zheng**  [0000-0002-1031-9424](#) ·  [syzheng](#) ·  [zhengsiyuan](#) Greehey  
74        Children's Cancer Research Institute, UT Health San Antonio

75     • **Peter J. Madsen**  [0000-0001-9266-3685](#) ·  [petermadsenmd](#) Division of  
76        Neurosurgery, Children's Hospital of Philadelphia; Center for Data-Driven Discovery in  
77        Biomedicine, Children's Hospital of Philadelphia

78     • **Nicholas Van Kuren**  [0000-0002-7414-9516](#) ·  [nicholasvk](#) Center for Data-Driven  
79        Discovery in Biomedicine, Children's Hospital of Philadelphia; Division of Neurosurgery,  
80        Children's Hospital of Philadelphia

81     • **Shannon Robins**  [0000-0003-0594-1953](#) Center for Data-Driven Discovery in  
82        Biomedicine, Children's Hospital of Philadelphia; Division of Neurosurgery, Children's  
83        Hospital of Philadelphia

84     • **Xiaoyan Huang**  [0000-0001-7267-4512](#) ·  [HuangXiaoyan0106](#) Center for Data-  
85        Driven Discovery in Biomedicine, Children's Hospital of Philadelphia; Division of  
86        Neurosurgery, Children's Hospital of Philadelphia

87     • **Angela J. Waanders**  [0000-0002-0571-2889](#) ·  [awaanders](#) Division of  
88        Hematology, Oncology, Neuro-Oncology, and Stem Cell Transplant, Ann & Robert H  
89        Lurie Children's Hospital of Chicago; Department of Pediatrics, Northwestern University  
90        Feinberg School of Medicine

91     • **Jung Kim**  [0000-0001-6274-2841](#) Clinical Genetics Branch, Division of Cancer  
92        Epidemiology and Genetics, National Cancer Institute



125 • **Ashley S. Margol**  [0000-0002-3038-8005](#) Division of Hematology and Oncology,  
126 Children's Hospital Los Angeles; Department of Pediatrics, Keck School of Medicine of  
127 University of Southern California

128 • **Zalman Vaksman** Division of Oncology, Children's Hospital of Philadelphia

129 • **Rebecca S. Kaufman**  [0000-0001-8535-9730](#) ·  [rebkau](#) Division of Oncology,  
130 Children's Hospital of Philadelphia; Department of Bioinformatics and Health Informatics,  
131 Children's Hospital of Philadelphia

132 • **Allison P. Heath**  [0000-0002-2583-9668](#) ·  [allisonheath](#) ·  [allig8r](#) Center for  
133 Data-Driven Discovery in Biomedicine, Children's Hospital of Philadelphia; Division of  
134 Neurosurgery, Children's Hospital of Philadelphia · Funded by NIH U2C HL138346-03;  
135 NCI/NIH Contract No. 75N91019D00024, Task Order No. 75N91020F00003; Australian  
136 Government, Department of Education

137 • **Brian M. Ennis**  [0000-0002-2653-5009](#) ·  [bmennis](#) Center for Data-Driven  
138 Discovery in Biomedicine, Children's Hospital of Philadelphia; Division of Neurosurgery,  
139 Children's Hospital of Philadelphia

140 • **Mariarita Santi**  [0000-0002-6728-3450](#) Department of Pathology and Laboratory  
141 Medicine, Children's Hospital of Philadelphia; Department of Pathology and Laboratory  
142 Medicine, University of Pennsylvania Perelman School of Medicine

143 • **Anna R. Poetsch**  [0000-0003-3056-4360](#) ·  [arpoe](#) ·  [APoetsch](#) Biotechnology  
144 Center, Technical University Dresden, Germany; National Center for Tumor Diseases,  
145 Dresden, Germany · Funded by The St. Anna Kinderkrebsforschung, Austria; The  
146 Mildred Scheel Early Career Center Dresden P2, funded by the German Cancer Aid

147 • **Angela N. Viaene**  [0000-0001-6430-8360](#) Department of Pathology and Laboratory  
148 Medicine, Children's Hospital of Philadelphia; Department of Pathology and Laboratory  
149 Medicine, University of Pennsylvania Perelman School of Medicine

150 • **Douglas R. Stewart**  [0000-0001-8193-1488](#) Clinical Genetics Branch, Division of  
151 Cancer Epidemiology and Genetics, National Cancer Institute

152 • **Steven M. Foltz**  [0000-0002-9526-8194](#) ·  [envest](#) Department of Systems  
153 Pharmacology and Translational Therapeutics, University of Pennsylvania; Childhood  
154 Cancer Data Lab, Alex's Lemonade Stand Foundation, Bala Cynwyd, PA, USA · Funded  
155 by Alex's Lemonade Stand Foundation GR-000002471; National Institutes of Health  
156 K12GM081259

157 • **Payal Jain**  [0000-0002-5914-9083](https://orcid.org/0000-0002-5914-9083) ·  [jainpayal022](https://orcid.org/0000-0002-5914-9083) ·  [jainpayal022](https://twitter.com/jainpayal022) Center for  
158 Data-Driven Discovery in Biomedicine, Children's Hospital of Philadelphia; Division of  
159 Neurosurgery, Children's Hospital of Philadelphia

160 • **Bo Zhang**  [0000-0002-0743-5379](https://orcid.org/0000-0002-0743-5379) ·  [zhangb1](https://orcid.org/0000-0002-0743-5379) Center for Data-Driven Discovery  
161 in Biomedicine, Children's Hospital of Philadelphia; Division of Neurosurgery, Children's  
162 Hospital of Philadelphia

163 • **Shrivats Kannan**  [0000-0002-1460-920X](https://orcid.org/0000-0002-1460-920X) ·  [shrivatsk](https://orcid.org/0000-0002-1460-920X) ·  [kshrivats](https://twitter.com/kshrivats) Center for  
164 Data-Driven Discovery in Biomedicine, Children's Hospital of Philadelphia; Division of  
165 Neurosurgery, Children's Hospital of Philadelphia

166 • **Michael Prados**  [0000-0002-9630-2075](https://orcid.org/0000-0002-9630-2075) University of California, San Francisco, San  
167 Francisco, CA, USA

168 • **Jena V. Lilly**  [0000-0003-1439-6045](https://orcid.org/0000-0003-1439-6045) ·  [jvlilly](https://orcid.org/0000-0003-1439-6045) ·  [jvlilly](https://twitter.com/jvlilly) Center for Data-Driven  
169 Discovery in Biomedicine, Children's Hospital of Philadelphia; Division of Neurosurgery,  
170 Children's Hospital of Philadelphia

171 • **Sabine Mueller**  [0000-0002-3452-5150](https://orcid.org/0000-0002-3452-5150) University of California, San Francisco, San  
172 Francisco, CA

173 • **Adam C. Resnick**  [0000-0003-0436-4189](https://orcid.org/0000-0003-0436-4189) ·  [adamcresnick](https://orcid.org/0000-0003-0436-4189) ·  [adamcresnick](https://twitter.com/adamcresnick)  
174 Center for Data-Driven Discovery in Biomedicine, Children's Hospital of Philadelphia;  
175 Division of Neurosurgery, Children's Hospital of Philadelphia · Funded by Alex's  
176 Lemonade Stand Foundation (Catalyst); Children's Brain Tumor Network; NIH 3P30  
177 CA016520-44S5, U2C HL138346-03, U24 CA220457-03; NCI/NIH Contract  
178 No. 75N91019D00024, Task Order No. 75N91020F00003; Children's Hospital of  
179 Philadelphia Division of Neurosurgery

180 • **Casey S. Greene**  [0000-0001-8713-9213](https://orcid.org/0000-0001-8713-9213) ·  [cgreenie](https://orcid.org/0000-0001-8713-9213) ·  [greenescientist](https://twitter.com/greenescientist)  
181 Department of Systems Pharmacology and Translational Therapeutics, Perelman  
182 School of Medicine, University of Pennsylvania, Philadelphia, PA, USA; Childhood  
183 Cancer Data Lab, Alex's Lemonade Stand Foundation, Bala Cynwyd, PA, USA; Center  
184 for Health AI, University of Colorado School of Medicine, Aurora, CO, USA; Department  
185 of Biomedical Informatics, University of Colorado School of Medicine, Aurora, CO, USA ·  
186 Funded by Alex's Lemonade Stand Foundation Childhood Cancer Data Lab (CCDL)

187 • **Jo Lynne Rokita**  [0000-0003-2171-3627](https://orcid.org/0000-0003-2171-3627) ·  [jharenza](https://orcid.org/0000-0003-2171-3627) ·  [jolynnerokita](https://twitter.com/jolynnerokita) Center  
188 for Data-Driven Discovery in Biomedicine, Children's Hospital of Philadelphia; Division of  
189 Neurosurgery, Children's Hospital of Philadelphia; Department of Bioinformatics and  
190 Health Informatics, Children's Hospital of Philadelphia · Funded by Alex's Lemonade

191 Stand Foundation (Young Investigator, Catalyst); NCI/NIH Contract  
192 No. 75N91019D00024, Task Order No. 75N91020F00003

193 • **Jaclyn N. Taroni**  [0000-0003-4734-4508](https://orcid.org/0000-0003-4734-4508) ·  [jaclyn-taroni](https://orcid.org/0000-0003-4734-4508) ·  [jaclyn\\_taroni](https://twitter.com/jaclyn_taroni)  
194 Childhood Cancer Data Lab, Alex's Lemonade Stand Foundation, Bala Cynwyd, PA,  
195 USA · Funded by Alex's Lemonade Stand Foundation Childhood Cancer Data Lab  
196 (CCDL)

197 • **Children's Brain Tumor Network**

198 • **Pacific Pediatric Neuro-Oncology Consortium**

## 199 **Contact information**

200  Correspondence: Jo Lynne Rokita <[rokita@chop.edu](mailto:rokita@chop.edu)>, Jaclyn N. Taroni  
201 <[jaclyn.taroni@ccdatalab.org](mailto:jaclyn.taroni@ccdatalab.org)>.

## 202 **In Brief**

203 The OpenPBTA is a global, collaborative open-science initiative which brought together  
204 researchers and clinicians to genomically characterize 1,074 pediatric brain tumors and 22  
205 patient-derived cell lines. Shapiro, et. al create over 40 open-source, scalable modules to  
206 perform cancer genomics analyses and provide a richly-annotated somatic dataset across 58  
207 brain tumor histologies. The OpenPBTA framework can be used as a model for large-scale data  
208 integration to inform basic research, therapeutic target identification, and clinical translation.

## 209 **Highlights**

210 OpenPBTA collaborative analyses establish resource for 1,074 pediatric brain tumors  
211 NGS-based WHO-aligned integrated diagnoses generated for 641 of 1,074 tumors  
212 RNA-Seq analysis infers medulloblastoma subtypes, *TP53* status, and telomerase activity  
213 OpenPBTA will accelerate therapeutic translation of genomic insights

## 214 **Summary**

215 Pediatric brain and spinal cancer are the leading disease-related cause of death in children,  
216 thus we urgently need curative therapeutic strategies for these tumors. To accelerate such  
217 discoveries, the Children's Brain Tumor Network and Pacific Pediatric Neuro-Oncology  
218 Consortium created a systematic process for tumor biobanking, model generation, and  
219 sequencing with immediate access to harmonized data. We leverage these data to create  
220 OpenPBTA, an open collaborative project which establishes over 40 scalable analysis modules  
221 to genomically characterize 1,074 pediatric brain tumors. Transcriptomic classification reveals

222 that *TP53* loss is a significant marker for poor overall survival in ependymomas and H3 K28-  
223 altered diffuse midline gliomas and further identifies universal *TP53* dysregulation in mismatch  
224 repair-deficient hypermutant high-grade gliomas. OpenPBTA is a foundational analysis platform  
225 actively being applied to other pediatric cancers and inform molecular tumor board decision-  
226 making, making it an invaluable resource to the pediatric oncology community.

## 227 **Keywords**

228 pediatric cancer, brain tumors, somatic variation, open science, reproducibility, classification,  
229 tumor atlas

## 230 **Introduction**

231 Pediatric brain and spinal cord tumors are collectively the second most common malignancy in  
232 children after leukemia, and they represent the leading disease-related cause of death in  
233 children<sup>1</sup>. Five-year survival rates vary widely across different histologic and molecular  
234 classifications of brain tumors. For example, most high-grade gliomas carry a universally fatal  
235 prognosis, while children with pilocytic astrocytoma have an estimated 10-year survival rate of  
236 92%<sup>2</sup>. Moreover, estimates from 2009 suggest that children and adolescents aged 0-19 with  
237 brain tumors in the United States have lost an average of 47,631 years of potential life<sup>3</sup>.

238 The low survival rates for some pediatric tumors are clearly multifactorial, explained partly by  
239 our lack of comprehensive understanding of the ever-evolving array of brain tumor molecular  
240 subtypes, difficulty drugging these tumors, and the shortage of drugs specifically labeled for  
241 pediatric malignancies. Historically, some of the most fatal, inoperable brain tumors, such as  
242 diffuse intrinsic pontine gliomas (DIPGs), were not routinely biopsied due to perceived risks of  
243 biopsy and the paucity of therapeutic options that would require tissue. Limited access to tissue  
244 to develop patient-derived cell lines and mouse models has been a barrier to research.  
245 Furthermore, the incidence of any single brain tumor molecular subtype is relatively low due to  
246 the rarity of pediatric tumors in general.

247 To address these long-standing barriers, multiple national and international consortia have  
248 come together to uniformly collect clinically-annotated surgical biosamples and associated  
249 germline materials as part of both observational and interventional clinical trials.  
250 Such accessible, centralized resources enable collaborative sharing of specimens and data  
251 across rare cancer subtypes to accelerate breakthroughs and clinical translation. The creation  
252 of the Pediatric Brain Tumor Atlas (PBTA) in 2018, led by the Children's Brain Tumor Network  
253 (CBTN, [cbtn.org](http://cbtn.org)) and the Pacific Pediatric Neuro-Oncology Consortium (PNOC, [PNOC.us](http://PNOC.us)) is  
254 one such effort that builds on nearly 10 years of multi-institutional enrollment, sample collection,  
255 and clinical followup across more than 30 institutions. Just as cooperation is required to share  
256 specimens and data, rigorous cancer genomic analysis requires collaboration among  
257 researchers with distinct expertise, such as computational scientists, bench scientists, clinicians,  
258 and pathologists.

259 Although there has been significant progress in recent years to elucidate the landscape of  
260 somatic variation responsible for pediatric brain tumor formation and progression, translation of

261 therapeutic agents to phase II or III clinical trials and subsequent FDA approvals have not kept  
262 pace. Within the last 20 years, the FDA has approved only five drugs for the treatment of  
263 pediatric brain tumors: mTOR inhibitor everolimus, for subependymal giant cell astrocytoma;  
264 anti-PD-1 immunotherapy pembrolizumab, for microsatellite instability-high or mismatch repair-  
265 deficient tumors; NTRK inhibitors larotrectinib and entrectinib, for tumors with an NTRK 1/2/3  
266 gene fusions; and MEK1/2 inhibitor selumetinib, for neurofibromatosis type 1 (NF1) and  
267 symptomatic, inoperable plexiform neurofibromas<sup>4</sup>.

268 This is, in part, due to pharmaceutical company priorities and concerns regarding toxicity,  
269 making it challenging for researchers to obtain new therapeutic agents for pediatric clinical  
270 trials. Critically, as of August 18, 2020, an amendment to the Pediatric Research Equity Act  
271 called the “Research to Accelerate Cures and Equity (RACE) for Children Act” mandates that all  
272 new adult oncology drugs also be tested in children when the molecular targets are relevant to a  
273 particular childhood cancer. The regulatory change introduced by the RACE Act, coupled with  
274 the identification of putative molecular targets in pediatric cancers through genomic  
275 characterization, is poised to accelerate identification of novel and effective therapeutic for  
276 pediatric diseases that have otherwise been overlooked.

277 To leverage diverse scientific and analytical expertise to analyze the PBTA data, we created an  
278 open science model and incorporated features such as analytical code review<sup>5,6</sup> and continuous  
279 integration to test data and code<sup>6,7</sup> to improve reproducibility throughout the life cycle of our  
280 project, termed OpenPBTA.

281 We anticipated that a model of open collaboration would enhance the value of our effort to the  
282 pediatric brain tumor research community and provide a framework for continuous, accelerated  
283 translation of pediatric brain tumor datasets. Openly sharing data and code in real time allows  
284 others to build upon the work more rapidly, and publications that include data and code sharing  
285 are poised for greater impact<sup>8,9</sup>. Here, we present a comprehensive, collaborative, open  
286 genomic analysis of 1,074 tumors and 22 cell lines, comprised of 58 distinct brain tumor  
287 histologies from 943 patients. The data and containerized infrastructure of OpenPBTA have  
288 been instrumental for discovery and translational research studies<sup>10-12</sup>, are actively integrated  
289 into PNOC molecular tumor board decision-making, and are a foundational layer for the NCI’s  
290 Childhood Cancer Data Initiative’s (CCDI) pediatric Molecular Targets Platform  
291 (<https://moleculartargets.ccdi.cancer.gov/>) recently built in support of the RACE Act<sup>13</sup>. We  
292 anticipate OpenPBTA will be an invaluable resource to the pediatric oncology community.

## 293 **Results**

### 294 **Crowd-sourced Somatic Analyses to Create an Open Pediatric** 295 **Brain Tumor Atlas**

296 We previously performed whole genome sequencing (WGS), whole exome sequencing (WXS),  
297 and RNA sequencing (RNA-Seq) on matched tumor and normal tissues as well as selected cell  
298 lines<sup>14</sup> from 943 patients from the Pediatric Brain Tumor Atlas (PBTA), consisting of samples  
299 from the [Children’s Brain Tumor Network \(CBTN\)](#) and the PNOC003 DIPG clinical trial<sup>12,15</sup> of the  
300 [Pacific Pediatric Neuro-Oncology Consortium \(PNOC\)](#) (**Figure 1A**). We then harnessed the

301 benchmarking efforts of the [Gabriella Miller Kids First Data Resource Center](#) to develop robust  
302 and reproducible data analysis workflows within the CAVATICA platform to perform primary  
303 somatic analyses including calling of single nucleotide variants (SNVs), copy number variants  
304 (CNVs), structural variants (SVs), and gene fusions, often implementing multiple complementary  
305 methods ([Figure S1](#)) and **STAR Methods**).

306 To facilitate analysis and visualization of this large, diverse cohort, we further categorized tumor  
307 broad histologies (i.e., broad 2016 WHO classifications) into smaller groupings we denote  
308 “cancer groups.” A summarized view of the number of biospecimens per phase of therapy  
309 across different broad histologies and cancer groups is shown in ([Figure 1B](#)). We maintained a  
310 data release folder on Amazon S3, downloadable directly from S3 or through the open-access  
311 [CAVATICA project](#), with merged files for each analysis (See **Data and code availability**  
312 section). As new analytical results (e.g., tumor mutation burden calculations) that we expected  
313 to be used across multiple analyses were produced, or issues with the data were identified, new  
314 data releases were made available in a versioned manner.

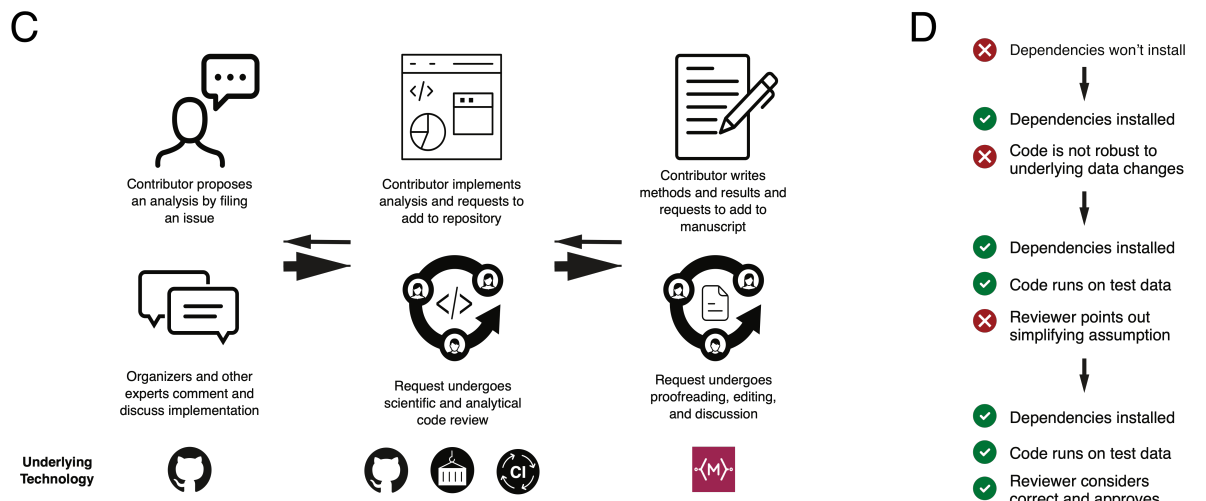
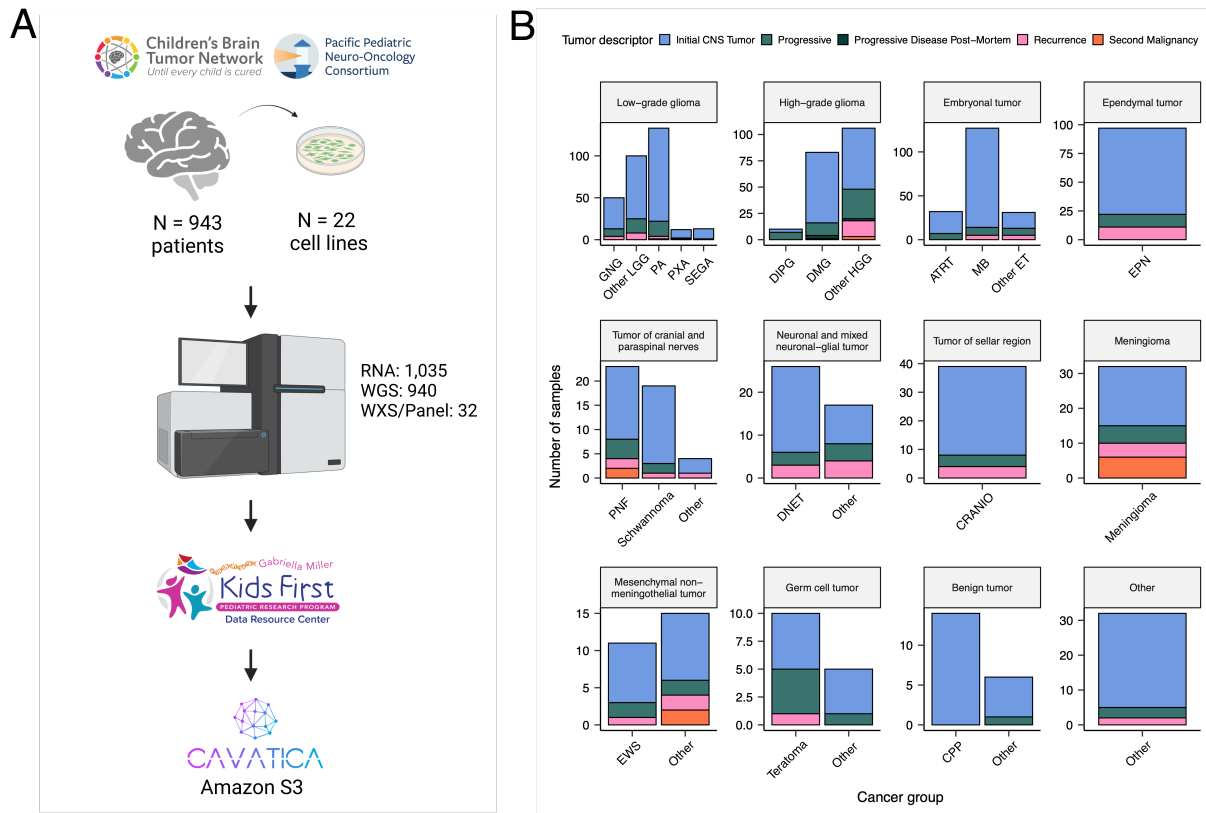
315 A key innovative feature of this project has been its open contribution model used for both  
316 analyses (i.e., analytical code) and scientific manuscript writing. We created a public Github  
317 analysis repository (<https://github.com/AlexsLemonade/OpenPBTA-analysis>) to hold all code  
318 associated with analyses downstream of the Kids First Data Resource Center workflows and a  
319 GitHub manuscript repository (<https://github.com/AlexsLemonade/OpenPBTA-manuscript>) with  
320 Manubot<sup>16</sup> integration to enable real-time manuscript creation using Markdown within GitHub.  
321 Importantly, all analyses and manuscript writing were conducted openly throughout the research  
322 project, allowing any researcher in the world the opportunity to contribute.

323 The process for analysis and manuscript contributions is outlined in [Figure 1C](#). First, a potential  
324 contributor would propose an analysis by filing an issue in the GitHub analysis repository. Next,  
325 organizers for the project, or other contributors with expertise, had the opportunity to provide  
326 feedback about the proposed analysis ([Figure 1C](#)). The contributor then made a copy (fork) of  
327 the analysis repository and added their proposed analysis code and results to their fork. The  
328 contributor would formally request to include their analytical code and results to the main  
329 OpenPBTA analysis repository by filing a pull request on GitHub. All pull requests to the  
330 analysis repository underwent peer review by organizers and/or other contributors to ensure  
331 scientific accuracy, maintainability, and readability of code and documentation ([Figure 1C-D](#)).

332 The collaborative nature of the project required additional steps beyond peer review of analytical  
333 code to ensure consistent results for all collaborators and over time ([Figure 1D](#)). We leveraged  
334 Docker®<sup>17</sup> and the Rocker project<sup>18</sup> to maintain a consistent software development  
335 environment, creating a monolithic image that contained all dependencies necessary for  
336 analyses. To ensure that new code would execute in the development environment, we used  
337 the continuous integration (CI) service CircleCI® to run analytical code on a small subset of data  
338 for testing before formal code review, allowing us to detect code bugs or sensitivity to changes  
339 in the underlying data.

340 We followed a similar process in our Manubot-powered<sup>16</sup> manuscript repository for additions to  
341 the manuscript ([Figure 1C](#)). Contributors forked the manuscript repository, added proposed  
342 content to their branch, and filed pull requests to the main manuscript repository with their

343 changes. Similarly, pull requests underwent a peer review process for clarity and correctness,  
 344 agreement with interpretation, and spell checking via Manubot.



345

346 **Figure 1: Overview of the OpenPBTA Project.** A, The Children's Brain Tumor Network and the  
 347 Pacific Pediatric Neuro-Oncology Consortium collected tumor samples from 943 patients. To  
 348 date, 22 cell lines were created from tumor tissue, and over 2000 specimens were sequenced  
 349 (N = 1035 RNA-Seq, N = 940 WGS, and N = 32 WXS or targeted panel). Data was harmonized  
 350 by the Kids First Data Resource Center using an Amazon S3 framework within CAVATICA. B,

351 *Stacked bar plot summary of the number of biospecimens per phase of therapy. Each panel*  
352 *denotes a broad histology and each bar denotes a cancer group. (Abbreviations: GNG =*  
353 *ganglioglioma, Other LGG = other low-grade glioma, PA = pilocytic astrocytoma, PXA =*  
354 *pleomorphic xanthoastrocytoma, SEGA = subependymal giant cell astrocytoma, DIPG = diffuse*  
355 *intrinsic pontine glioma, DMG = diffuse midline glioma, Other HGG = other high-grade glioma,*  
356 *ATRT = atypical teratoid rhabdoid tumor, MB = medulloblastoma, Other ET = other embryonal*  
357 *tumor, EPN = ependymoma, PNF = plexiform neurofibroma, DNET = dysembryoplastic*  
358 *neuroepithelial tumor, CRANIO = craniopharyngioma, EWS = Ewing sarcoma, CPP = choroid*  
359 *plexus papilloma). Only samples with available descriptors were included. C, Overview of the*  
360 *open analysis and manuscript contribution model. In the analysis GitHub repository, a*  
361 *contributor would propose an analysis that other participants can comment on. Contributors*  
362 *would then implement the analysis and file a request to add their changes to the analysis*  
363 *repository (“pull request”). Pull requests underwent review for scientific rigor and correctness of*  
364 *implementation. Pull requests were additionally checked to ensure that all software*  
365 *dependencies were included and the code was not sensitive to underlying data changes using*  
366 *container and continuous integration technologies. Finally, a contributor would file a pull request*  
367 *documenting their methods and results to the Manubot-powered manuscript repository. Pull*  
368 *requests in the manuscript repository were also subject to review. D, A potential path for an*  
369 *analytical pull request. Arrows indicate revisions to a pull request. Prior to review, a pull request*  
370 *was tested for dependency installation and whether or not the code would execute. Pull*  
371 *requests also required approval by organizers and/or other contributors, who checked for*  
372 *scientific correctness. Panel A created with BioRender.com.*

## 373 **Molecular Subtyping of OpenPBTA CNS Tumors**

374 Over the past two decades, experts in neuro-oncology have worked with the World Health  
375 Organization (WHO) to iteratively redefine the classifications of central nervous system (CNS)  
376 tumors<sup>19,20</sup>. More recently, in 2016 and 2021<sup>21,22</sup>, molecular subtypes have been integrated into  
377 these classifications. In 2011, the Children’s Brain Tumor Tissue Consortium, now known as the  
378 Children’s Brain Tumor Network (CBTN), opened its protocol for brain tumor and matched  
379 normal sample collection. Since the CBTN opened its collection protocol in 2011, before  
380 molecular data were integrated into classifications, the majority of the samples within the  
381 OpenPBTA lacked molecular subtype annotations at the time of tissue collection. Moreover, the  
382 OpenPBTA data does not yet feature methylation arrays which are increasingly used to inform  
383 molecular subtyping. Therefore, we jointly considered key genomic features of tumor entities  
384 described by the WHO in 2016, low-grade glioma (LGG) subtypes described by Ryall and  
385 colleagues<sup>23</sup>, as well as clinician and pathologist review, to generate research-grade integrated  
386 diagnoses for 60% (641/1074) of tumor samples with high confidence (**Table S1**).

387 Importantly, this collaborative molecular subtyping process allowed us to identify potential data  
388 entry errors (e.g., an ETMR incorrectly entered as a medulloblastoma) and histologically mis-  
389 identified specimens (e.g., Ewing sarcoma sample labeled as a craniopharyngioma), update  
390 diagnoses using current WHO terms (e.g., tumors formerly ascribed primitive neuro-ectodermal  
391 tumor [PNET] diagnoses), and discover rarer tumor entities within the OpenPBTA (e.g., H3-  
392 mutant ependymoma, meningioma with *YAP1::FAM118B* fusion). **Table 1** lists the subtypes we  
393 defined within OpenPBTA, comprising low-grade gliomas (N = 290), high-grade gliomas (N =

394 141), embryonal tumors (N = 126), ependymomas (N = 30), tumors of sellar region (N = 27),  
395 mesenchymal non-meningothelial tumors (N = 11), glialneuronal tumors (N = 10), and  
396 chordomas (N = 6). For detailed methods, see **STAR Methods** and **Figure S1**.

397 **Table 1: Molecular subtypes generated through the OpenPBTA project.** Listed are broad  
398 tumor histologies, molecular subtypes generated, and number of specimens subtyped within the  
399 OpenPBTA project.

| Broad histology group | OpenPBTA molecular subtype       | n  |
|-----------------------|----------------------------------|----|
| Chordoma              | CHDM, conventional               | 2  |
| Chordoma              | CHDM, poorly differentiated      | 4  |
| Embryonal tumor       | CNS Embryonal, NOS               | 13 |
| Embryonal tumor       | CNS HGNET-MN1                    | 1  |
| Embryonal tumor       | CNS NB-FOXR2                     | 3  |
| Embryonal tumor       | ETMR, C19MC-altered              | 5  |
| Embryonal tumor       | ETMR, NOS                        | 1  |
| Embryonal tumor       | MB, Group3                       | 14 |
| Embryonal tumor       | MB, Group4                       | 49 |
| Embryonal tumor       | MB, SHH                          | 30 |
| Embryonal tumor       | MB, WNT                          | 10 |
| Ependymal tumor       | EPN, H3 K28                      | 1  |
| Ependymal tumor       | EPN, ST RELA                     | 28 |
| Ependymal tumor       | EPN, ST YAP1                     | 1  |
| High-grade glioma     | DMG, H3 K28                      | 24 |
| High-grade glioma     | DMG, H3 K28, TP53 activated      | 13 |
| High-grade glioma     | DMG, H3 K28, TP53 loss           | 40 |
| High-grade glioma     | HGG, H3 G35                      | 3  |
| High-grade glioma     | HGG, H3 G35, TP53 loss           | 1  |
| High-grade glioma     | HGG, H3 wildtype                 | 31 |
| High-grade glioma     | HGG, H3 wildtype, TP53 activated | 5  |
| High-grade glioma     | HGG, H3 wildtype, TP53 loss      | 21 |
| High-grade glioma     | HGG, IDH, TP53 activated         | 2  |
| High-grade glioma     | HGG, IDH, TP53 loss              | 1  |
| Low-grade glioma      | GNG, BRAF V600E                  | 13 |
| Low-grade glioma      | GNG, BRAF V600E, CDKN2A/B        | 1  |
| Low-grade glioma      | GNG, FGFR                        | 1  |
| Low-grade glioma      | GNG, H3                          | 1  |
| Low-grade glioma      | GNG, IDH                         | 2  |
| Low-grade glioma      | GNG, KIAA1549-BRAF               | 5  |
| Low-grade glioma      | GNG, MYB/MYBL1                   | 1  |

| Broad histology group                   | OpenPBTA molecular subtype               | n   |
|---|--|-----|
| Low-grade glioma                        | GNG, NF1-germline                        | 1   |
| Low-grade glioma                        | GNG, NF1-somatic, BRAF V600E             | 1   |
| Low-grade glioma                        | GNG, other MAPK                          | 4   |
| Low-grade glioma                        | GNG, other MAPK, IDH                     | 1   |
| Low-grade glioma                        | GNG, RTK                                 | 3   |
| Low-grade glioma                        | GNG, wildtype                            | 14  |
| Low-grade glioma                        | LGG, BRAF V600E                          | 27  |
| Low-grade glioma                        | LGG, BRAF V600E, CDKN2A/B                | 5   |
| Low-grade glioma                        | LGG, FGFR                                | 8   |
| Low-grade glioma                        | LGG, IDH                                 | 3   |
| Low-grade glioma                        | LGG, KIAA1549-BRAF                       | 113 |
| Low-grade glioma                        | LGG, KIAA1549-BRAF, NF1-germline         | 1   |
| Low-grade glioma                        | LGG, KIAA1549-BRAF, other MAPK           | 1   |
| Low-grade glioma                        | LGG, MYB/MYBL1                           | 2   |
| Low-grade glioma                        | LGG, NF1-germline                        | 6   |
| Low-grade glioma                        | LGG, NF1-germline, CDKN2A/B              | 1   |
| Low-grade glioma                        | LGG, NF1-germline, FGFR                  | 2   |
| Low-grade glioma                        | LGG, NF1-somatic                         | 2   |
| Low-grade glioma                        | LGG, NF1-somatic, FGFR                   | 1   |
| Low-grade glioma                        | LGG, NF1-somatic, NF1-germline, CDKN2A/B | 1   |
| Low-grade glioma                        | LGG, other MAPK                          | 12  |
| Low-grade glioma                        | LGG, RTK                                 | 10  |
| Low-grade glioma                        | LGG, RTK, CDKN2A/B                       | 1   |
| Low-grade glioma                        | LGG, wildtype                            | 34  |
| Low-grade glioma                        | SEGA, RTK                                | 1   |
| Low-grade glioma                        | SEGA, wildtype                           | 11  |
| Mesenchymal non-meningothelial tumor    | EWS                                      | 11  |
| Neuronal and mixed neuronal-glial tumor | CNC                                      | 2   |
| Neuronal and mixed neuronal-glial tumor | EVN                                      | 1   |
| Neuronal and mixed neuronal-glial tumor | GNT, BRAF V600E                          | 1   |
| Neuronal and mixed neuronal-glial tumor | GNT, KIAA1549-BRAF                       | 2   |
| Neuronal and mixed neuronal-glial tumor | GNT, other MAPK                          | 1   |
| Neuronal and mixed neuronal-glial tumor | GNT, other MAPK, FGFR                    | 1   |
| Neuronal and mixed neuronal-glial tumor | GNT, RTK                                 | 2   |
| Tumor of sellar region                  | CRANIO, ADAM                             | 27  |
|   | Total                                    | 641 |

## 400 **Somatic Mutational Landscape of Pediatric Brain Tumors**

401 We performed a comprehensive genomic analysis of somatic SNVs, CNVs, SVs, and fusions  
402 across 1,074 tumors (N = 1,019 RNA-Seq, N = 918 WGS, N = 32 WXS/Panel) and 22 cell lines  
403 (N = 16 RNA-Seq, N = 22 WGS), from 943 patients, 833 with paired normal specimens (N = 801  
404 WGS, N = 32 WXS/Panel). Following SNV consensus calling (Figure S1 and Figure S2A-G),  
405 we observed as expected lower tumor mutation burden (TMB) Figure S2H in pediatric tumors  
406 compared to adult brain tumors from The Cancer Genome Atlas (TCGA), Figure S2I, with  
407 hypermutant (> 10 Mut/Mb) and ultra-hypermutant (> 100 Mut/Mb) tumors<sup>24</sup> only found within  
408 HGGs. Figure 2 and Figure S3A depict oncprints of histology-specific driver genes across  
409 PBTA histologies.

### 410 **Low-grade gliomas**

411 As expected, the majority (62%, 140/227) of LGGs harbored a somatic alteration in *BRAF*, with  
412 canonical *BRAF*::*KIAA1549* fusions as the major oncogenic driver<sup>25</sup> (Figure 2A). We observed  
413 additional mutations in *FGFR1* (2%), *PIK3CA* (2%), *KRAS* (2%), *TP53* (1%), and *ATRX* (1%)  
414 and fusions in *NTRK2* (2%), *RAF1* (2%), *MYB* (1%), *QKI* (1%), *ROS1* (1%), and *FGFR2* (1%),  
415 concordant with previous studies reporting the near universal upregulation of the RAS/MAPK  
416 pathway in these tumors resulting from activating mutations and/or oncogenic fusions<sup>23,25</sup>.  
417 Indeed, we observed significant upregulation (ANOVA Bonferroni-corrected p < 0.01) of the  
418 KRAS signaling pathway in LGGs (Figure 5B).

### 419 **Embryonal tumors**

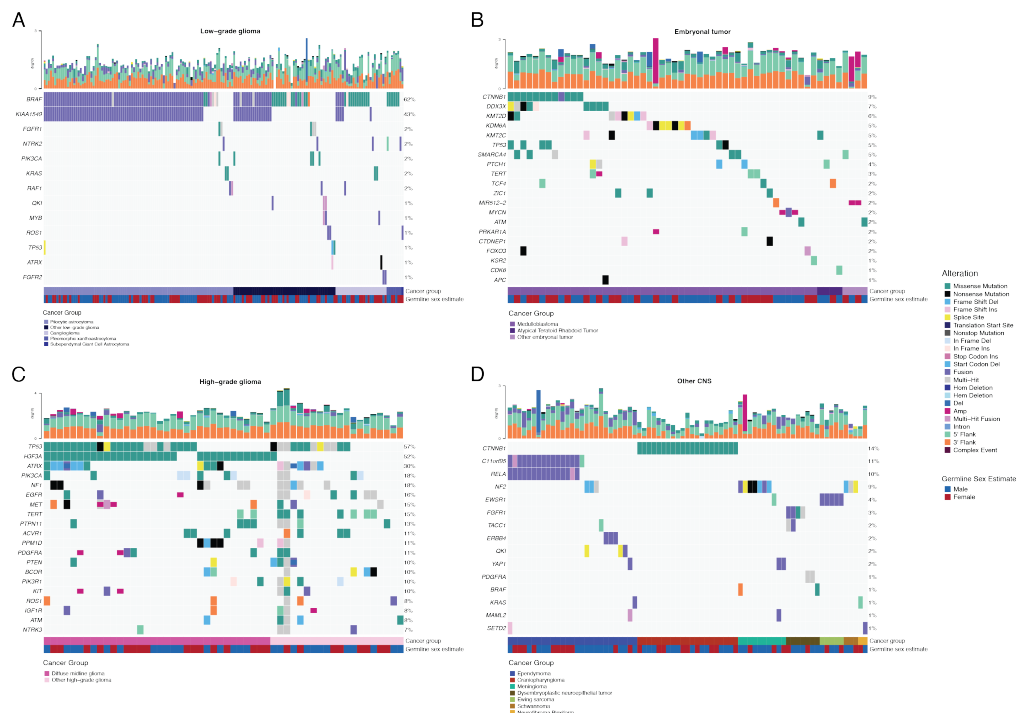
420 The majority (N = 95) of embryonal tumor samples were medulloblastomas that spanned the  
421 spectrum of molecular subtypes (WNT, SHH, Group3, and Group 4; see **Molecular Subtyping**  
422 **of CNS Tumors**), as identified by subtype-specific canonical mutations (Figure 2B). We  
423 detected canonical *SMARCB1*/*SMARCA4* deletions or inactivating mutations in atypical teratoid  
424 rhabdoid tumors (ATRTs) and C19MC amplification in the embryonal tumors with multilayer  
425 rosettes (ETMRs, displayed as other embryonal tumors)<sup>26-29</sup>.

### 426 **High-grade gliomas**

427 Across HGGs, we found that *TP53* (57%, 35/61) and *H3F3A* (52%, 32/61) were both most  
428 mutated and co-occurring genes (Figure 2A and C), followed by frequent mutations in *ATRX*  
429 (30%, 18/61). We observed recurrent amplifications and fusions in *EGFR*, *MET*, *PDGFRA*, and  
430 *KIT*, highlighting that these tumors utilize multiple oncogenic mechanisms to activate tyrosine  
431 kinases, as has been previously reported<sup>15,30,31</sup>. Gene set enrichment analysis showed  
432 upregulation (ANOVA Bonferroni-corrected p < 0.01) of DNA repair, G2M checkpoint, and MYC  
433 pathways as well as downregulation of the TP53 pathway (Figure 5B). The two tumors with  
434 ultra-high TMB (> 100 Mutations/Mb) were from patients with known mismatch repair deficiency  
435 syndrome<sup>14</sup>.

## 436 Other CNS tumors

437 We observed that 25% (15/60) of ependymoma tumors were *C11orf95::RELA* (now,  
438 *ZFTA::RELA*) fusion-positive ependymomas and that 68% (21/31) of craniopharyngiomas were  
439 driven by mutations in *CTNNB1* (**Figure 2D**). Multiple histologies contained somatic mutations  
440 or fusions in *NF2*: 41% (7/17) of meningiomas, 5% (3/60) of ependymomas, and 27% (3/11)  
441 schwannomas. Rare fusions in *ERBB4*, *YAP1*, *KRAS*, and *MAML2* were observed in 10%  
442 (6/60) of ependymoma tumors. DNETs harbored alterations in MAPK/PI3K pathway genes as  
443 previously reported<sup>32</sup>, including *FGFR1* (21%, 4/19), *PDGFRA* (10%, 2/19), and *BRAF* (5%,  
444 1/19). Frequent mutations in additional rare brain tumor histologies are depicted in **Figure S3A**.



445

446 **Figure 2: Mutational landscape of PBTA tumors.** Shown are frequencies of canonical somatic  
447 gene mutations, CNVs, fusions, and TMB (top bar plot) for the top 20 genes mutated across  
448 primary tumors within the OpenPBTA dataset. A, Low-grade astrocytic tumors (N = 227):  
449 pilocytic astrocytoma (N = 104), other low-grade glioma (N = 69), ganglioglioma (N = 35),  
450 pleomorphic xanthoastrocytoma (N = 9), subependymal giant cell astrocytoma (N = 10); B,  
451 Embryonal tumors (N = 128): medulloblastomas (N = 95), atypical teratoid rhabdoid tumors (N =  
452 24), other embryonal tumors (N = 9); C, Diffuse astrocytic and oligodendroglial tumors (N = 61):  
453 diffuse midline gliomas (N = 34) and other high-grade gliomas (N = 27); D, Other CNS tumors  
454 (N = 194): ependymomas (N = 60), craniopharyngiomas (N = 31), meningiomas (N = 17),  
455 dysembryoplastic neuroepithelial tumors (N = 19), Ewing sarcomas (N = 7), schwannomas (N =  
456 11), and neurofibroma plexiforms (N = 7). Additional, rare CNS tumors are displayed in **Figure**

457 **S3A. Tumor histology (Cancer Group) and patient sex (Germline sex estimate) are**  
458 **displayed as annotations at the bottom of each plot. Only samples with mutations in the listed**  
459 **genes are shown. Multiple CNVs are denoted as a complex event.**

## 460 **Mutational co-occurrence, CNV, and signatures highlight key** 461 **oncogenic drivers**

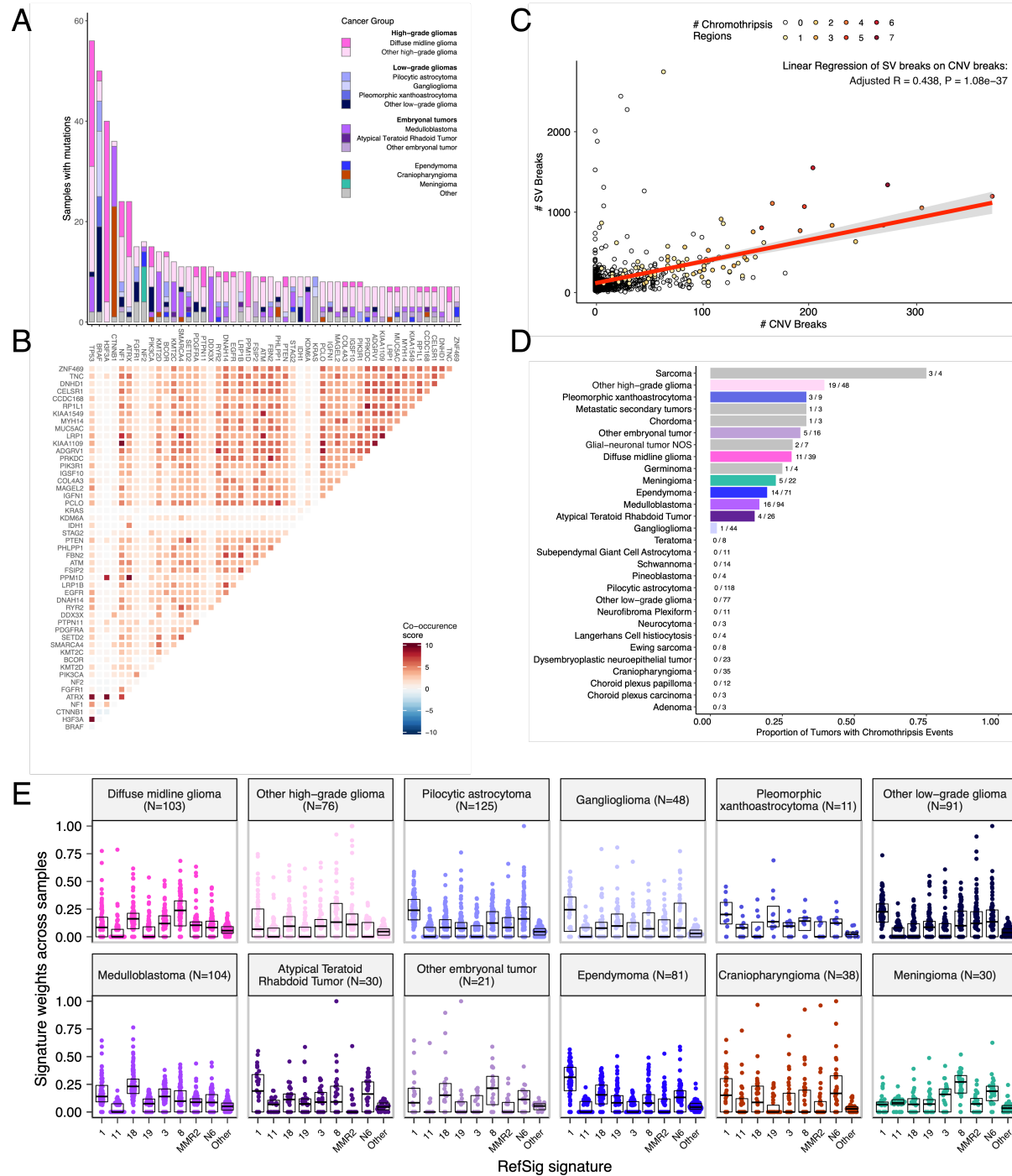
462 We analyzed mutational co-occurrence among OpenPBTA tumors, using a single sequencing  
463 sample from each individual with available WGS (N = 666). The top 50 mutated genes (see  
464 **STAR Methods** for details) in primary tumors are shown in **Figure 3** by tumor type (**A**, bar  
465 plots), with co-occurrence scores illustrated in the heatmap (**B**). *TP53* was the most frequently  
466 mutated gene across OpenPBTA tumors (8.4%, 56/666), significantly co-occurring with *H3F3A*  
467 (OR = 32, 95% CI: 15.3 - 66.7, q = 8.46e-17), *ATRX* (OR = 20, 95% CI: 8.4 - 47.7, q = 4.43e-8),  
468 *NF1* (OR = 8.62, 95% CI: 3.7 - 20.2, q = 5.45e-5), and *EGFR* (OR = 18.2, 95% CI: 5 - 66.5, q =  
469 1.6e-4). Other canonical cancer driver genes that were frequently mutated included *BRAF*,  
470 *H3F3A*, *CTNNB1*, *NF1*, *ATRX*, *FGFR1*, and *PIK3CA*.

471 At the broad histology level, mutations in *CTNNB1* significantly co-occurred with mutations in  
472 *TP53* (OR = 42.9, 95% CI: 7 - 261.4, q = 1.63e-3) and *DDX3X* (OR = 21.1, 95% CI: 4.6 - 96.3, q  
473 = 4.46e-3) in embryonal tumors. Mutations in *FGFR1* and *PIK3CA* significantly co-occurred in  
474 LGGs (OR = 76.1, 95% CI: 9.85 - 588.1, q = 3.26e-3), consistent with previous findings<sup>33,34</sup>. Of  
475 HGG tumors with mutations in *TP53* or *PPM1D*, 52/54 (96.3%) had mutations in only one of  
476 these genes (OR = 0.188, 95% CI: 0.04 - 0.94, p = 0.0413, q = 0.0587). This trend recapitulates  
477 previous observations that *TP53* and *PPM1D* mutations tend to be mutually exclusive in  
478 HGGs<sup>35</sup>.

479 We summarized broad CNV and SV and observed that HGGs and DMGs, followed by  
480 medulloblastomas, had the most unstable genomes (**Figure S3B**). By contrast,  
481 craniopharyngiomas and schwannomas generally lacked somatic CNV. Together, these CNV  
482 patterns largely aligned with our estimates of tumor mutational burden (**Figure S2H**). The  
483 breakpoint density estimated from SV and CNV data was significantly correlated across tumors  
484 (p = 1.08e-37) (**Figure 3C**) and as expected, the number of chromothripsis regions called  
485 increased as breakpoint density increased (**Figure S3B-C**). We identified chromothripsis events  
486 in 28% (N = 11/39) of diffuse midline gliomas and in 40% (N = 19/48) of other HGGs (non-  
487 midline HGGs) (**Figure 3D**). We also found evidence of chromothripsis in over 15% of  
488 sarcomas, PXAs, metastatic secondary tumors, chordomas, glial-neuronal tumors, germinomas,  
489 meningiomas, ependymomas, medulloblastomas, ATRTs, and other embryonal tumors,  
490 highlighting the genomic instability and complexity of these pediatric brain tumors.

491 We next assessed the contributions of eight previously identified adult CNS-specific mutational  
492 signatures from the RefSig database<sup>36</sup> across samples (**Figure 3E** and **Figure S4A**). Stage 0  
493 and/or 1 tumors characterized by low TMBs (**Figure S2H**) such as pilocytic astrocytomas,  
494 gangliogliomas, other LGGs, and craniopharyngiomas, were dominated by Signature 1 (**Figure**  
495 **S4A**), which results from the normal process of spontaneous deamination of 5-methylcytosine.  
496 Signature N6 is a CNS-specific signature which we observed nearly universally across samples.  
497 Drivers of Signature 18, *TP53*, *APC*, *NOTCH1* (found at

498 https://signal.mutationalsignatures.com/explore/referenceCancerSignature/31/drivers), are also  
499 canonical drivers of medulloblastoma, and indeed, we observed Signature 18 as the signature  
500 with the highest weight in medulloblastoma tumors. Signatures 3, 8, 18, and MMR2 were  
501 prevalent in HGGs, including DMGs. Finally, we found that the Signature 1 weight was higher at  
502 diagnosis (pre-treatment) and was almost always lower in tumors at later phases of therapy  
503 (progression, recurrence, post-mortem, secondary malignancy; **Figure S4B**). This trend may  
504 have resulted from therapy-induced mutations that produced additional signatures (e.g.,  
505 temozolamide treatment has been suggested to drive Signature 11<sup>37</sup>), subclonal expansion,  
506 and/or acquisition of additional driver mutations during tumor progression, leading to higher  
507 overall TMBs and additional signatures.



508

509 **Figure 3: Mutational co-occurrence and signatures highlight key oncogenic drivers.** A, Bar  
 510 plot of occurrence and co-occurrence of nonsynonymous mutations for the 50 most commonly  
 511 mutated genes across all tumor types, which are denoted as “Other” when there are fewer than  
 512 10 samples per grouping; B, Co-occurrence and mutual exclusivity of nonsynonymous  
 513 mutations between genes; The co-occurrence score is defined as  $I(-\log_{10}(P))$  where  $P$  is  
 514 defined by Fisher’s exact test and  $I$  is 1 when mutations co-occur more often than expected and  
 515 -1 when exclusivity is more common; C, The number of SV breaks significantly correlate with

516 CNV breaks (Adjusted  $R = 0.436$ ,  $p = 1.08e-37$ ). *D*, Chromothripsis frequency across pediatric  
517 brain tumors for all cancer groups with  $N \geq 3$  samples. *E*, Sina plots of RefSig signature  
518 weights for signatures 1, 11, 18, 19, 3, 8, N6, MMR2, and Other across cancer groups. Box plot  
519 lines represent the first quartile, median, and third quartile.

## 520 Transcriptomic Landscape of Pediatric Brain Tumors

### 521 Prediction of *TP53* oncogenicity and telomerase activity

522 To understand the *TP53* phenotype in each tumor, we ran a classifier previously trained on  
523 TCGA<sup>38</sup> to calculate a *TP53* score and infer *TP53* inactivation status. We compared results of  
524 this classifier to “true positive” alterations derived using high-confidence SNVs, CNVs, SVs, and  
525 fusions in *TP53*. Specifically, we annotated *TP53* alterations as “activated” if samples harbored  
526 one of p.R273C or p.R248W gain-of-function mutations<sup>39</sup>, or “lost” if the given patient either had  
527 a Li Fraumeni Syndrome (LFS) predisposition diagnosis, the tumor harbored a known hotspot  
528 mutation, or the tumor contained two hits (e.g. both SNV and CNV), which would suggest both  
529 alleles had been affected. If the *TP53* mutation did not reside within the DNA-binding domain or  
530 we did not detect any alteration in *TP53*, we annotate the tumor as “other,” reflecting its  
531 unknown *TP53* alteration status. The classifier achieved a high accuracy (AUROC = 0.85) for  
532 rRNA-depleted, stranded samples compared to randomly shuffled *TP53* scores (Figure 4A). By  
533 contrast, while this classifier has previously shown strong performance on poly-A data from both  
534 adult<sup>38</sup> tumors and pediatric patient-derived xenografts<sup>40</sup>, it did not perform as well on the poly-A  
535 samples in this cohort (AUROC = 0.62; Figure S5A).

536 While we expected that samples annotated as “lost” would have higher *TP53* scores than would  
537 samples annotated as “other,” we observed that samples annotated as “activated” had similar  
538 *TP53* scores to those annotated as “lost” (Figure 4B, Wilcoxon  $p = 0.23$ ). This result suggests  
539 that the classifier actually detects an oncogenic, or altered, *TP53* phenotype (scores  $> 0.5$ )  
540 rather than solely *TP53* inactivation, as interpreted previously<sup>38</sup>. Moreover, tumors with  
541 “activating” *TP53* mutations showed higher *TP53* expression compared to those with *TP53*  
542 “loss” mutations (Wilcoxon  $p = 3.5e-3$ , Figure 4C). Tumor types with the highest median *TP53*  
543 scores were those known to harbor somatic *TP53* alterations and included DMGs,  
544 medulloblastomas, HGGs, DNETs, ependymomas, and craniopharyngiomas (Figure 4D), while  
545 gangliogliomas, LGGs, meningiomas, and schwannomas had the lowest median scores.

546 To further validate the classifier’s accuracy, we assessed *TP53* scores for patients with LFS,  
547 hypothesizing that all of these tumors would have high scores. Indeed, we observed higher  
548 scores in LFS tumors ( $N = 8$ ) for which we detected high-confidence *TP53* somatic alterations  
549 (Tables S1 and S3). Although we did not detect canonical somatic *TP53* mutations in two  
550 patients whose tumors had low *TP53* scores (BS\_DEHF4C7 with a score of 0.09 and  
551 BS\_ZD5HN296 with a score of 0.28), we confirmed from pathology reports these patients were  
552 both diagnosed with LFS and had pathogenic germline variants in *TP53*. In addition, the tumor  
553 purity of these two LFS samples was low (16% and 37%, respectively), suggesting the classifier  
554 may require a certain level of tumor purity to achieve good performance, as we expect *TP53* to  
555 be intact in normal cells.

556 We next used gene expression data to predict telomerase activity using EXpression-based  
557 Telomerase ENzymatic activity Detection (EXTEND)<sup>41</sup> as a surrogate measure of malignant  
558 potential<sup>41,42</sup>, such that higher EXTEND scores suggest increased malignant potential. As  
559 expected, EXTEND scores significantly correlated with *TERC* ( $R = 0.619$ ,  $p < 0.01$ ) and *TERT* ( $R$   
560 = 0.491,  $p < 0.01$ ) expression (Figure S5B-C). We found aggressive tumors such as HGGs  
561 (DMGs and other high-grade gliomas) and MB had high EXTEND scores (Figure 4D), while low-  
562 grade lesions such as schwannomas, GNGs, DNETs, and other low-grade gliomas had among  
563 the lowest scores (Table S3). These findings support previous reports of a more aggressive  
564 phenotype in tumors with higher telomerase activity<sup>43-46</sup>.

## 565 **Hypermutant tumors share mutational signatures and have dysregulated 566 *TP53***

567 We further investigated the mutational signature profiles of the hypermutant ( $TMB > 10$  Mut/Mb;  
568  $N = 3$ ) and ultra-hypermutant ( $TMB > 100$  Mut/Mb;  $N = 4$ ) tumors and/or derived cell lines from  
569 six patients in the OpenPBTA cohort (Figure 4E). Five of six tumors were diagnosed as HGGs  
570 and one was a brain metastasis of a MYCN non-amplified neuroblastoma tumor. Signature 11,  
571 which is associated with exposure to temozolomide plus *MGMT* promoter and/or mismatch  
572 repair deficiency<sup>47</sup>, was indeed present in tumors with previous exposure to the drug (Table 2).  
573 We detected the MMR2 signature in tumors of four patients (PT\_0SPKM4S8, PT\_3CHB9PK5,  
574 PT\_JNEV57VK, and PT\_VTM2STE3) diagnosed with either constitutional mismatch repair  
575 deficiency (CMMRD) or Lynch syndrome (Table 2), genetic predisposition syndromes caused  
576 by a variant in a mismatch repair gene such as *PMS2*, *MLH1*, *MSH2*, *MSH6*, or others<sup>48</sup>. Three  
577 of these patients harbored pathogenic germline variants in one of the aforementioned genes.  
578 While we did not find a *known* pathogenic variant in the germline of PT\_VTM2STE3, this patient  
579 had a self-reported *PMS2* variant noted in their pathology report and we did find 19 intronic  
580 variants of unknown significance (VUS) in *PMS2*. This is not surprising since an estimated 49%  
581 of germline *PMS2* variants in patients with CMMRD and/or Lynch syndrome are VUS<sup>48</sup>.  
582 Interestingly, while the cell line derived from patient PT\_VTM2STE3's tumor at progression was  
583 not hypermutated ( $TMB = 5.7$  Mut/Mb), it solely showed the MMR2 signature of the eight CNS  
584 signatures examined, suggesting selective pressure to maintain a mismatch repair (MMR)  
585 phenotype *in vitro*. From patient PT\_JNEV57VK, only one of the two cell lines derived from the  
586 progressive tumor was hypermutated ( $TMB = 35.9$  Mut/Mb). This hypermutated cell line was  
587 strongly weighted towards signature 11, while this patient's non-hypermutated cell line showed  
588 a number of lesser signature weights (1, 11, 18, 19, MMR2; Table S2), highlighting the plasticity  
589 of mutational processes and the need to carefully genetically characterize and select models  
590 for preclinical studies based on research objectives.

591 We observed that signature 18, which has been associated with high genomic instability and  
592 can lead to a hypermutator phenotype<sup>36</sup>, was uniformly represented among hypermutant solid  
593 tumors. Additionally, we found that all of the HGG tumors or cell lines had dysfunctional *TP53*  
594 (Table 2), consistent with a previous report showing *TP53* dysregulation is a dependency in  
595 tumors with high genomic instability<sup>36</sup>. With one exception, hypermutant and ultra-hypermutant  
596 tumors had high *TP53* scores ( $> 0.5$ ) and telomerase activity. Interestingly, none of the  
597 hypermutant samples showed evidence of signature 3 (present in homologous recombination  
598 deficient tumors), signature 8 (arises from double nucleotide substitutions/unknown etiology), or

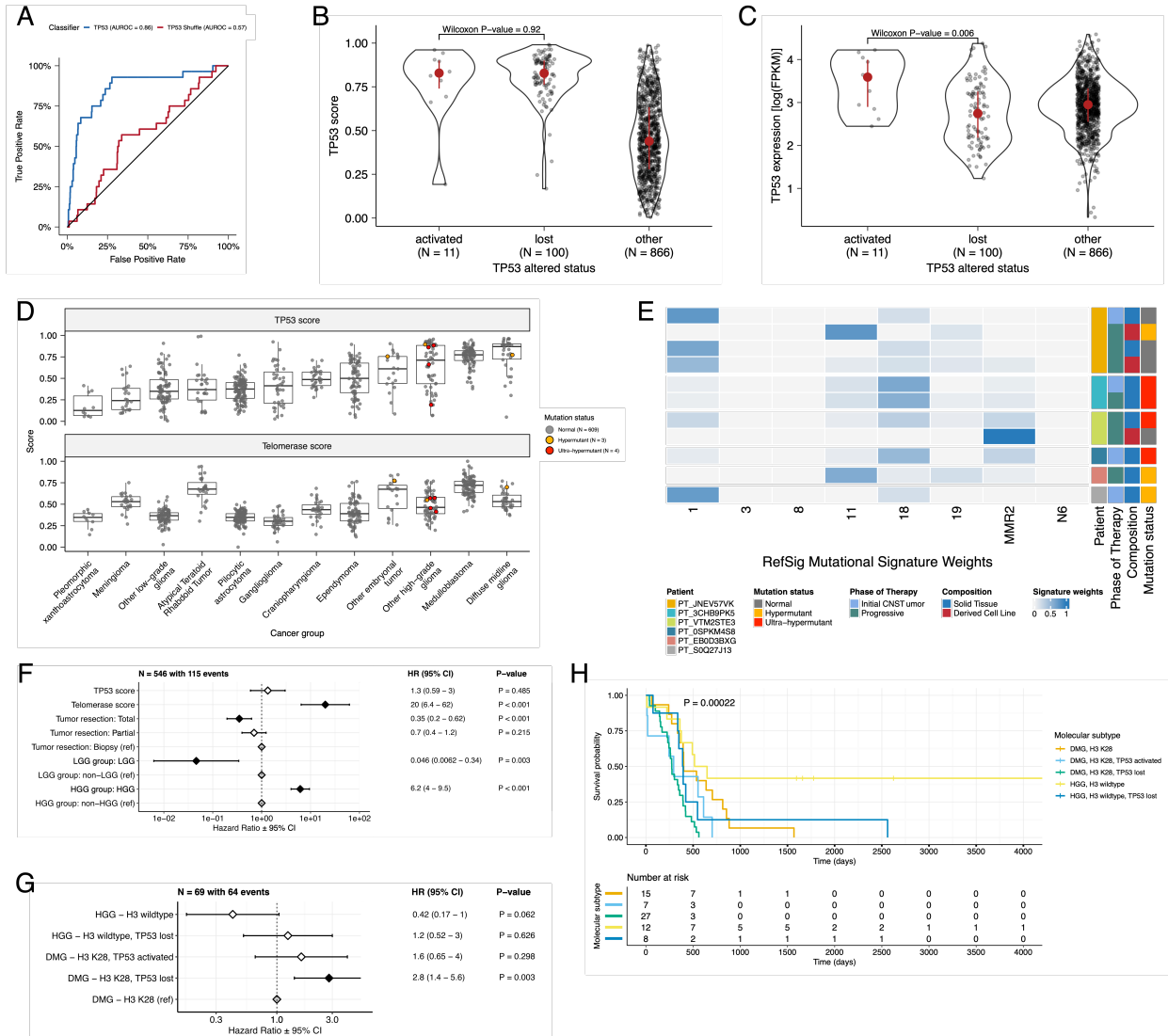
599 signature N6 (a universal CNS tumor signature). The mutual exclusivity of signatures 3 and  
600 MMR2 corroborates a previous report suggesting tumors do not tend to feature both deficient  
601 homologous repair and mismatch repair<sup>38</sup>.

602 **Table 2: Patients with hypermutant tumors.** Listed are patients with at least one hypermutant  
603 or ultra-hypermutant tumor or cell line. Pathogenic (P) or likely pathogenic (LP) germline  
604 variants, coding region TMB, phase of therapy, therapeutic interventions, cancer predisposition  
605 (CMMRD = Constitutional mismatch repair deficiency), and molecular subtypes are included.

| Kids First Participant ID | Kids First Biospecimen ID | CBTN ID   | Phase of therapy  | Composition       | Therapy post-biopsy                              | Cancer predisposition | Pathogenic germline variant                   | TMB   | OpenPBTA molecular subtype         |
|---------------------------|---------------------------|-----------|-------------------|-------------------|--|-----------------------|---|-------|------------------------------------|
| PT_0SPKM4S8               | BS_VW4XN9Y7               | 7316-2640 | Initial CNS Tumor | Solid Tissue      | Radiation, Temozolomide, CCNU                    | None documented       | NM_000535.7(PS2):c.137G>T (p.Ser46Ile) (LP)   | 187.4 | HGG, H3 wildtype, TP53 activated   |
| PT_3CHB9PK5               | BS_20TBZG09               | 7316-515  | Initial CNS Tumor | Solid Tissue      | Radiation, Temozolomide, Irinotecan, Bevacizumab | CMMRD                 | NM_000179.3(MSH6):c.3439-2A>G (LP)            | 307   | HGG, H3 wildtype, TP53 loss        |
| PT_3CHB9PK5               | BS_8AY2GM4G               | 7316-2085 | Progressive       | Solid Tissue      | Radiation, Temozolomide, Irinotecan, Bevacizumab | CMMRD                 | NM_000179.3(MSH6):c.3439-2A>G (LP)            | 321.6 | HGG, H3 wildtype, TP53 loss        |
| PT_EB0D3BXG               | BS_F0GNWEJJ               | 7316-3311 | Progressive       | Solid Tissue      | Radiation, Nivolumab                             | None documented       | None detected                                 | 26.3  | Metastatic NBL, MYCN non-amplified |
| PT_JNEV57VK               | BS_85Q5P8GF               | 7316-2594 | Initial CNS Tumor | Solid Tissue      | Radiation, Temozolomide                          | Lynch Syndrome        | NM_000251.3(MSH2):c.1906G>C (p.Ala636Pro) (P) | 4.7   | DMG, H3 K28, TP53 loss             |
| PT_JNEV57VK               | BS_HM5GFJN8               | 7316-3058 | Progressive       | Derived Cell Line | Radiation, Temozolomide, Nivolumab               | Lynch Syndrome        | NM_000251.3(MSH2):c.1906G>C (p.Ala636Pro) (P) | 35.9  | DMG, H3 K28, TP53 loss             |
| PT_JNEV57VK               | BS_QWM9BPDY               | 7316-3058 | Progressive       | Derived Cell Line | Radiation, Temozolomide, Nivolumab               | Lynch Syndrome        | NM_000251.3(MSH2):c.1906G>C (p.Ala636Pro) (P) | 7.4   | DMG, H3 K28, TP53 loss             |
| PT_JNEV57VK               | BS_P0QJ1QAH               | 7316-3058 | Progressive       | Solid Tissue      | Radiation, Temozolomide, Nivolumab               | Lynch Syndrome        | NM_000251.3(MSH2):c.1906G>C (p.Ala636Pro) (P) | 6.3   | DMG, H3 K28, TP53 activated        |
| PT_S0Q27J13               | BS_P3PF53V8               | 7316-2307 | Initial CNS Tumor | Solid Tissue      | Radiation, Temozolomide, Irinotecan              | None documented       | None detected                                 | 15.5  | HGG, H3 wildtype, TP53 activated   |
| PT_VTM2STE3               | BS_ERFMPQN3               | 7316-2189 | Progressive       | Derived Cell Line | Unknown  | Lynch Syndrome        | None detected                                 | 5.7   | HGG, H3 wildtype, TP53 loss        |
| PT_VTM2STE3               | BS_02YBZSBY               | 7316-2189 | Progressive       | Solid Tissue      | Unknown  | Lynch Syndrome        | None detected                                 | 274.5 | HGG, H3 wildtype, TP53 activated   |

606 Next, we asked whether transcriptomic classification of *TP53* dysregulation and/or telomerase  
607 activity recapitulate the known prognostic influence of these oncogenic biomarkers. To this end,  
608 we conducted a multivariate Cox regression on overall survival (**Figure 4F; STAR Methods**),  
609 controlling for extent of tumor resection and whether a tumor was low-grade (LGG group) or  
610 high-grade (HGG group). We identified several expected trends, including a significant overall  
611 survival benefit if the tumor had been fully resected (HR = 0.35, 95% CI = 0.2 - 0.62, p < 0.001)  
612 or if the tumor belonged to the LGG group (HR = 0.046, 95% CI = 0.0062 - 0.34, p = 0.003) as  
613 well as a significant risk if the tumor belonged to the HGG group (HR = 6.2, 95% CI = 4.0 - 9.5,  
614 p < 0.001). High telomerase scores were associated with poor prognosis across brain tumor  
615 histologies (HR = 20, 95% CI = 6.4 - 62, p < 0.001), demonstrating that EXTEND scores  
616 calculated from RNA-Seq are an effective rapid surrogate measure for telomerase activity.  
617 Although higher *TP53* scores, which predict *TP53* gene or pathway dysregulation, were not a  
618 significant predictor of risk across the entire OpenPBTA cohort (**Table S4**), we did find a

619 significant survival risk associated with higher *TP53* scores within DMGs (HR = 6436, 95% CI =  
620 2.67 - 1.55e7, p = 0.03) and ependymomas (HR = 2003, 95% CI = 9.9 - 4.05e5, p = 0.005).  
621 Since we observed the negative prognostic effect of *TP53* scores for HGGs, we assessed the  
622 effect of molecular subtypes within HGG samples on survival risk. We found that DMG H3 K28  
623 tumors with *TP53* loss had significantly worse prognosis (HR = 2.8, CI = 1.4-5.6, p = 0.003) than  
624 did DMG H3 K28 tumors with wildtype *TP53* (Figure 4G and Figure 4H). This finding was also  
625 recently reported in a retrospective analysis of DIPG tumors from the PNOC003 clinical trial<sup>12</sup>.



626

627 **Figure 4: TP53 and telomerase activity** A, Receiver Operating Characteristic for *TP53*  
628 classifier run on FPKM of stranded RNA-Seq samples. B, Violin and strip plots of *TP53*  
629 scores from stranded RNA-Seq samples plotted by *TP53* alteration type (Nactivated = 11, Nlost = 100,  
630 Nother = 866). C, Violin and strip plots of *TP53* RNA expression from stranded RNA-Seq  
631 samples plotted by *TP53* activation status (Nactivated = 11, Nlost = 100, Nother = 866). D, Box  
632 plots of *TP53* and telomerase (EXTEND) scores across cancer groups. Mutation status is  
633 highlighted in orange (hypermutant) or red (ultra-hypermutant). E, Heatmap of RefSig  
634 mutational signatures for patients who have least one tumor or cell line with a hypermutant

635 phenotype. *F*, Forest plot depicting the prognostic effects of TP53 and telomerase scores on  
636 overall survival, controlling for extent of tumor resection, LGG group, and HGG group. *G*, Forest  
637 plot depicting the effect of molecular subtype on overall survival of HGGs. For *F* and *G*, hazard  
638 ratios (HR) with 95% confidence intervals and *p*-values are listed. Significant *p*-values are  
639 denoted with black diamonds. Reference groups are denoted by grey diamonds. *H*, Kaplan-  
640 Meier curve of HGG tumors by molecular subtype.

## 641 Histologic and oncogenic pathway clustering

642 UMAP visualization of gene expression variation across brain tumors (**Figure 5A**) showed the  
643 expected clustering of brain tumors by histology. We additionally explored UMAP projections of  
644 gene expression within molecular subtypes for certain cancer groups. We observed that, except  
645 for three outliers, *C11orf95::RELA* (*ZFTA::RELA*) fusion-positive ependymomas fell within  
646 distinct clusters (**Figure S6A**). Medulloblastoma (MB) samples cluster by molecular subtype,  
647 with WNT and SHH in distinct clusters and Groups 3 and 4 showing some overlap (**Figure**  
648 **S6B**), as expected. Of note, two MB samples annotated as the SHH subtype did not cluster with  
649 the other MB samples, and one clustered with Group 3 and 4 samples, suggesting potential  
650 subtype misclassification or different underlying biology of these two tumors. *BRAF*-driven low-  
651 grade gliomas (**Figure S6C**) were present in three separate clusters, suggesting that there  
652 might be additional shared biology within each cluster. Histone H3 G35-mutant high-grade  
653 gliomas generally clustered together and away from K28-mutant tumors (**Figure S6D**).  
654 Interestingly, although H3 K28-mutant tumors have different biological drivers than do H3  
655 wildtype tumors<sup>49</sup>, they did not form distinct clusters. This pattern suggests these subtypes may  
656 be driven by common transcriptional programs, have other much stronger biological drivers than  
657 their known distinct epigenetic drivers, or our sample size is too small to detect transcriptional  
658 differences.

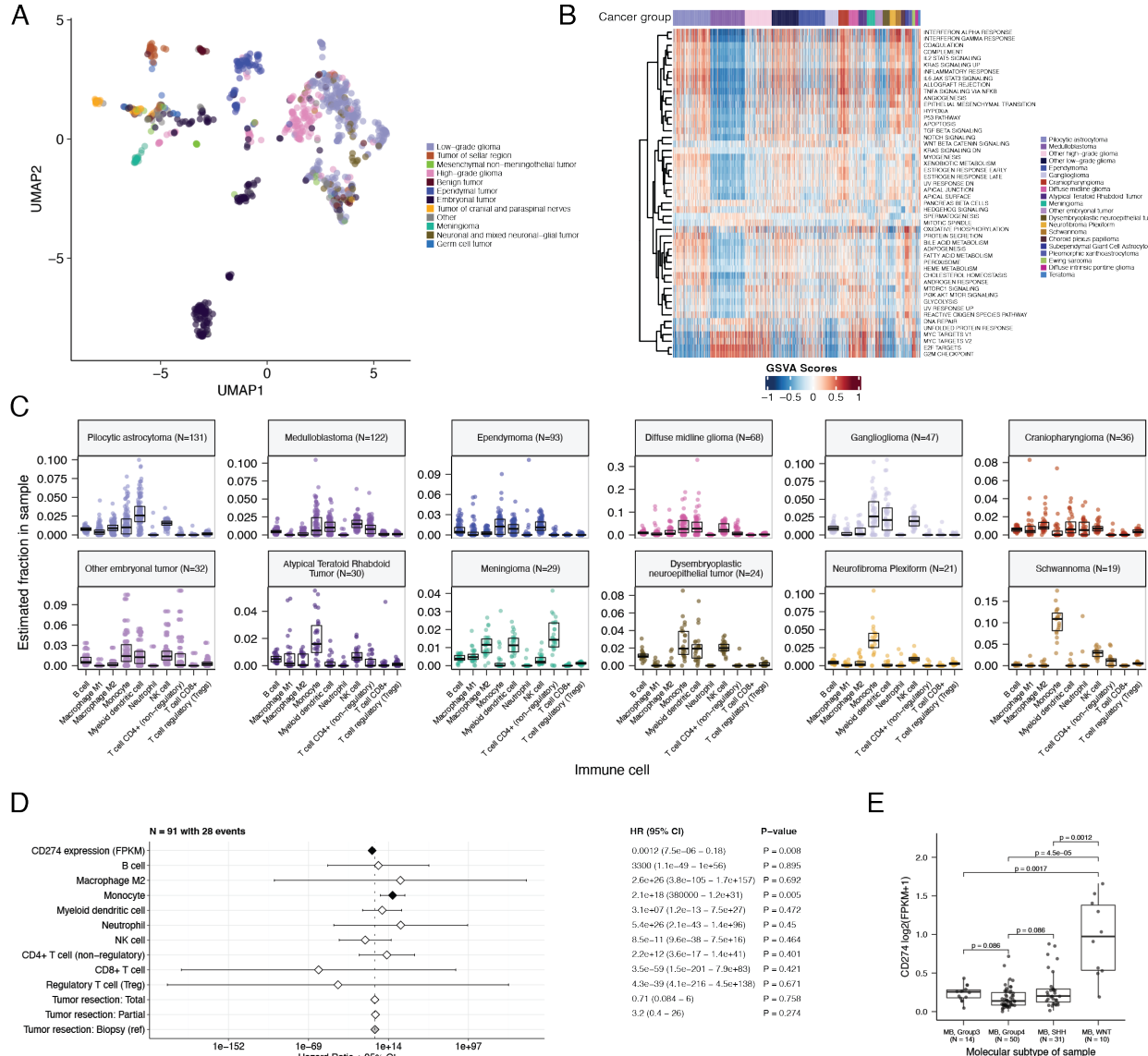
659 We next performed gene set variant analysis (GSVA) for Hallmark cancer gene sets to  
660 demonstrate activation of underlying oncogenic pathways (**Figure 5B** and quantified immune  
661 cell fractions across OpenPBTA tumors using quanTlseq (**Figure 5C** and **Figure S6E**). Through  
662 these analyses, we were able to recapitulate previously-described tumor biology. For example,  
663 HGG, DMG, MB, and ATRT tumors are known to upregulate *MYC*<sup>50</sup> which in turn activates *E2F*  
664 and S phase<sup>51</sup>. Indeed, we detected significant (Bonferroni-corrected *p* < 0.05) upregulation of  
665 *MYC* and *E2F* targets, as well as G2M (cell cycle phase following S phase) in MBs, ATRTs, and  
666 HGGs compared to several other cancer groups. In contrast, LGGs showed significant  
667 downregulation (Bonferroni-corrected *p* < 0.05) of these pathways. Schwannomas and  
668 neurofibromas, which have a documented inflammatory immune microenvironment of T and B  
669 lymphocytes as well as tumor-associated macrophages (TAMs), are driven by upregulation of  
670 cytokines such as *IFN $\gamma$* , *IL-1*, and *IL-6*, and *TNF $\alpha$* <sup>52</sup>. Indeed, we observed significant  
671 upregulation of these cytokines in GSVA hallmark pathways (Bonferroni-corrected *p* < 0.05)  
672 (**Figure 5B**) and found immune cell types dominated by monocytes in these tumors (**Figure**  
673 **5C**). We also observed significant upregulation of pro-inflammatory cytokines *IFN $\alpha$*  and *IFN $\gamma$*  in  
674 LGGs and craniopharyngiomas compared to medulloblastoma and ependymoma tumors  
675 (Bonferroni-corrected *p* < 0.05), both of which showed significant down-regulation of these  
676 cytokines (**Figure 5B**). Together, these results supported previous proteogenomic findings of

677 lower immune infiltration in aggressive medulloblastomas and ependymomas versus higher  
678 immune infiltration in *BRAF*-driven LGG and craniopharyngiomas<sup>53</sup>.

679 Although CD8+ T-cell infiltration across all cancer groups was quite low (**Figure 5C**), we  
680 observed some signal in specific cancer molecular subtypes (Groups 3 and 4 medulloblastoma)  
681 as well as outlier tumors (*BRAF*-driven LGG, *BRAF*-driven and wildtype ganglioglioma, and  
682 CNS embryonal NOS; **Figure S6E**) Surprisingly, the classically immunologically-cold HGG and  
683 DMG tumors<sup>54,55</sup> contained higher overall fractions of immune cells, where monocytes, dendritic  
684 cells, and NK cells were the most prevalent (**Figure 5C**). Thus, we suspect that quanTlseq  
685 might actually have captured microglia within these immune cell fractions.

686 While we did not detect notable prognostic effects of immune cell infiltration on overall survival  
687 in HGG or DMG tumors, we did find that high levels of macrophage M1 and monocytes were  
688 associated with poorer overall survival (monocyte HR = 2.1e18, 95% CI = 3.80e5 - 1.2e31, p =  
689 0.005) in medulloblastoma tumors (**Figure 5D**). We further reproduced previous findings  
690 (**Figure 5E**) that medulloblastomas typically have low expression of *CD274* (PD-L1)<sup>56</sup>. However,  
691 we also found that higher expression of *CD274* was significantly associated with improved  
692 overall prognosis for medulloblastoma samples, although with a marginal effect size (HR =  
693 0.0012, 95% CI = 7.5e-06 - 0.18, p = 0.008) (**Figure 5D**). This result may be explained by the  
694 higher expression of *CD274* found in WNT subtype tumors by us and others<sup>57</sup>, as this diagnosis  
695 carries the best prognosis of all medulloblastoma subgroups (**Figure 5E**).

696 Finally, we asked whether any molecular subtypes might show an immunologically-hot  
697 phenotype, as roughly defined by a greater proportion of CD8+ to CD4+ T cells<sup>58,59</sup>. While  
698 adamantinomatous craniopharyngiomas and Group 3 and Group 4 medulloblastomas had the  
699 highest CD8+ to CD4+ T cell ratios (**Figure S6F**), very few tumors had ratios greater than 1,  
700 highlighting an urgent need to identify novel therapeutics for these immunologically-cold  
701 pediatric brain tumors with poor prognosis.



702

703 **Figure 5: Transcriptomic and immune landscape of pediatric brain tumors** A, First two  
 704 dimensions from UMAP of sample transcriptome data. Points are colored by the broad histology  
 705 of the samples they represent. B, Heatmap of GSVA scores for Hallmark gene sets with  
 706 significant differences, with samples ordered by cancer group. C, Box plots of quanTlseq  
 707 estimates of immune cell proportions in select cancer groups with  $N > 15$  samples. Note: Other  
 708 HGGs and other LGGs have immune cell proportions similar to DMG and pilocytic astrocytoma,  
 709 respectively, and are not shown. D, Forest plot depicting the additive effects of CD274  
 710 expression, immune cell proportion, and extent of tumor resection on overall survival of  
 711 medulloblastoma patients. Hazard ratios (HR) with 95% confidence intervals and p-values are  
 712 listed. Significant p-values are denoted with black diamonds. Reference groups are denoted by  
 713 grey diamonds. Of note, the Macrophage M1 HR was 0 (coefficient = -9.90e+4) with infinite  
 714 upper and lower CIs, and thus it was not included in the figure. E, Box plot of CD274 expression

715 ( $\log_2 FPKM$ ) for medulloblastoma samples grouped by molecular subtype. Bonferroni-corrected  
716 *p*-values from Wilcoxon tests are shown.

## 717 Discussion

718 We created OpenPBTA to define an open, real-time, reproducible analysis framework to  
719 genomically characterize pediatric brain tumors that brings together basic and translational  
720 researchers, clinicians, and data scientists on behalf of accelerated discovery and clinical  
721 impact. We provide robust reusable code and data resources, paired with cloud-based  
722 availability of source and derived data resources, to the pediatric oncology community,  
723 encouraging interdisciplinary scientists to collaborate on new analyses in order to accelerate  
724 therapeutic translation for children with cancer, goals we are seeing play out in real-time. To our  
725 knowledge, this initiative represents the first large-scale, collaborative, open analysis of genomic  
726 data coupled with open manuscript writing, in which we comprehensively analyzed the largest  
727 cohort of pediatric brain tumors to date, comprising 1,074 tumors across 58 distinct histologies.  
728 We used available WGS, WXS, and RNA-Seq data to generate high-confidence consensus  
729 SNV and CNV calls, prioritize putative oncogenic fusions, and establish over 40 scalable  
730 modules to perform common downstream cancer genomics analyses, all of which have  
731 undergone rigorous scientific and analytical code review. We detected and showed expected  
732 patterns of genomic lesions, mutational signatures, and aberrantly regulated signaling pathways  
733 across multiple pediatric brain tumor histologies.

734 Assembling large, pan-histology cohorts of fresh frozen samples and associated clinical  
735 phenotypes and outcomes requires a multi-year, multi-institutional framework, like those  
736 provided by CBTN and PNOC. As such, uniform clinical molecular subtyping was largely not  
737 performed for most of this cohort at the time of diagnosis and/or at surgery, and when available  
738 (e.g., sparse medulloblastoma subtypes), it required manual curation from pathology reports  
739 and/or free text clinical data fields. Furthermore, rapid classification to derive molecular  
740 subtypes could not be immediately performed since research-based DNA methylation data for  
741 these samples are not yet available. Thus, to enable biological interrogation of specific tumor  
742 subtypes, we created RNA- and DNA-based subtyping modules aligned with WHO molecularly-  
743 defined diagnoses. We worked closely with pathologists and clinicians to build modules from  
744 which we determined a research-grade integrated diagnosis for 60% of samples while  
745 discovering incorrectly diagnosed or mis-identified samples in the OpenPBTA cohort.

746 We harnessed RNA expression data for a number of analyses, yielding important biological  
747 insights across multiple brain tumor histologies. For example, we performed subtyping of  
748 medulloblastoma tumors, for which only 35% (43/122) had subtype information from pathology  
749 reports. Among the subtyped tumors, we accurately recapitulated subtypes using MM2S (91%;  
750 39/43) or medulloPackage (95%; 41/43)<sup>[60,61](#)</sup>. We then applied the consensus of these methods  
751 to subtype all medulloblastoma tumors lacking pathology-based subtypes.

752 We advanced the integrative analyses and cross-cohort comparison via a number of validated  
753 modules. We used an expression classifier to determine whether tumors have dysfunctional  
754 *TP53*<sup>[38](#)</sup> and the EXTEND algorithm to determine their degree of telomerase activity using a 13-  
755 gene signature<sup>[41](#)</sup>. Interestingly, in contrast to adult colorectal cancer and gastric

756 adenocarcinoma, in which *TP53* loss of function is less frequent in hypermutated tumors<sup>62,63</sup>, we  
757 found that hypermutant HGG tumors universally displayed dysregulation of *TP53*. Furthermore,  
758 high *TP53* scores were a significant prognostic marker for poor overall survival for patients with  
759 certain tumor types, such as H3 K28-altered DMGs and ependymomas. We also show that  
760 EXTEND scores are a robust surrogate measure for telomerase activity in pediatric brain  
761 tumors. By assessing *TP53* and telomerase activity prospectively from expression data,  
762 information usually only attainable with DNA sequencing and/or qPCR, we can quickly  
763 incorporate oncogenic biomarker and prognostic knowledge and expand our biological  
764 understanding of these tumors.

765 We identified enrichment of hallmark cancer pathways and characterized the immune cell  
766 landscape across pediatric brain tumors, demonstrating tumors in some histologies, such as  
767 schwannomas, craniopharyngiomas, and low-grade gliomas, may have a inflammatory tumor  
768 microenvironment. Of note, we observed upregulation of IFN $\gamma$ , IL-1, and IL-6, and TNF $\alpha$  in  
769 craniopharyngiomas, tumors difficult to resect due to their anatomical location and critical  
770 surrounding structures. Neurotoxic side effects have been reported when interferon alpha  
771 immunotherapy is administered to reduce cystic craniopharyngioma tumor size and/or delay  
772 progression<sup>64,65</sup>. Thus, additional immune vulnerabilities, such as IL-6 inhibition and immune  
773 checkpoint blockade, have recently been proposed as therapies for cystic adamantinomatous  
774 craniopharyngiomas<sup>66-70</sup> and our results noted above support this approach. Finally, our study  
775 reproduced the overall known poor infiltration of CD8+ T cells and general low expression of  
776 CD274 (PD-L1) in pediatric brain tumors, further highlighting the urgent need to identify novel  
777 therapeutic strategies for these immunologically cold tumors.

778 OpenPBTA has rapidly become a foundational data analysis and processing layer for a number  
779 of discovery research and translational projects which will continue to add other genomic  
780 modalities and analyses, such as germline, methylation, single cell, epigenomic, mRNA splicing,  
781 imaging, and model drug response data. For example, the RNA fusion filtering module created  
782 within OpenPBTA set the stage for development of the R package *annoFuse*<sup>71</sup> and an R Shiny  
783 application *shinyFuse*. Using medulloblastoma subtyping and immune deconvolution analyses  
784 performed herein, Dang and colleagues showed enrichment of monocyte and microglia-derived  
785 macrophages within the SHH subgroup which they suggest may accumulate following radiation  
786 therapy<sup>10</sup>. Expression and copy number analyses were used to demonstrate that *GPC2* is a  
787 highly expressed and copy number gained immunotherapeutic target in ETMRs,  
788 medulloblastomas, choroid plexus carcinomas, H3 wildtype high-grade gliomas, as well as  
789 DMGs. This led Foster and colleagues to subsequently develop a chimeric antigen receptor  
790 (CAR) directed against *GPC2*, for which they show preclinical efficacy in mouse models<sup>11</sup>.  
791 Moreover, OpenPBTA has enabled a framework to support real-time integration of clinical trial  
792 subjects as each was enrolled on the PNOC008 high-grade glioma clinical trial<sup>72</sup>, allowing  
793 researchers and clinicians to link tumor biology to translational impact through clinical decision  
794 support during tumor board discussions. Finally, as part of the the NCI's Childhood Cancer Data  
795 Initiative (CCDI), the OpenPBTA project was recently expanded into a pan-pediatric cancer  
796 effort (<https://github.com/PediatricOpenTargets/OpenPedCan-analysis>) to build the Molecular  
797 Targets Platform (<https://moleculartargets.ccdi.cancer.gov/>) in support of the RACE Act. An  
798 additional, large-scale cohort of >2,500 tumor samples and associated germline DNA is in the  
799 process of undergoing sequence data generation as part of CBTN CCDI-Kids First NCI and

800 Common Fund project ([https://commonfund.nih.gov/kidsfirst/2021X01projects#FY21\\_Resnick](https://commonfund.nih.gov/kidsfirst/2021X01projects#FY21_Resnick)).  
801 Like the original OpenPBTA cohort, data will be processed and released in near real-time via  
802 the Kids First Data Resource and integrated with OpenPBTA. The OpenPBTA project has  
803 paved the way for new modes of collaborative data-driven discovery, open, reproducible, and  
804 scalable analyses that will extend beyond the current research described herein, and we  
805 anticipate this foundational work will continue to have a long-term impact within the pediatric  
806 brain tumor translational research community and beyond, ultimately leading to accelerated  
807 impact and improved outcomes for children with cancer.  
808 All code and processed data are openly available through GitHub, CAVATICA, and  
809 PedcBioPortal (see **STAR METHODS**).

## 810 Acknowledgments

811 We graciously thank the patients and families who have donated their tumors to the Children's  
812 Brain Tumor Network (CBTN) and/or the Pacific Pediatric Neuro-oncology Consortium, without  
813 which this research would not be possible.  
814 Philanthropic support has ensured the CBTN's ability to collect, store, manage, and distribute  
815 specimen and data since it was founded in 2013. In addition to the support from the CBTN  
816 Executive Council members and Brain Tumor Board of Visitors, the following donors have  
817 provided leadership level support for CBTN: Children's Brain Tumor Foundation, Easie Family  
818 Foundation, Kortney Rose Foundation, Lilabean Foundation, Minnick Family Charitable Fund,  
819 Perricelli Family, Psalm 103 Foundation, and Swifty Foundation.  
820 This work was funded through the Alex's Lemonade Stand Foundation (ALSF) Childhood  
821 Cancer Data Lab (CSG), ALSF Young Investigator Award (JLR), ALSF Catalyst Award (JLR,  
822 ACR, PBS), ALSF Catalyst Award (SJS), ALSF CCDL Postdoctoral Training Grant (SMF),  
823 Children's Hospital of Philadelphia Division of Neurosurgery (PBS and ACR), the Australian  
824 Government, Department of Education (APH), the St. Anna Kinderkrebsforschung, Austria  
825 (ARP), the Mildred Scheel Early Career Center Dresden P2, funded by the German Cancer Aid  
826 (ARP), and NIH Grants 3P30 CA016520-44S5 (ACR), U2C HL138346-03 (ACR, APH), U24  
827 CA220457-03 (ACR), K12GM081259 (SMF), R03-CA23036 (SJD), and NIH Contract  
828 No. HHSN261200800001E (SJD). This project has been funded in part with Federal funds from  
829 the National Cancer Institute, National Institutes of Health, under Contract  
830 No. 75N91019D00024, Task Order No. 75N91020F00003 (JLR, ACR, APH). Additionally, this  
831 work was supported by the Intramural Research Program of the Division of Cancer  
832 Epidemiology and Genetics of the National Cancer Institute. The content of this publication does  
833 not necessarily reflect the views or policies of the Department of Health and Human Services,  
834 nor does mention of trade names, commercial products or organizations imply endorsement by  
835 the U.S. Government.  
836 The authors would like to thank the following collaborators who contributed or supervised  
837 analyses present in the analysis repository that were not included in the manuscript: William  
838 Amadio, Holly C. Beale, Ellen T. Kephart, A. Geoffrey Lyle, and Olena M. Vaske. Finally, we  
839 would like to thank Yuanchao Zhang and Eric Wafula for adding to the project codebase,

840 Jessica B. Foster for helpful discussions while drafting the manuscript, and Gina D. Mawla for  
841 identifying and reporting issues in OpenPBTA data.

## 842 **Author Contributions**

| Author                | Contributions   |
|-----------------------|---|
| Joshua A. Shapiro     | Methodology, Software, Validation, Formal analysis, Investigation, Writing - Original draft, Writing - Review and editing, Visualization, Supervision |
| Krutika S. Gaonkar    | Data curation, Formal analysis, Investigation, Methodology, Software, Writing – Original draft, Writing - Review and editing                          |
| Candace L. Savonen    | Methodology, Software, Validation, Formal analysis, Investigation, Writing - Original draft, Writing - Review and editing, Visualization              |
| Stephanie J. Spielman | Validation, Formal analysis, Writing - Review and editing, Visualization, Supervision, Funding acquisition  |
| Chante J. Bethell     | Methodology, Validation, Formal analysis, Investigation, Writing - Original draft, Visualization  |
| Run Jin               | Data curation, Formal analysis, Visualization, Writing – Original draft, Writing - Review and editing   |
| Komal S. Rathi        | Formal analysis, Investigation, Methodology, Writing – Original draft   |
| Yuankun Zhu           | Data curation, Formal analysis, Investigation, Methodology, Supervision   |
| Laura E. Egolf        | Formal analysis, Writing - Original draft   |
| Bailey K. Farrow      | Data curation, Software   |
| Daniel P. Miller      | Formal analysis   |
| Yang Yang             | Formal analysis, Software   |
| Tejaswi Koganti       | Formal analysis, Investigation  |
| Nighat Noureen        | Formal analysis, Visualization, Writing - Original draft  |
| Mateusz P. Koptyra    | Formal analysis, Writing – Original draft   |
| Nhat Duong            | Formal analysis, Investigation, Methodology   |
| Adam A. Kraya         | Methodology   |
| Cassie Kline          | Supervision, Investigation, Writing - Review and editing  |
| Yiran Guo             | Formal analysis, Writing - Review and editing   |
| Phillip B. Storm      | Conceptualization, Funding acquisition, Resources   |
| Javad Nazarian        | Conceptualization   |
| Stephen C. Mack       | Writing - Review and editing  |
| Pichai Raman          | Conceptualization, Formal analysis, Methodology   |
| Siyuan Zheng          | Formal analysis, Visualization, Writing - Original draft, Supervision, Writing - Review and editing   |
| Peter J. Madsen       | Writing – Review & editing  |
| Nicolas Van Kuren     | Data curation, Software   |
| Shannon Robins        | Data curation   |

| Author             | Contributions   |
|--------------------|---|
| Xiaoyan Huang      | Formal analysis   |
| Angela J. Waanders | Supervision, Conceptualization  |
| Jung Kim           | Investigation, Writing - Review and editing   |
| Derek Hanson       | Validation  |
| Carl J. Koschmann  | Conceptualization   |
| Sharon J. Diskin   | Investigation, Supervision, Validation, Funding acquisition, Writing - Review and editing   |
| Rishi R. Lulla     | Conceptualization   |
| Miguel A. Brown    | Data curation, Methodology, Formal analysis   |
| Jessica Wong       | Writing – Original draft  |
| Jennifer L. Mason  | Supervision   |
| Laura Scolaro      | Data curation   |
| Meen Chul Kim      | Data curation   |
| Hongbo M. Xie      | Methodology, Supervision  |
| Brian R. Rood      | Conceptualization   |
| Kristina A. Cole   | Writing - Review and editing  |
| Ashley S. Margol   | Writing - Review and editing  |
| Zalman Vaksman     | Formal analysis, Investigation  |
| Rebecca S. Kaufman | Formal analysis, Investigation, Validation  |
| Allison P. Heath   | Project administration, Funding acquisition   |
| Brian M. Ennis     | Data curation, Formal analysis  |
| Mariarita Santi    | Investigation, Validation, Writing - Review and editing   |
| Anna R. Poetsch    | Formal analysis, Funding acquisition, Writing – Review and editing  |
| Angela N. Viaene   | Investigation, Validation   |
| Douglas R. Stewart | Supervision, Writing - Review and editing   |
| Steven M. Foltz    | Validation, Funding acquisition   |
| Payal Jain         | Data curation, Investigation, Validation  |
| Bo Zhang           | Data curation, Formal analysis  |
| Shrivats Kannan    | Formal analysis, Methodology, Writing – Original draft  |
| Michael Prados     | Conceptualization   |
| Jena V. Lilly      | Conceptualization, Funding acquisition, Project administration  |
| Sabine Mueller     | Conceptualization   |
| Adam C. Resnick    | Conceptualization, Funding acquisition, Resources, Supervision  |
| Casey S. Greene    | Conceptualization, Funding acquisition, Methodology, Project administration, Software, Supervision, Writing – Review & editing  |
| Jo Lynne Rokita    | Conceptualization, Data curation, Formal analysis, Funding acquisition, Investigation, Methodology, Software, Supervision, Writing – Original draft, Writing - Review and editing |

| Author                                      | Contributions  |
|---|--|
| Jaclyn N. Taroni                            | Methodology, Software, Validation, Formal analysis, Investigation, Data curation, Writing - Review and editing, Visualization, Supervision, Project administration |
| Children's Brain Tumor Network              | Conceptualization  |
| Pacific Pediatric Neuro-Oncology Consortium | Conceptualization  |

843 Except for the first and last four authors, authorship order was determined as follows: Authors  
844 who contributed to the OpenPBTA code base are listed based on number of modules included  
845 in the manuscript to which that individual contributed and, in the case of ties, a random order is  
846 used. All remaining authors are then listed in a random order.

847 Code for determining authorship order can be found in the `count-contributions` module of  
848 the OpenPBTA analysis repository.

## 849 **Declarations of Interest**

850 CSG's spouse was an employee of Alex's Lemonade Stand Foundation, which was a sponsor  
851 of this research. JAS, CLS, CJB, SJS, and JNT are or were employees of Alex's Lemonade  
852 Stand Foundation, a sponsor of this research. AJW is a member of the Scientific Advisory  
853 boards for Alexion and DayOne Biopharmaceuticals.

## 854 **Figure Titles and Legends**

855 **Figure 1. Overview of the OpenPBTA Project.** A, The Children's Brain Tumor Network and  
856 the Pacific Pediatric Neuro-Oncology Consortium collected tumor samples from 943 patients. To  
857 date, 22 cell lines were created from tumor tissue, and over 2000 specimens were sequenced  
858 ( $N = 1035$  RNA-Seq,  $N = 940$  WGS, and  $N = 32$  WXS or targeted panel). Data was harmonized  
859 by the Kids First Data Resource Center using an Amazon S3 framework within CAVATICA. B,  
860 Stacked bar plot summary of the number of biospecimens per phase of therapy per broad  
861 histology (Abbreviations: GNG = ganglioglioma, Other LGG = other low-grade glioma, PA =  
862 pilocytic astrocytoma, PXA = pleomorphic xanthoastrocytoma, SEGA = subependymal giant cell  
863 astrocytoma, DIPG = diffuse intrinsic pontine glioma, DMG = diffuse midline glioma, Other HGG  
864 = other high-grade glioma, ATRT = atypical teratoid rhabdoid tumor, MB = medulloblastoma,  
865 Other ET = other embryonal tumor, EPN = ependymoma, PNF = plexiform neurofibroma, DNET  
866 = dysembryoplastic neuroepithelial tumor, CRANIO = craniopharyngioma, EWS = Ewing  
867 sarcoma, CPP = choroid plexus papilloma). Only samples with available descriptors were  
868 included. C, Overview of the open analysis and manuscript contribution model. In the analysis  
869 GitHub repository, a contributor would propose an analysis that other participants can comment  
870 on. Contributors would then implement the analysis and file a request to add their changes to  
871 the analysis repository ("pull request"). Pull requests underwent review for scientific rigor and  
872 correctness of implementation. Pull requests were additionally checked to ensure that all  
873 software dependencies were included and the code was not sensitive to underlying data

874 changes using container and continuous integration technologies. Finally, a contributor would  
875 file a pull request documenting their methods and results to the Manubot-powered manuscript  
876 repository. Pull requests in the manuscript repository were also subject to review. D, A potential  
877 path for an analytical pull request. Arrows indicate revisions to a pull request. Prior to review, a  
878 pull request was tested for dependency installation and whether or not the code would execute.  
879 Pull requests also required approval by organizers and/or other contributors, who checked for  
880 scientific correctness. Panel A created with [BioRender.com](https://biorender.com).

881 **Figure 2. Mutational landscape of PBTA tumors.** Shown are frequencies of canonical  
882 somatic gene mutations, CNVs, fusions, and TMB (top bar plot) for the top 20 genes mutated  
883 across primary tumors within the OpenPBTA dataset. A, Low-grade astrocytic tumors (N = 227):  
884 pilocytic astrocytoma (N = 104), other low-grade glioma (N = 69), ganglioglioma (N = 35),  
885 pleomorphic xanthoastrocytoma (N = 9), subependymal giant cell astrocytoma (N = 10); B,  
886 Embryonal tumors (N = 128): medulloblastomas (N = 95), atypical teratoid rhabdoid tumors (N =  
887 24), other embryonal tumors (N = 9); C, Diffuse astrocytic and oligodendroglial tumors (N = 61):  
888 diffuse midline gliomas (N = 34) and other high-grade gliomas (N = 27); D, Other CNS tumors  
889 (N = 194): ependymomas (N = 60), craniopharyngiomas (N = 31), meningiomas (N = 17),  
890 dysembryoplastic neuroepithelial tumors (N = 19), Ewing sarcomas (N = 7), schwannomas (N =  
891 11), and neurofibroma plexiforms (N = 7). Additional, rare CNS tumors are displayed in **Figure**  
892 **S3A**. Tumor histology (Cancer Group) and patient sex (Germline sex estimate) are  
893 displayed as annotations at the bottom of each plot. Only samples with mutations in the listed  
894 genes are shown. Multiple CNVs are denoted as a complex event.

895 **Figure 3. Mutational co-occurrence and signatures highlight key oncogenic drivers.** A,  
896 Bar plot of occurrence and co-occurrence of nonsynonymous mutations for the 50 most  
897 commonly mutated genes across all tumor types (annotated from `cancer_group` if N >= 10 or  
898 `Other` if N < 10); B, Co-occurrence and mutual exclusivity of nonsynonymous mutations  
899 between genes; The co-occurrence score is defined as  $I(-\log_{10}(P))$  where  $P$  is defined by  
900 Fisher's exact test and  $I$  is 1 when mutations co-occur more often than expected and -1 when  
901 exclusivity is more common; C, The number of SV breaks significantly correlates with the  
902 number of CNV breaks (Adjusted R = 0.438, p = 1.08e-37). D, Chromothripsis frequency across  
903 pediatric brain tumors shown by `cancer_group` with N >= 3. E, Sina plots of RefSig signature  
904 weights for signatures 1, 11, 18, 19, 3, 8, N6, MMR2, and Other across cancer groups. Box plot  
905 lines represent the first quartile, median, and third quartile.

906 **Figure 4. TP53 and telomerase activity** A, Receiver Operating Characteristic for *TP53*  
907 classifier run on FPKM of stranded RNA-Seq samples. B, Violin and box plots of *TP53* scores  
908 plotted by *TP53* alteration type (Nactivated = 11, Nlost = 100, Nother = 866). C, Violin and box  
909 plots of *TP53* RNA expression plotted by *TP53* activation status (Nactivated = 11, Nlost = 100,  
910 Nother = 866). D, Box plots of *TP53* and telomerase (EXTEND) scores grouped by  
911 `cancer_group`. Mutation status is highlighted in orange (hypermutant) or red (ultra-  
912 hypermutant). E, Heatmap of RefSig mutational signatures for patients who have least one  
913 tumor or cell line with a TMB >= 10 Mut/Mb. F, Forest plot depicting the prognostic effects of  
914 *TP53* and telomerase scores on overall survival, controlling for extent of tumor resection, LGG  
915 group, and HGG group. G, Forest plot depicting the effect of molecular subtype on overall  
916 survival of HGGs. For F and G, hazard ratios (HR) with 95% confidence intervals and p-values

917 are listed. Significant p-values are denoted with black diamonds. Reference groups are denoted  
918 by grey diamonds. H, Kaplan-Meier curve of HGG tumors by molecular subtype.

919 **Figure 5. Transcriptomic and immune landscape of pediatric brain tumors** A, First two  
920 dimensions from UMAP of sample transcriptome data. Points are colored by the broad histology  
921 of the samples they represent. B, Heatmap of GSVA scores for Hallmark gene sets with  
922 significant differences, with samples ordered by cancer group. C, Box plots of quanTlseq  
923 estimates of immune cell proportions in select cancer groups with  $N > 15$  samples. Note: Other  
924 HGGs and other LGGs have immune cell proportions similar to DMG and pilocytic astrocytoma,  
925 respectively, and are not shown. D, Forest plot depicting the additive effects of *CD274*  
926 expression, immune cell proportion, and extent of tumor resection on overall survival of  
927 medulloblastoma patients. Hazard ratios (HR) with 95% confidence intervals and p-values are  
928 listed. Significant p-values are denoted with black diamonds. Reference groups are denoted by  
929 grey diamonds. Of note, the Macrophage M1 HR was 0 (coefficient = -9.90e+4) with infinite  
930 upper and lower CIs, and thus it was not included in the figure. E, Box plot of *CD274* expression  
931 (log2 FPKM) for medulloblastoma samples grouped by molecular subtype. Bonferroni-corrected  
932 p-values from Wilcoxon tests are shown.

## 933 **Table Titles and Legends**

934 **Table 1. Molecular subtypes generated through the OpenPBTA project.** Listed are broad  
935 tumor histologies, molecular subtypes generated, and number of specimens subtyped within the  
936 OpenPBTA project.

937 **Table 2. Patients with hypermutant tumors.** Listed are patients with at least one hypermutant  
938 or ultra-hypermutant tumor or cell line. Pathogenic (P) or likely pathogenic (LP) germline  
939 variants, coding region TMB, phase of therapy, therapeutic interventions, cancer predisposition  
940 (CMMRD = Constitutional mismatch repair deficiency), and molecular subtypes are included.

## 941 **STAR METHODS**

## 942 **RESOURCE AVAILABILITY**

### 943 **Lead contact**

944 Requests for access to OpenPBTA raw data and/or specimens may be directed to, and will be  
945 fulfilled by Jo Lynne Rokita (rokita@chop.edu).

### 946 **Materials availability**

947 This study did not create new, unique reagents.

### 948 **Data and code availability**

949 Raw and harmonized WGS, WXS, and RNA-Seq data derived from human samples are  
950 available within the KidsFirst Portal<sup>73</sup> upon access request to the CBTN (<https://cbtn.org/>) as of

951 the date of the publication. In addition, merged summary files are openly accessible at  
952 <https://cavatica.sbggenomics.com/u/cavatica/openpbta> or via download script in the  
953 <https://github.com/AlexsLemonade/OpenPBTA-analysis> repository. Summary data are visible  
954 within PedcBioPortal at <https://pedcbioportal.kidsfirstdrc.org/study/summary?id=openpbta>.  
955 Associated DOIs are listed in the **Key Resources Table**.

956 All original code was developed within the following repositories and is publicly available as  
957 follows. Primary data analyses can be found at <https://github.com/d3b-center/OpenPBTA-workflows>. Downstream data analyses can be found at  
958 <https://github.com/AlexsLemonade/OpenPBTA-analysis>. Manuscript code can be found at  
959 <https://github.com/AlexsLemonade/OpenPBTA-manuscript>. Associated DOIs are listed in the  
960 **Key Resources Table**. Software versions are documented in **Table S5** as an appendix to the  
961 **Key Resources Table**.  
962

963 Any additional information required to reanalyze the data reported in this paper is available from  
964 the lead contact upon request.

## 965 **METHOD DETAILS**

### 966 **Biospecimen Collection**

967 The Pediatric Brain Tumor Atlas specimens are comprised of samples from Children's Brain  
968 Tumor Network (CBTN) and the Pediatric Pacific Neuro-Oncology Consortium (PNOC). The  
969 [CBTN](#) is a collaborative, multi-institutional (26 institutions worldwide) research program  
970 dedicated to the study of childhood brain tumors. [PNOC](#) is an international consortium  
971 dedicated to bringing new therapies to children and young adults with brain tumors. We also  
972 include blood and tumor biospecimens from newly-diagnosed diffuse intrinsic pontine glioma  
973 (DIPG) patients as part of the PNOC003 clinical trial [PNOC003/NCT02274987<sup>15</sup>](https://clinicaltrials.gov/ct2/show/NCT02274987).

974 The CBTN-generated cell lines were derived from either fresh tumor tissue directly obtained  
975 from surgery performed at Children's Hospital of Philadelphia (CHOP) or from prospectively  
976 collected tumor specimens stored in Recover Cell Culture Freezing medium (cat# 12648010,  
977 Gibco). We dissociated tumor tissue using enzymatic method with papain as described<sup>14</sup>.  
978 Briefly, we washed tissue with HBSS (cat# 14175095, Gibco), and we minced and incubated the  
979 tissue with activated papain solution (cat# LS003124, SciQuest) for up to 45 minutes. We used  
980 ovomucoid solution (cat# 542000, SciQuest) to inactivate the papain, briefly treated tissue with  
981 DNase (cat# 10104159001, Roche), passed it through the 100µm cell strainer (cat# 542000,  
982 Greiner Bio-One). We initiated two cell culture conditions based on the number of cells  
983 available. For cultures utilizing the fetal bovine serum (FBS), we plated a minimum density of  
984 3×105 cells/mL in DMEM/F-12 medium (cat# D8062, Sigma) supplemented with 20% FBS (cat#  
985 SH30910.03, Hyclone), 1% GlutaMAX (cat# 35050061, Gibco), Penicillin/Streptomycin-  
986 Amphotericin B Mixture (cat# 17-745E, Lonza), and 0.2% Normocin (cat# ant-nr-2, Invivogen).  
987 For serum-free media conditions, we plated cells at minimum density of 1×106 cells/mL in  
988 DMEM/F12 medium supplemented with 1% GlutaMAX, 1X B-27 supplement minus vitamin A  
989 (cat# 12587-010, Gibco), 1x N-2 supplement (cat# 17502001, Gibco), 20 ng/ml epidermal  
990 growth factor (cat# PHG0311L, Gibco), 20 ng/mL basic fibroblast growth factor (cat# 100-18B,

991 PeproTech), 2.5µg/mL heparin (cat# H3149, Sigma), Penicillin/Streptomycin-Amphotericin B  
992 Mixture, and 0.2% Normocin.

### 993 **Nucleic acids extraction and library preparation**

#### 994 **PNOc samples**

995 The Translational Genomic Research Institute (TGEN; Phoenix, AZ) performed DNA and RNA  
996 extractions on tumor biopsies using a DNA/RNA AllPrep Kit (Qiagen, #80204). All RNA used for  
997 library prep had a minimum RIN of seven, but no QC thresholds were implemented for the DNA.  
998 For library preparation, 500 ng of nucleic acids were used as input for RNA-Seq, WXS, and  
999 targeted DNA panel (panel) sequencing. RNA library preparation was performed using the  
1000 TruSeq RNA Sample Prep Kit (Illumina, #FC-122-1001) and the exome prep was performed  
1001 using KAPA Library Preparation Kit (Roche, #KK8201) using Agilent's SureSelect Human All  
1002 Exon V5 backbone with custom probes. The targeted DNA panel developed by Ashion Analytics  
1003 (formerly known as the GEM Cancer panel) consisted of exonic probes against 541 cancer  
1004 genes. Both panel and WXS assays contained 44,000 probes across evenly spaced genomic  
1005 loci used for genome-wide copy number analysis. For the panel, additional probes tiled across  
1006 intronic regions of 22 known tumor suppressor genes and 22 genes involved in common cancer  
1007 translocations for structural analysis. All extractions and library preparations were performed  
1008 according to manufacturer's instructions.

#### 1009 **CBTN samples**

1010 Blood, tissue, and cell line DNA/RNA extractions were performed at the Biorepository Core at  
1011 CHOP. Briefly, 10-20 mg frozen tissue, 0.4-1ml of blood, or 2e6 cells pellet was used for  
1012 extractions. Tissues were lysed using a Qiagen TissueLyser II (Qiagen) with 2×30 sec at 18Hz  
1013 settings using 5 mm steel beads (cat# 69989, Qiagen). Both tissue and cell pellets processes  
1014 included a CHCl3 extraction and were run on the QIAcube automated platform (Qiagen) using  
1015 the AllPrep DNA/RNA/miRNA Universal kit (cat# 80224, Qiagen). Blood was thawed and treated  
1016 with RNase A (cat#, 19101, Qiagen); 0.4-1ml was processed using the Qiagen QIAsymphony  
1017 automated platform (Qiagen) using the QIAsymphony DSP DNA Midi Kit (cat# 937255, Qiagen).  
1018 DNA and RNA quantity and quality was assessed by PerkinElmer DropletQuant UV-VIS  
1019 spectrophotometer (PerkinElmer) and an Agilent 4200 TapeStation (Agilent, USA) for RIN and  
1020 DIN (RNA Integrity Number and DNA Integrity Number, respectively). The NantHealth  
1021 Sequencing Center, BGI at CHOP, or the Genomic Clinical Core at Sidra Medical and Research  
1022 Center performed library preparation and sequencing. BGI at CHOP and Sidra Medical and  
1023 Research Center used in house, center-specific workflows for sample preparation. At  
1024 NantHealth Sequencing Center, DNA sequencing libraries were prepared for tumor and  
1025 matched-normal DNA using the KAPA HyperPrep kit (cat# 08098107702, Roche), and tumor  
1026 RNA-Seq libraries were prepared using KAPA Stranded RNA-Seq with RiboErase kit (cat#  
1027 07962304001, Roche).

#### 1028 **Data generation**

1029 NantHealth and Sidra performed 2x150 bp WGS on paired tumor (~60X) and constitutive DNA  
1030 (~30X) samples on an Illumina X/400. BGI at CHOP performed 2x100 bp WGS sequenced at

1031 60X depth for both tumor and normal samples. NantHealth performed ribosomal-depleted whole  
1032 transcriptome stranded RNA-Seq to an average depth of 200M. BGI at CHOP performed poly-A  
1033 or ribosomal-depleted whole transcriptome stranded RNA-Seq to an average depth of 100M.  
1034 The Translational Genomic Research Institute (TGEN; Phoenix, AZ) performed paired tumor  
1035 (~200X) and constitutive whole exome sequencing (WXS) or targeted DNA panel (panel) and  
1036 poly-A selected RNA-Seq (~200M reads) for PNOC tumor samples. The panel tumor sample  
1037 was sequenced to 470X, and the normal panel sample was sequenced to 308X. PNOC 2x100  
1038 bp WXS and RNA-Seq libraries were sequenced on an Illumina HiSeq 2500.

## 1039 **DNA WGS Alignment**

1040 We used BWA-MEM<sup>74</sup> to align paired-end DNA-seq reads to the version 38 patch release 12 of  
1041 the *Homo sapiens* genome reference, obtained as a FASTA file from UCSC (see **Key**  
1042 **Resources Table**). Next, we used the Broad Institute's Best Practices<sup>75</sup> to process Binary  
1043 Alignment/Map files (BAMs) in preparation for variant discovery. We marked duplicates using  
1044 SAMBLASTER<sup>76</sup>, and we merged and sorted BAMs using Sambamba<sup>77</sup>. We used the  
1045 BaseRecalibrator submodule of the Broad's Genome Analysis Tool Kit GATK<sup>78</sup> to process  
1046 BAM files. Lastly, for normal/germline input, we used the GATK HaplotypeCaller<sup>79</sup>  
1047 submodule on the recalibrated BAM to generate a genomic variant call format (GVCF) file. This  
1048 file is used as the basis for germline calling, described in the **SNV calling for B-allele**  
1049 **Frequency (BAF) generation** section.

1050 We obtained references from the [Broad Genome References on AWS](#) bucket with a general  
1051 description of references at <https://s3.amazonaws.com/broad-references/broad-references-readme.html>.

## 1053 **Quality Control of Sequencing Data**

1054 To confirm sample matches and remove mis-matched samples from the dataset, we performed  
1055 NGSCheckMate<sup>80</sup> on matched tumor/normal CRAM files. Briefly, we processed CRAMs using  
1056 BCFtools to filter and call 20k common single nucleotide polymorphisms (SNPs) using default  
1057 parameters. We used the resulting VCFs to run NGSCheckMate. Per NGSCheckMate author  
1058 recommendations, we used  $\leq 0.61$  as a correlation coefficient cutoff at sequencing depths  $>$   
1059 10 to predict mis-matched samples. We determined RNA-Seq read strandedness by running the  
1060 infer\_experiment.py script from RNA-SeqC<sup>81</sup> on the first 200k mapped reads. We removed  
1061 any samples whose calculated strandedness did not match strandedness information provided  
1062 by the sequencing center. We required that at least 60% of RNA-Seq reads mapped to the  
1063 human reference for samples to be included in analysis.

## 1064 **Germline Variant Calling**

### 1065 **SNP calling for B-allele Frequency (BAF) generation**

1066 We performed germline haplotype calls using the GATK Joint Genotyping Workflow on individual  
1067 GVCFs from the normal sample alignment workflow. Using only SNPs, we applied the GATK  
1068 generic hard filter suggestions to the VCF, with an additional requirement of 10 reads minimum

1069 depth per SNP. We used the filtered VCF as input to Control-FREEC and CNVkit (below) to  
1070 generate B-allele frequency (BAF) files. This single-sample workflow is available in the [D3b](#)  
1071 [GitHub repository](#). References can be obtained from the [Broad Genome References on AWS](#)  
1072 bucket, and a general description of references can be found at  
1073 <https://s3.amazonaws.com/broad-references/broad-references-readme.html>.

## 1074 **Assessment of germline variant pathogenicity**

1075 For patients with hypermutant samples, we first added population frequency of germline variants  
1076 using ANNOVAR<sup>82</sup> and pathogenicity scoring from ClinVar<sup>83</sup> using SnpSift<sup>84</sup>. We then filtered  
1077 for variants with read depth  $\geq 15$ , variant allele fraction  $\geq 0.20$ , and which were observed at  $<$   
1078 0.1% allele frequency across each population in the Genome Aggregation Database (see **Key**  
1079 **Resources Table**). Finally, we retained variants in genes included in the KEGG MMR gene set  
1080 (see **Key Resources Table**), *POLE*, and/or *TP53* which were ClinVar-annotated as pathogenic  
1081 (P) or likely pathogenic (LP) with review status of  $\geq 2$  stars. All P/LP variants were manually  
1082 reviewed by an interdisciplinary team of scientists, clinicians, and genetic counselors. This  
1083 workflow is available in the [D3b GitHub repository](#).

## 1084 **Somatic Mutation Calling**

### 1085 **SNV and indel calling**

1086 For PBTA samples, we used four variant callers to call SNVs and indels from panel, WXS, and  
1087 WGS data: Strelka2<sup>85</sup>, Mutect2<sup>86</sup>, Lancet<sup>87</sup>, and VarDictJava<sup>88</sup>. VarDictJava-only calls  
1088 were not retained since  $\sim 39M$  calls with low VAF were uniquely called and may be potential  
1089 false positives. ( $\sim 1.2M$  calls were called by Mutect2, Strelka2, and Lancet and included  
1090 consensus CNV calling as described below.) We used only Strelka2, Mutect2 and Lancet  
1091 to analyze WXS samples from TCGA. TCGA samples were captured using various WXS target  
1092 capture kits and we downloaded the BED files from the GDC portal. The manufacturers  
1093 provided the input interval BED files for both panel and WXS data for PBTA samples. We  
1094 padded all panel and WXS BED files by 100 bp on each side for Strelka2, Mutect2,  
1095 and VarDictJava runs and by 400 bp for the Lancet run. For WGS calling, we utilized the  
1096 non-padded BROAD Institute interval calling list  
1097 `wgs_calling_regions.hg38.interval_list`, comprised of the full genome minus N  
1098 bases, unless otherwise noted below. We ran Strelka2<sup>85</sup> using default parameters for  
1099 canonical chromosomes (chr1-22, X,Y,M), as recommended by the authors, and we filtered the  
1100 final Strelka2 VCF for PASS variants. We ran Mutect2 from GATK according to Broad best  
1101 practices outlined from their Workflow Description Language (WDL), and we filtered the final  
1102 Mutect2 VCF for PASS variants. To manage memory issues, we ran VarDictJava<sup>88</sup> using 20  
1103 Kb interval chunks of the input BED, padded by 100 bp on each side, such that if an indel  
1104 occurred in between intervals, it would be captured. Parameters and filtering followed [BCBIO](#)  
1105 [standards](#) except that variants with a variant allele frequency (VAF)  $\geq 0.05$  (instead of  $\geq 0.10$ )  
1106 were retained. The 0.05 VAF increased the true positive rate for indels and decreased the false  
1107 positive rate for SNVs when using VarDictJava in consensus calling. We filtered the final  
1108 VarDictJava VCF for PASS variants with `TYPE=StronglySomatic`. We ran Lancet using

1109 default parameters, except for those noted below. For input intervals to `Lancet` WGS, we  
1110 created a reference BED from only the UTR, exome, and start/stop codon features of the  
1111 GENCODE 31 reference, augmented as recommended with PASS variant calls from `Strelka2`  
1112 and `Mutect2`. We then padded these intervals by 300 bp on each side during `Lancet` variant  
1113 calling. Per recommendations for WGS samples, we augmented the `Lancet` input intervals  
1114 described above with PASS variant calls from `Strelka2` and `Mutect2` as validation<sup>89</sup>.

## 1115 **VCF annotation and MAF creation**

1116 We normalized INDELS with `bcftools norm` on all PASS VCFs using the  
1117 `kfdrc_annot_vcf_sub_wf.cwl` subworkflow, release v3 (See **Table S5**). The Ensembl  
1118 Variant Effect Predictor (VEP)<sup>90</sup>, reference release 93, was used to annotate variants and  
1119 `bcftools` was used to add population allele frequency (AF) from gnomAD<sup>91</sup>. We annotated SNV  
1120 and INDEL hotspots from v2 of Memorial Sloan Kettering Cancer Center's (MSKCC) database  
1121 (See **Key Resources Table**) as well as the *TERT* promoter mutations C228T and C250T<sup>92</sup>. We  
1122 annotated SNVs by matching amino acid position (`Protein_position` column in MAF file)  
1123 with SNVs in the MSKCC database, we matched splice sites to `HGVSp_Short` values in the  
1124 MSKCC database, and we matched INDELS based on amino acid present within the range of  
1125 INDEL hotspots values in the MSKCC database. We removed non-hotspot annotated variants  
1126 with a normal depth less than or equal to 7 and/or gnomAD allele frequency (AF) greater than  
1127 0.001 as potential germline variants. We matched *TERT* promoter mutations using hg38  
1128 coordinates as indicated in ref.<sup>92</sup>: C228T occurs at 5:1295113 is annotated as existing variant  
1129 s1242535815, COSM1716563, or COSM1716558, and is 66 bp away from the TSS; C250T  
1130 occurs at Chr5:1295135, is annotated as existing variant COSM1716559, and is 88 bp away  
1131 from the TSS. We retained variants annotated as PASS or `HotSpotAllele=1` in the final set,  
1132 and we created MAFs using MSKCC's `vcf2maf` tool.

## 1133 **Gather SNV and INDEL Hotspots**

1134 We retained all variant calls from `Strelka2`, `Mutect2`, or `Lancet` that overlapped with an  
1135 SNV or INDEL hotspot in a hotspot-specific MAF file, which we then used for select analyses as  
1136 described below.

## 1137 **Consensus SNV Calling**

1138 Our SNV calling process led to separate sets of predicted mutations for each caller. We  
1139 considered mutations to describe the same change if they were identical for the following MAF  
1140 fields: `Chromosome`, `Start_Position`, `Reference_Allele`, `Allele`, and  
1141 `Tumor_Sample_Barcode`. `Strelka2` does not call multinucleotide variants (MNV), but  
1142 instead calls each component SNV as a separate mutation, so we separated MNV calls from  
1143 `Mutect2` and `Lancet` into consecutive SNVs before comparing them to `Strelka2` calls. We  
1144 examined VAFs produced by each caller and compared their overlap with each other (**Figure S2**).  
1145 `VarDictJava` calls included many variants that were not identified by other callers  
1146 (**Figure S2C**), while the other callers produced results that were relatively consistent with one  
1147 another. Many of these `VarDictJava`-specific calls were variants with low allele frequency

1148 (Figure S2B). We therefore derived consensus mutation calls as those shared among the other  
1149 three callers (Strelka2, Mutect2, and Lancet), and we did not further consider  
1150 VarDictJava calls due to concerns it called a large number of false positives. This decision  
1151 had minimal impact on results because VarDictJava also identified nearly every mutation that  
1152 the other three callers identified, in addition to many unique mutations.

## 1153 **Somatic Copy Number Variant Calling (WGS samples only)**

1154 We used Control-FREEC<sup>93,94</sup> and CNVkit<sup>95</sup> for copy number variant calls. For both  
1155 algorithms, the germline\_sex\_estimate (described below) was used as input for sample  
1156 sex and germline variant calls (above) were used as input for BAF estimation. Control-FREEC  
1157 was run on human genome reference hg38 using the optional parameters of a 0.05 coefficient  
1158 of variation, ploidy choice of 2-4, and BAF adjustment for tumor-normal pairs. Theta2<sup>96</sup> used  
1159 VarDictJava germline and somatic calls, filtered on PASS and strongly somatic, to infer tumor  
1160 purity. Theta2 purity was added as an optional parameter to CNVkit to adjust copy number  
1161 calls. CNVkit was run on human genome reference hg38 using the optional parameters of  
1162 Theta2 purity and BAF adjustment for tumor-normal pairs. We used GISTIC<sup>97</sup> on the CNVkit  
1163 and the consensus CNV segmentation files to generate gene-level copy number abundance  
1164 (Log R Ratio) as well as chromosomal arm copy number alterations using the parameters  
1165 specified in the (run-gistic analysis module in the OpenPBTA Analysis repository).

## 1166 **Consensus CNV Calling**

1167 For each caller and sample, we called CNVs based on consensus among Control-FREEC<sup>93,94</sup>,  
1168 CNVkit<sup>95</sup>, and Manta<sup>98</sup>. We specifically included CNVs called significant by Control-FREEC  
1169 (p-value < 0.01) and Manta calls that passed all filters in consensus calling. We removed  
1170 sample and consensus caller files with more than 2,500 CNVs because we expected these to  
1171 be noisy and derive poor quality samples based on cutoffs used in GISTIC<sup>97</sup>. For each sample,  
1172 we included the regions in the final consensus set: 1) regions with reciprocal overlap of 50% or  
1173 more between at least two of the callers; 2) smaller CNV regions in which more than 90% of  
1174 regions are covered by another caller. We did not include any copy number alteration called by  
1175 a single algorithm in the consensus file. We defined copy number as NA for any regions that had  
1176 a neutral call for the samples included in the consensus file. We merged CNV regions within  
1177 10,000 bp of each other with the same direction of gain or loss into single region. We filtered out  
1178 any CNVs that overlapped 50% or more with immunoglobulin, telomeric, centromeric, segment  
1179 duplicated regions, or that were shorter than 3000 bp.

## 1180 **Somatic Structural Variant Calling (WGS samples only)**

1181 We used Manta<sup>98</sup> for structural variant (SV) calls, and we limited to regions used in Strelka2.  
1182 The hg38 reference for SV calling used was limited to canonical chromosome regions. We used  
1183 AnnotSV<sup>99</sup> to annotate Manta output. All associated workflows are available in the [workflows](#)  
1184 [GitHub repository](#).

1185 **Gene Expression**

1186 **Abundance Estimation**

1187 We used `STAR`<sup>100</sup> to align paired-end RNA-seq reads, and we used the associated alignment for  
1188 all subsequent RNA analysis. We used Ensembl GENCODE 27 “Comprehensive gene  
1189 annotation” (see **Key Resources Table**) as a reference. We used `RSEM`<sup>101</sup> for both FPKM and  
1190 TPM transcript- and gene-level quantification.

1191 **Gene Expression Matrices with Unique HUGO Symbols**

1192 To enable downstream analyses, we next identified gene symbols that map to multiple Ensembl  
1193 gene identifiers (in GENCODE v27, 212 gene symbols map to 1866 Ensembl gene identifiers),  
1194 known as multi-mapped gene symbols, and ensured unique mappings (`collapse-rnaseq`  
1195 analysis module in the OpenPBTA Analysis repository). To this end, we first removed genes  
1196 with no expression from the `RSEM` abundance data by requiring an `FPKM > 0` in at least 1  
1197 sample across the PBTA cohort. We computed the mean `FPKM` across all samples per gene.  
1198 For each multi-mapped gene symbol, we chose the Ensembl identifier corresponding to the  
1199 maximum mean `FPKM`, using the assumption that the gene identifier with the highest  
1200 expression best represented the expression of the gene. After collapsing gene identifiers,  
1201 46,400 uniquely-expressed genes remained in the poly-A dataset, and 53,011 uniquely-  
1202 expressed genes remained in the stranded dataset.

1203 **Gene fusion detection**

1204 We set up `Arriba`<sup>102</sup> and `STAR-Fusion`<sup>103</sup> fusion detection tools using CWL on CAVATICA.  
1205 For both of these tools, we used aligned BAM and chimeric SAM files from `STAR` as inputs and  
1206 `GRCh38_gencode_v27` GTF for gene annotation. We ran `STAR-Fusion` with default  
1207 parameters and annotated all fusion calls with the  
1208 `GRCh38_v27_CTAT_lib_Feb092018.plugin-n-play.tar.gz` file from the `STAR-Fusion`  
1209 release. For `Arriba`, we used a blacklist file `blacklist_hg38_GRCh38_2018-11-  
1210 04.tsv.gz` from the `Arriba` release to remove recurrent fusion artifacts and transcripts  
1211 present in healthy tissue. We provided `Arriba` with strandedness information for stranded  
1212 samples, or we set it to auto-detection for poly-A samples. We used `FusionAnnotator` on  
1213 `Arriba` fusion calls to harmonize annotations with those of `STAR-Fusion`. The RNA  
1214 expression and fusion workflows can be found in the [D3b GitHub repository](#). The  
1215 `FusionAnnotator` workflow we used for this analysis can be found in the [D3b GitHub](#)  
1216 [repository](#).

## 1217 QUANTIFICATION AND STATISTICAL ANALYSIS

### 1218 Recurrently mutated genes and co-occurrence of gene mutations (interaction- 1219 plots analysis module)

1220 Using the consensus SNV calls, we identified genes that were recurrently mutated in the  
1221 OpenPBTA cohort, including nonsynonymous mutations with a VAF > 5% among the set of  
1222 independent samples. We used VEP<sup>90</sup> annotations, including "High" and "Moderate"  
1223 consequence types as defined in the R package Maftools<sup>104</sup>, to determine the set of  
1224 nonsynonymous mutations. For each gene, we then tallied the number of samples that had at  
1225 least one nonsynonymous mutation.

1226 For genes that contained nonsynonymous mutations in multiple samples, we calculated  
1227 pairwise mutation co-occurrence scores. This score was defined as  $I(-\log_{10}(P))$  where  $I$  is 1  
1228 when the odds ratio is > 1 (indicating co-occurrence), and -1 when the odds ratio is < 1  
1229 (indicating mutual exclusivity), with  $P$  defined by Fisher's Exact Test.

### 1230 Focal Copy Number Calling (focal-cn-file-preparation analysis module)

1231 We added the ploidy inferred via Control-FREEC to the consensus CNV segmentation file and  
1232 used the ploidy and copy number values to define gain and loss values broadly at the  
1233 chromosome level. We used bedtools coverage<sup>105</sup> to add cytoband status using the UCSC  
1234 cytoband file<sup>106</sup> (See **Key Resources Table**). The output status call fractions, which are values  
1235 of the loss, gain, and callable fractions of each cytoband region, were used to define dominant  
1236 status at the cytoband-level. We calculated the weighted means of each status call fraction  
1237 using band length. We used the weighted means to define the dominant status at the  
1238 chromosome arm-level.

1239 A status was considered dominant if more than half of the region was callable and the status  
1240 call fraction was greater than 0.9 for that region. We adopted this 0.9 threshold to ensure that  
1241 the dominant status fraction call was greater than the remaining status fraction calls in a region.

1242 We aimed to define focal copy number units to avoid calling adjacent genes in the same  
1243 cytoband or arm as copy number losses or gains where it would be more appropriate to call the  
1244 broader region a loss or gain. To determine the most focal units, we first considered the  
1245 dominant status calls at the chromosome arm-level. If the chromosome arm dominant status  
1246 was callable but not clearly defined as a gain or loss, we instead included the cytoband-level  
1247 status call. Similarly, if a cytoband dominant status call was callable but not clearly defined as a  
1248 gain or loss, we instead included gene-level status call. To obtain the gene-level data, we used  
1249 the IRanges package in R<sup>107</sup> to find overlaps between the segments in the consensus CNV file  
1250 and the exons in the GENCODE v27 annotation file (See **Key Resources Table**) . If the copy  
1251 number value was 0, we set the status to "deep deletion". For autosomes only, we set the status  
1252 to "amplification" when the copy number value was greater than two times the ploidy value. We  
1253 plotted genome-wide gains and losses in (**Figure S3B**) using the R package  
1254 ComplexHeatmap<sup>108</sup>.

1255 **Breakpoint Density (WGS samples only; chromosomal-instability analysis**  
1256 **module)**

1257 We defined breakpoint density as the number of breaks per genome or exome per sample. For  
1258 Manta SV calls, we filtered to retain “PASS” variants and used breakpoints from the algorithm.  
1259 For consensus CNV calls, if  $|\log_2 \text{ratio}| > \log_2(1)$ , we annotated the segment as a break. We  
1260 then calculated breakpoint density as:

1261 
$$\text{breakpoint density} = \frac{\text{N breaks}}{\text{Size in Mb of effectively surveyed genome}}$$

1262 **Chromothripsy Analysis (WGS samples only; chromothripsy analysis**  
1263 **module)**

1264 Considering only chromosomes 1-22 and X, we identified candidate chromothripsy regions in  
1265 the set of independent tumor WGS samples with ShatterSeek<sup>109</sup>, using Manta SV calls that  
1266 passed all filters and consensus CNV calls. We modified the consensus CNV data to fit  
1267 ShatterSeek input requirements as follows: we set CNV-neutral or excluded regions as the  
1268 respective sample’s ploidy value from Control-FREEC, and we then merged consecutive  
1269 segments with the same copy number value. We classified candidate chromothripsy regions as  
1270 high- or low-confidence using the statistical criteria described by the ShatterSeek authors.

1271 **Immune Profiling and Deconvolution (immune-deconv analysis module)**

1272 We used the R package `immunedeconv`<sup>110</sup> with the method `quantiSeq`<sup>111</sup> to deconvolute  
1273 various immune cell types across tumors from the PBTA cohort in the stranded and poly-A  
1274 collapsed FPKM RNA-seq datasets (immune-deconv [analysis module](#)). The `quantiSeq`  
1275 deconvolution method directly estimates absolute fractions of 10 immune cell types that  
1276 represent inferred proportions of the cell types in the mixture. Therefore, we utilized `quantiSeq`  
1277 for inter-sample, intra-sample, and inter-histology score comparisons.

1278 **Gene Set Variation Analysis (gene-set-enrichment-analysis analysis module)**

1279 We performed Gene Set Variation Analysis (GSVA) on collapsed, log2-transformed RSEM  
1280 FPKM data using the `GSVA` Bioconductor package<sup>112</sup>. We specified the parameter  
1281 `mx.diff=TRUE` to obtain Gaussian-distributed scores for each of the MSigDB hallmark gene  
1282 sets<sup>113</sup>. We compared GSVA scores among histology groups using ANOVA and subsequent  
1283 Tukey tests; p-values were Bonferroni-corrected for multiple hypothesis testing. We plotted  
1284 scores by cancer group using the `ComplexHeatmap` R package ([Figure 5B](#))<sup>108</sup>.

1285 **Transcriptomic Dimension Reduction (transcriptomic-dimension-reduction**  
1286 **analysis module)**

1287 We applied Uniform Manifold Approximation and Projection (UMAP)<sup>114</sup> to log2-transformed  
1288 FPKM data using the `umap` R package (See **Key Resources Table**). We set the number of  
1289 neighbors to 15.

1290 **Fusion prioritization (fusion\_filtering analysis module)**

1291 We performed artifact filtering and additional annotation on fusion calls to prioritize putative  
1292 oncogenic fusions. Briefly, we considered all in-frame and frameshift fusion calls with at least  
1293 one junction read and at least one gene partner expressed (TPM > 1) to be true calls. If a fusion  
1294 call had a large number of spanning fragment reads compared to junction reads (spanning  
1295 fragment minus junction read greater than ten), we removed these calls as potential false  
1296 positives. We prioritized a union of fusion calls as true calls if the fused genes were detected by  
1297 both callers, the same fusion was recurrent within a broad histology grouping (> 2 samples), or  
1298 the fusion was specific to the given broad histology. If either 5' or 3' genes fused to more than  
1299 five different genes within a sample, we removed these calls as potential false positives. We  
1300 annotated putative driver fusions and prioritized fusions based on partners containing known  
1301 [kinases](#), [oncogenes](#), [tumor suppressors](#), curated transcription factors<sup>115</sup>, [COSMIC genes](#),  
1302 and/or known [TCGA fusions](#) from curated references. Based on pediatric cancer literature  
1303 review, we added *MYBL1*<sup>116</sup>, *SNCAIP*<sup>117</sup>, *FOXR2*<sup>118</sup>, *TTYH1*<sup>119</sup>, and *TERT*<sup>120-123</sup> to the oncogene  
1304 list, and we added *BCOR*<sup>118</sup> and *QKI*<sup>124</sup> to the tumor suppressor gene list.

1305 **Oncoprint figure generation (oncoprint-landscape analysis module)**

1306 We used `Maftools`<sup>104</sup> to generate oncoprints depicting the frequencies of canonical somatic  
1307 gene mutations, CNVs, and fusions for the top 20 genes mutated across primary tumors within  
1308 broad histologies of the OpenPBTA dataset. We collated canonical genes from the literature for  
1309 low-grade astrocytic tumors<sup>25</sup>, embryonal tumors<sup>26,28,29,125,126</sup>, diffuse astrocytic and  
1310 oligodendroglial tumors<sup>15,22,30,31</sup>, and other tumors: ependymal tumors, craniopharyngiomas,  
1311 neuronal-glial mixed tumors, histiocytic tumors, chordoma, meningioma, and choroid plexus  
1312 tumors<sup>127-136</sup>.

1313 **Mutational Signatures (mutational-signatures analysis module)**

1314 We obtained weights (i.e., exposures) for signature sets using the `deconstructSigs` R  
1315 package function `whichSignatures()`<sup>137</sup> from consensus SNVs with the  
1316 `BSgenome.Hsapiens.UCSC.hg38` annotations (see **Key Resources Table**). Specifically, we  
1317 estimated signature weights across samples for eight signatures previously identified in the  
1318 Signal reference set of signatures ("RefSig") as associated with adult central nervous system  
1319 (CNS) tumors<sup>36</sup>. These eight RefSig signatures are 1, 3, 8, 11, 18, 19, N6, and MMR2. Weights  
1320 for signatures fall in the range zero to one inclusive. `deconstructSigs` estimates the weights  
1321 for each signature across samples and allows for a proportion of unassigned weights referred to  
1322 as "Other" in the text. These results do not include signatures with small contributions;  
1323 `deconstructSigs` drops signature weights that are less than 6%<sup>137</sup>. We plotted mutational

1324 signatures for patients with hypermutant tumors (**Figure 4E**) using the R package  
1325 ComplexHeatmap<sup>108</sup>.

## 1326 **Tumor Mutation Burden (snv-callers analysis module)**

1327 We consider tumor mutation burden (TMB) to be the number of consensus SNVs per effectively  
1328 surveyed base of the genome. We considered base pairs to be effectively surveyed if they were  
1329 in the intersection of the genomic ranges considered by the callers used to generate the  
1330 consensus and where appropriate, regions of interest, such as coding sequences. We  
1331 calculated TMB as:

1332 
$$TMB = \frac{\text{\# of coding sequence SNVs}}{\text{Size in Mb of effectively surveyed genome}}$$

1333 We used the total number coding sequence consensus SNVs for the numerator and the size of  
1334 the intersection of the regions considered by Strelka2 and Mutect2 with coding regions  
1335 (CDS from GENCODE v27 annotation, see **Key Resources Table**) as the denominator.

## 1336 **Clinical Data Harmonization**

### 1337 **WHO Classification of Disease Types**

1338 **Table S1** contains a README, along with sample technical, clinical, and additional metadata  
1339 used for this study.

### 1340 **Molecular Subtyping**

1341 We performed molecular subtyping on tumors in the OpenPBTA to the extent possible. The  
1342 molecular\_subtype field in pbta-histologies.tsv contains molecular subtypes for  
1343 tumor types selected from pathology\_diagnosis and  
1344 pathology\_free\_text\_diagnosis fields as described below, following World Health  
1345 Organization 2016 classification criteria<sup>21</sup>.

1346 Medulloblastoma (MB) subtypes SHH, WNT, Group 3, and Group 4 were predicted using the  
1347 consensus of two RNA expression classifiers: Medulloblastoma<sup>61</sup> and MM2S<sup>60</sup> on the  
1348 RSEM FPKM data (molecular-subtyping-MB analysis module).

1349 High-grade glioma (HGG) subtypes were derived (molecular-subtyping-HGG analysis  
1350 module) using the following criteria:

- 1351 1. If any sample contained an *H3F3A* p.K28M, *HIST1H3B* p.K28M, *HIST1H3C* p.K28M, or  
1352 *HIST2H3C* p.K28M mutation and no *BRAF* p.V600E mutation, it was subtyped as DMG,  
1353 H3 K28.
- 1354 2. If any sample contained an *HIST1H3B* p.K28M, *HIST1H3C* p.K28M, or *HIST2H3C*  
1355 p.K28M mutation and a *BRAF* p.V600E mutation, it was subtyped as DMG, H3 K28,  
1356 BRAF V600E.

1357 3. If any sample contained an *H3F3A* p.G35V or p.G35R mutation, it was subtyped as<sup>HGG</sup>,  
1358 H3 G35.

1359 4. If any high-grade glioma sample contained an *IDH1* p.R132 mutation, it was subtyped as  
1360 HGG, IDH.

1361 5. If a sample was initially classified as HGG, had no defining histone mutations, and a  
1362 *BRAF* p.V600E mutation, it was subtyped as<sup>BRAF</sup> V600E.

1363 6. All other high-grade glioma samples that did not meet any of these criteria were  
1364 subtyped as HGG, H3 wildtype.

1365 Embryonal tumors were included in non-MB and non-ATRT embryonal tumor subtyping  
1366 (molecular-subtyping-embryonal analysis module) if they met any of the following  
1367 criteria:

1368 1. A *TTYH1* (5' partner) fusion was detected.

1369 2. A *MN1* (5' partner) fusion was detected, with the exception of<sup>MN1::PATZ1</sup> since it is an  
1370 entity separate of CNS HGNET-MN1 tumors<sup>138</sup>.

1371 3. Pathology diagnoses included “Supratentorial or Spinal Cord PNET” or “Embryonal  
1372 Tumor with Multilayered Rosettes”.

1373 4. A pathology diagnosis of “Neuroblastoma”, where the tumor was not indicated to be  
1374 peripheral or metastatic and was located in the CNS.

1375 5. Any sample with “embryonal tumor with multilayer rosettes, ros (who grade iv)”,  
1376 “embryonal tumor, nos, congenital type”, “ependymoblastoma” or “medulloepithelioma”  
1377 in pathology free text.

1378 Non-MB and non-ATRT embryonal tumors identified with the above criteria were further  
1379 subtyped (molecular-subtyping-embryonal analysis module) using the criteria below<sup>139–</sup>  
1380 [142](#).

1381 1. Any RNA-seq biospecimen with *LIN28A* overexpression, plus a *TYH1* fusion (5' partner)  
1382 with a gene adjacent or within the C19MC miRNA cluster and/or copy number  
1383 amplification of the C19MC region was subtyped as<sup>ETMR</sup>, C19MC-altered  
1384 (Embryonal tumor with multilayer rosettes, chromosome 19 miRNA cluster altered)<sup>119,143</sup>.

1385 2. Any RNA-seq biospecimen with *LIN28A* overexpression, a *TTYH1* fusion (5' partner)  
1386 with a gene adjacent or within the C19MC miRNA cluster but no evidence of copy  
1387 number amplification of the C19MC region was subtyped as<sup>ETMR</sup>, NOS (Embryonal  
1388 tumor with multilayer rosettes, not otherwise specified)<sup>119,143</sup>.

1389 3. Any RNA-seq biospecimen with a fusion having a 5' *MN1* and 3' *BEND2* or *CXXC5*  
1390 partner were subtyped as<sup>CNS HGNET-MN1</sup> [Central nervous system (CNS) high-grade  
1391 neuroepithelial tumor with *MN1* alteration].

1392 4. Non-MB and non-ATRT embryonal tumors with internal tandem duplication (as defined  
1393 in<sup>144</sup>) of *BCOR* were subtyped as<sup>CNS HGNET-BCOR</sup> (CNS high-grade neuroepithelial  
1394 tumor with *BCOR* alteration).

1395 5. Non-MB and non-ATRT embryonal tumors with over-expression and/or gene fusions in  
1396 *FOXR2* were subtyped as CNS NB-FOXR2 (CNS neuroblastoma with *FOXR2*  
1397 activation).

1398 6. Non-MB and non-ATRT embryonal tumors with *C/C::NUTM1* or other *C/C* fusions, were  
1399 subtyped as CNS EFT-CIC (CNS Ewing sarcoma family tumor with *C/C* alteration)<sup>118</sup>

1400 7. Non-MB and non-ATRT embryonal tumors that did not fit any of the above categories  
1401 were subtyped as CNS Embryonal, NOS (CNS Embryonal tumor, not otherwise  
1402 specified).

1403 Neurocytoma subtypes central neurocytoma (CNC) and extraventricular neurocytoma (EVN)  
1404 were assigned (molecular-subtyping-neurocytoma analysis module) based on the  
1405 primary site of the tumor<sup>145</sup>. If the tumor's primary site was "ventricles," we assigned the subtype  
1406 as CNC; otherwise, we assigned the subtype as EVN.

1407 Craniopharyngiomas (CRANIO) were subtyped (molecular-subtyping-CRANIO analysis  
1408 module) into adamantinomatous (CRANIO, ADAM), papillary (CRANIO, PAP) or undetermined  
1409 (CRANIO, To be classified) based on the following criteria<sup>146,147</sup>:

1410 1. Craniopharyngiomas from patients over 40 years old with a *BRAF* p.V600E mutation  
1411 were subtyped as CRANIO, PAP.

1412 2. Craniopharyngiomas from patients younger than 40 years old with mutations in exon 3 of  
1413 *CTNNB1* were subtyped as CRANIO, ADAM.

1414 3. Craniopharyngiomas that did not fall into the above two categories were subtyped as  
1415 CRANIO, To be classified.

1416 A molecular subtype of EWS was assigned to any tumor with a *EWSR1* fusion or with a  
1417 pathology\_diagnosis of Ewings Sarcoma (molecular-subtyping-EWS analysis  
1418 module).

1419 Low-grade gliomas (LGG) or glialneuronal tumors (GNT) were subtyped (molecular-  
1420 subtyping-LGAT analysis module), based on SNV, fusion and CNV status based on<sup>23</sup>, and as  
1421 described below.

1422 1. If a sample contained a *NF1* somatic mutation, either nonsense or missense, it was  
1423 subtyped as LGG, NF1-somatic.

1424 2. If a sample contained *NF1* germline mutation, as indicated by a patient having the  
1425 neurofibromatosis cancer predisposition, it was subtyped as LGG, NF1-germline.

1426 3. If a sample contained the *IDH* p.R132 mutation, it was subtyped as LGG, IDH.

1427 4. If a sample contained a histone p.K28M mutation in either *H3F3A*, *H3F3B*, *HIST1H3B*,  
1428 *HIST1H3C*, or *HIST2H3C*, or if it contained a p.G35R or p.G35V mutation in *H3F3A*, it  
1429 was subtyped as LGG, H3.

1430 5. If a sample contained *BRAF* p.V600E or any other non-canonical *BRAF* mutations in the  
1431 kinase (PK\_Tyr\_Ser-Thr) domain PF07714 (see **Key Resources Table**), it was  
1432 subtyped as LGG, BRAF V600E.

1433 6. If a sample contained KIAA1549::BRAF fusion, it was subtyped as LGG,  
1434 KIAA1549::BRAF.

1435 7. If a sample contained SNV or indel in either KRAS, NRAS, HRAS, MAP2K1, MAP2K2,  
1436 MAP2K1, ARAF, RAF1, or non-kinase domain of BRAF, or if it contained RAF1 fusion,  
1437 or BRAF fusion that was not KIAA1549::BRAF, it was subtyped as LGG, other  
1438 MAPK.

1439 8. If a sample contained SNV in either MET, KIT or PDGFRA, or if it contained fusion in  
1440 ALK, ROS1, NTRK1, NTRK2, NTRK3 or PDGFRA, it was subtyped as LGG, RTK.

1441 9. If a sample contained FGFR1 p.N546K, p.K656E, p.N577, or p. K687 hotspot mutations,  
1442 or tyrosine kinase domain tandem duplication (See **Key Resources Table**), or FGFR1  
1443 or FGFR2 fusions, it was subtyped as LGG, FGFR.

1444 10. If a sample contained MYB or MYBL1 fusion, it was subtyped as LGG, MYB/MYBL1.

1445 11. If a sample contained focal CDKN2A and/or CDKN2B deletion, it was subtyped as LGG,  
1446 CDKN2A/B.

1447 For LGG tumors that did not have any of the above molecular alterations, if both RNA and DNA  
1448 samples were available, it was subtyped as LGG, wildtype. Otherwise, if either RNA or DNA  
1449 sample was unavailable, it was subtyped as LGG, To be classified.

1450 If pathology diagnosis was Subependymal Giant Cell Astrocytoma (SEGA), the LGG  
1451 portion of molecular subtype was recoded to SEGA.

1452 Lastly, for all LGG- and GNT- subtyped samples, if the tumors were glialneuronal in origin,  
1453 based on pathology\_free\_text\_diagnosis entries of desmoplastic  
1454 infantile,desmoplastic infantile ganglioglioma, desmoplastic infantile  
1455 astrocytoma or glioneuronal, each was recoded as follows: If pathology diagnosis is Low-  
1456 grade glioma/astrocytoma (WHO grade I/II) or Ganglioglioma, the LGG portion of  
1457 the molecular subtype was recoded to GNT.

1458 Ependymomas (EPN) were subtyped (molecular-subtyping-EPN analysis module) into  
1459 EPN, ST RELA, EPN, ST YAP1, EPN, PF A and EPN, PF B based on evidence for these  
1460 molecular subgroups as described in Pajtler et al.<sup>128</sup>. Briefly, fusion, CNV and gene expression  
1461 data were used to subtype EPN as follows:

1462 1. Any tumor with fusions containing RELA as fusion partner, e.g., C11orf95::RELA,  
1463 LTBP3::RELA, was subtyped as EPN, ST RELA.

1464 2. Any tumor with fusions containing YAP1 as fusion partner, such as C11orf95::YAP1,  
1465 YAP1::MAMLD1 and YAP1::FAM118B, was subtyped as EPN, ST YAP1.

1466 3. Any tumor with the following molecular characterization would be subtyped as EPN, PF  
1467 A:  
1468 • CXorf67 expression z-score of over 3  
1469 • TKTL1 expression z-score of over 3 and 1q gain

1470 4. Any tumor with the following molecular characterization would be subtyped as EPN, PF  
1471 B:

1472     • *GPBP17* expression z-score of over 3 and loss of 6q or 6p  
1473     • *IFT46* expression z-score of over 3 and loss of 6q or 6p

1474     Any tumor with the above molecular characteristics would be exclusively subtyped to the  
1475     designated group.

1476     For all other remaining EPN tumors without above molecular characteristics, they would be  
1477     subtyped to EPN, ST RELA and EPN, ST YAP1 in a non-exclusive way (e.g., a tumor could  
1478     have both EPN, ST RELA and EPN, ST YAP1 subtypes) if any of the following alterations  
1479     were present.

1480     1. Any tumor with the following alterations was assigned EPN, ST RELA:  
1481         • *PTEN* :: *TAS2R1* fusion  
1482         • chromosome 9 arm (9p or 9q) loss  
1483         • *RELA* expression z-score of over 3  
1484         • *L1CAM* expression z-score of over 3  
1485     2. Any tumor with the following alterations was assigned EPN, ST YAP1:  
1486         • *C11orf95* :: *MAML2* fusion  
1487         • chromosome 11 short arm (11p) loss  
1488         • chromosome 11 long arm (11q) gain  
1489         • *ARL4D* expression z-score of over 3  
1490         • *CLDN1* expression z-score of over 3

1491     After all relevant tumor samples were subtyped by the above molecular subtyping modules, the  
1492     results from these modules, along with other clinical information (such as pathology diagnosis  
1493     free text), were compiled in the molecular-subtyping-pathology module and integrated  
1494     into the OpenPBTA data in the molecular-subtyping-integrate module.

## 1495 **TP53 Alteration Annotation (tp53\_nf1\_score analysis module)**

1496     We annotated *TP53* altered HGG samples as either *TP53* lost or *TP53* activated and  
1497     integrated this within the molecular subtype. To this end, we applied a *TP53* inactivation  
1498     classifier originally trained on TCGA pan-cancer data<sup>38</sup> to the matched RNA expression data for  
1499     each sample. Along with the *TP53* classifier scores, we collectively used consensus SNV and  
1500     CNV, SV, and reference databases that list *TP53* hotspot mutations<sup>148,149</sup> and functional  
1501     domains<sup>150</sup> to determine *TP53* alteration status for each sample. We adopted the following rules  
1502     for calling either *TP53* lost or *TP53* activated:

- 1503         1. If a sample had either of the two well-characterized *TP53* gain-of-function mutations,  
1504             p.R273C or p.R248W<sup>39</sup>, we assigned *TP53* activated status.
- 1505         2. Samples were annotated as *TP53* lost if they contained i) a *TP53* hotspot mutation as  
1506             defined by IARC *TP53* database or the MSKCC cancer hotspots database<sup>148,149</sup> (see  
1507             also, **Key Resources Table**), ii) two *TP53* alterations, including SNV, CNV or SV,  
1508             indicative of probable bi-allelic alterations; iii) one *TP53* somatic alteration, including

1509 SNV, CNV, or SV or a germline *TP53* mutation indicated by the diagnosis of Li-Fraumeni  
1510 syndrome (LFS)<sup>151</sup>, or iv) one germline *TP53* mutation indicated by LFS and the *TP53*  
1511 classifier score for matched RNA-Seq was greater than 0.5.

## 1512 **Prediction of participants' genetic sex**

1513 Participant metadata included a reported gender. We used WGS germline data, in concert with  
1514 the reported gender, to predict participant genetic sex so that we could identify sexually  
1515 dimorphic outcomes. This analysis may also indicate samples that may have been  
1516 contaminated. We used the `idxstats` utility from `SAMtools`<sup>152</sup> to calculate read lengths, the  
1517 number of mapped reads, and the corresponding chromosomal location for reads to the X and Y  
1518 chromosomes. We used the fraction of total normalized X and Y chromosome reads that were  
1519 attributed to the Y chromosome as a summary statistic. We manually reviewed this statistic in  
1520 the context of reported gender and determined that a threshold of less than 0.2 clearly  
1521 delineated female samples. We marked fractions greater than 0.4 as predicted males, and we  
1522 marked samples with values in the inclusive range 0.2-0.4 as unknown. We performed this  
1523 analysis through [CWL](#) on CAVATICA. We added resulting calls to the histologies file under the  
1524 column header `germline_sex_estimate`.

## 1525 **Selection of independent samples (independent-samples analysis module)**

1526 Certain analyses required that we select only a single representative specimen for each  
1527 individual. In these cases, we identified a single specimen by prioritizing primary tumors and  
1528 those with whole-genome sequencing available. If this filtering still resulted in multiple  
1529 specimens, we randomly selected a single specimen from the remaining set.

## 1530 **Quantification of Telomerase Activity using Gene Expression Data** 1531 **(telomerase-activity-prediction analysis module)**

1532 We predicted telomerase activity of tumor samples using the recently developed `EXTEND`  
1533 method<sup>41</sup>. Briefly, `EXTEND` estimates telomerase activity based on the expression of a 13-gene  
1534 signature. We derived this signature by comparing telomerase-positive tumors and tumors with  
1535 activated alternative lengthening of telomeres pathway, a group presumably negative of  
1536 telomerase activity.

## 1537 **Survival models (survival-analysis analysis module)**

1538 We calculated overall survival (OS) as days since initial diagnosis and performed several  
1539 survival analyses on the OpenPBTA cohort using the `survival` [R package](#). We performed  
1540 survival analysis for patients by HGG subtype using the Kaplan-Meier estimator<sup>153</sup> and a log-  
1541 rank test (Mantel-Cox test)<sup>154</sup> on the different HGG subtypes. Next, we used multivariate Cox  
1542 (proportional hazards) regression analysis<sup>155</sup> to model the following: a) `tp53` scores +  
1543 telomerase scores + extent of tumor resection + LGG group + HGG group,  
1544 in which `tp53` scores and telomerase scores are numeric, extent of tumor  
1545 resection is categorical, and LGG group and HGG group are binary variables indicating

1546 whether the sample is in either broad histology grouping, b) tp53 scores + telomerase  
1547 scores + extent of tumor resection for each cancer\_group with an N>=3  
1548 deceased patients (DIPG, DMG, HGG, MB, and EPN), and c) quantiseq cell type  
1549 fractions + CD274 expression + extent of tumor resection for each  
1550 cancer\_group with an N>=3 deceased patients (DIPG, DMG, HGG, MB, and EPN), in which  
1551 quantiseq cell type fractions and CD274 expression are numeric.

## 1552 KEY RESOURCES TABLE

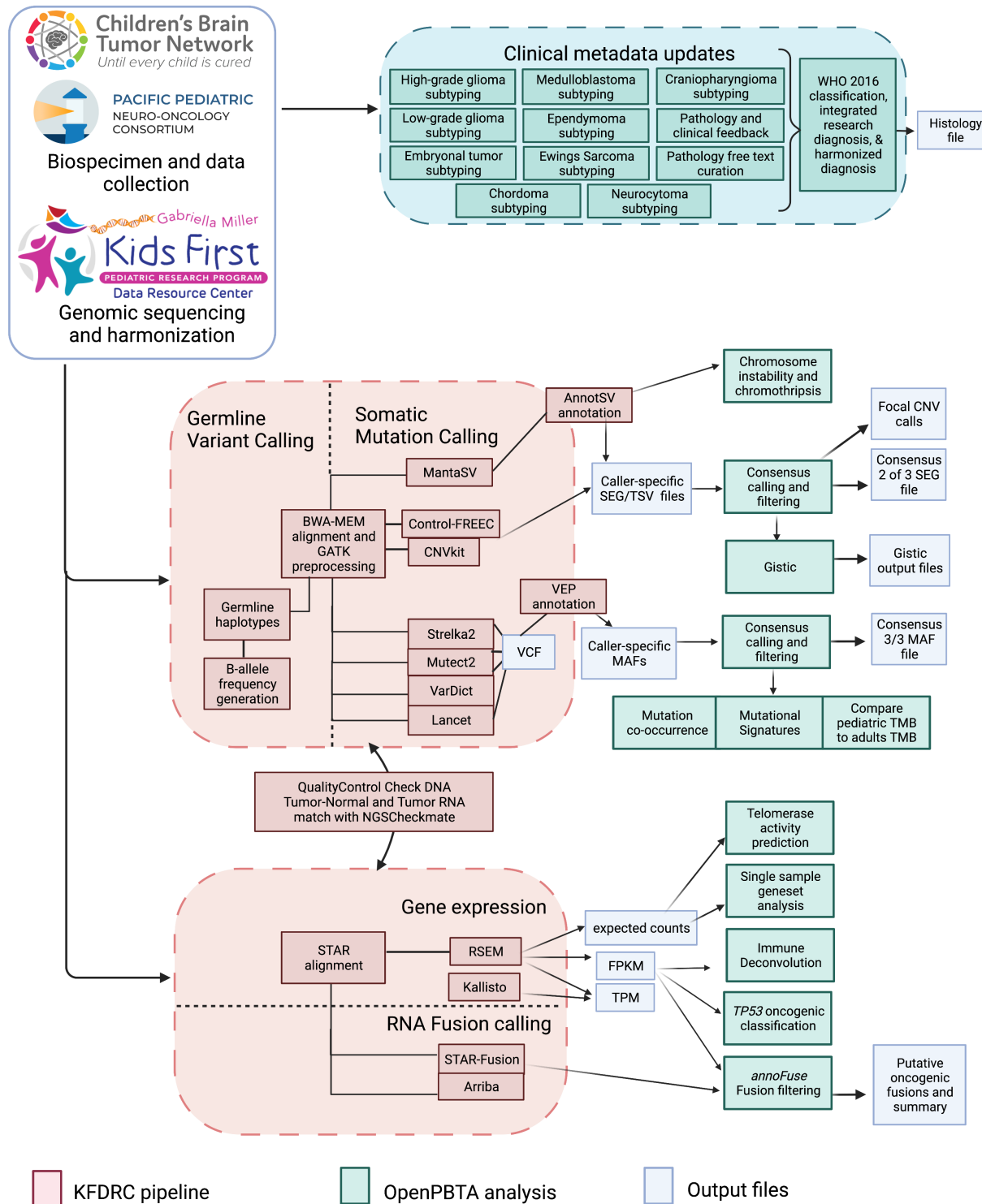
| REAGENT or RESOURCE                     | SOURCE          | IDENTIFIER  |
|---|-----------------|-------------|
| Critical commercial assays              |                 |             |
| Recover Cell Culture Freezing media     | Gibco           | 12648010    |
| Hank's Balanced Salt Solution (HBSS)    | Gibco           | 14175095    |
| Papain                                  | SciQuest        | LS003124    |
| Ovomucoid                               | SciQuest        | 542000      |
| DNase                                   | Roche           | 10104159001 |
| 100µm cell strainer                     | Greiner Bio-One | 542000      |
| DMEM/F-12 medium                        | Sigma           | D8062       |
| Fetal Bovine Serum (FBS)                | Hyclone         | SH30910.03  |
| GlutaMAX                                | Gibco           | 35050061    |
| Penicillin/Streptomycin -Amphotericin B | Lonza           | 17-745E     |
| Normocin                                | Invivogen       | ant-nr-2    |
| B-27 supplement minus vitamin A         | Gibco           | 12587-010   |
| N-2 supplement                          | Gibco           | 17502001    |
| Epidermal growth factor                 | Gibco           | PHG0311L    |
| Basic fibroblast growth factor          | PeproTech       | 100-18B     |
| Heparin                                 | Sigma           | H3149       |
| DNA/RNA AllPrep Kit                     | Qiagen          | 80204       |
| TruSeq RNA Sample Prep Kit              | Illumina        | FC-122-1001 |
| KAPA Library Preparation Kit            | Roche           | KK8201      |

| REAGENT or RESOURCE                           | SOURCE                                       | IDENTIFIER  |
|---|--|---|
| AllPrep DNA/RNA/miRNA Universal kit           | Qiagen                                       | 80224   |
| RNase A                                       | Qiagen                                       | 19101   |
| QIAAsymphony DSP DNA Midi Kit                 | Qiagen                                       | 937255  |
| KAPA HyperPrep kit                            | Roche  | 08098107702   |
| RiboErase kit                                 | Roche  | 07962304001   |
| Raw and harmonized WGS, WXS, Panel, RNA-Seq   | KidsFirst Data Resource Center, this project | <a href="#">73</a>  |
| Merged summary files                          | this project                                 | <a href="https://cavatica.sbggenomics.com/u/cavatica/openpbta">https://cavatica.sbggenomics.com/u/cavatica/openpbta</a>                         |
| Merged summary files and downstream analyses  | this project                                 | <a href="https://github.com/AlexsLemonade/OpenPBTA-analysis/">https://github.com/AlexsLemonade/OpenPBTA-analysis/</a>                           |
| Processed data                                | this project                                 | <a href="https://pedcobiportal.kidsfirstdrc.org/study/summary?id=openpbta">https://pedcobiportal.kidsfirstdrc.org/study/summary?id=openpbta</a> |
| Experimental models: Cell lines               |  |   |
| CBTN pediatric brain tumor-derived cell lines | <a href="#">14</a>                           | See <b>Table S1</b> for identifiers   |
| Software and algorithms                       |  |   |
| Data processing and analysis software         | Multiple                                     | See <b>Table S5</b> for identifiers   |
| OpenPBTA workflows repository                 | this project                                 | <a href="#">156</a>   |
| OpenPBTA analysis repository                  | this project                                 | <a href="#">157</a>   |
| OpenPBTA manuscript repository                | this project                                 |   |
|   |  |   |
| Other   |  |   |
| TCGA WXS dataset                              | National Institutes of Health The            | dbGAP phs000178.v11.p8  |

| REAGENT or RESOURCE                     | SOURCE                      | IDENTIFIER  |
|---|-----------------------------|---|
|   | Cancer Genome Atlas (TCGA)  |   |
| Cancer hotspots                         | MSKCC                       | <a href="https://www.cancerhotspots.org/#/download (v2)">https://www.cancerhotspots.org/#/download (v2)</a>   |
| Reference genomes                       | Broad                       | <a href="https://s3.console.aws.amazon.com/s3/buckets/broad-references/hg38/v0/">https://s3.console.aws.amazon.com/s3/buckets/broad-references/hg38/v0/</a>   |
| Reference genome hg38, patch release 12 | UCSC                        | <a href="http://hgdownload.soe.ucsc.edu/goldenPath/hg38/bigZips/">http://hgdownload.soe.ucsc.edu/goldenPath/hg38/bigZips/</a>   |
| Human Cytoband file                     | UCSC                        | <a href="http://hgdownload.cse.ucsc.edu/goldenpath/hg38/database/cytoBand.txt.gz">http://hgdownload.cse.ucsc.edu/goldenpath/hg38/database/cytoBand.txt.gz</a>   |
| CDS from GENCODE v27 annotation         | GENCODE                     | <a href="https://www.gencodegenes.org/human/release_27.html">https://www.gencodegenes.org/human/release_27.html</a>   |
| PFAM domains and locations              | UCSC                        | <a href="http://hgdownload.soe.ucsc.edu/goldenPath/hg38/database/pfamDes.txt.gz">http://hgdownload.soe.ucsc.edu/goldenPath/hg38/database/pfamDes.txt.gz</a> ; <a href="https://pfam.xfam.org/family/PF07714">https://pfam.xfam.org/family/PF07714</a> |
| BSgenome.Hsapiens.UCSC.hg38 annotations | Bioconductor                | <a href="https://bioconductor.org/packages/release/data/annotation/html/BSgenome.Hsapiens.UCSC.hg38.html">https://bioconductor.org/packages/release/data/annotation/html/BSgenome.Hsapiens.UCSC.hg38.html</a>   |
| gnomAD v2.1.1 (exome and genome)        | Genome Aggregation Database | <a href="https://gnomad.broadinstitute.org/downloads#v2-liftover-variants">https://gnomad.broadinstitute.org/downloads#v2-liftover-variants</a>   |
| KEGG MMR gene set v7.5.1                | BROAD Institute             | <a href="https://www.gsea-msigdb.org/gsea/msigdb/download_geneset.jsp?geneSetName=KEGG_MISMATCH_REPAIR">https://www.gsea-msigdb.org/gsea/msigdb/download_geneset.jsp?geneSetName=KEGG_MISMATCH_REPAIR</a>   |
| ClinVar Database (2022-05-07)           | NCBI                        | <a href="https://ftp.ncbi.nlm.nih.gov/pub/clinvar/vcf_GRCh38/archive_2.0/2022/clinvar_20220507.vcf.gz">https://ftp.ncbi.nlm.nih.gov/pub/clinvar/vcf_GRCh38/archive_2.0/2022/clinvar_20220507.vcf.gz</a>   |

1553

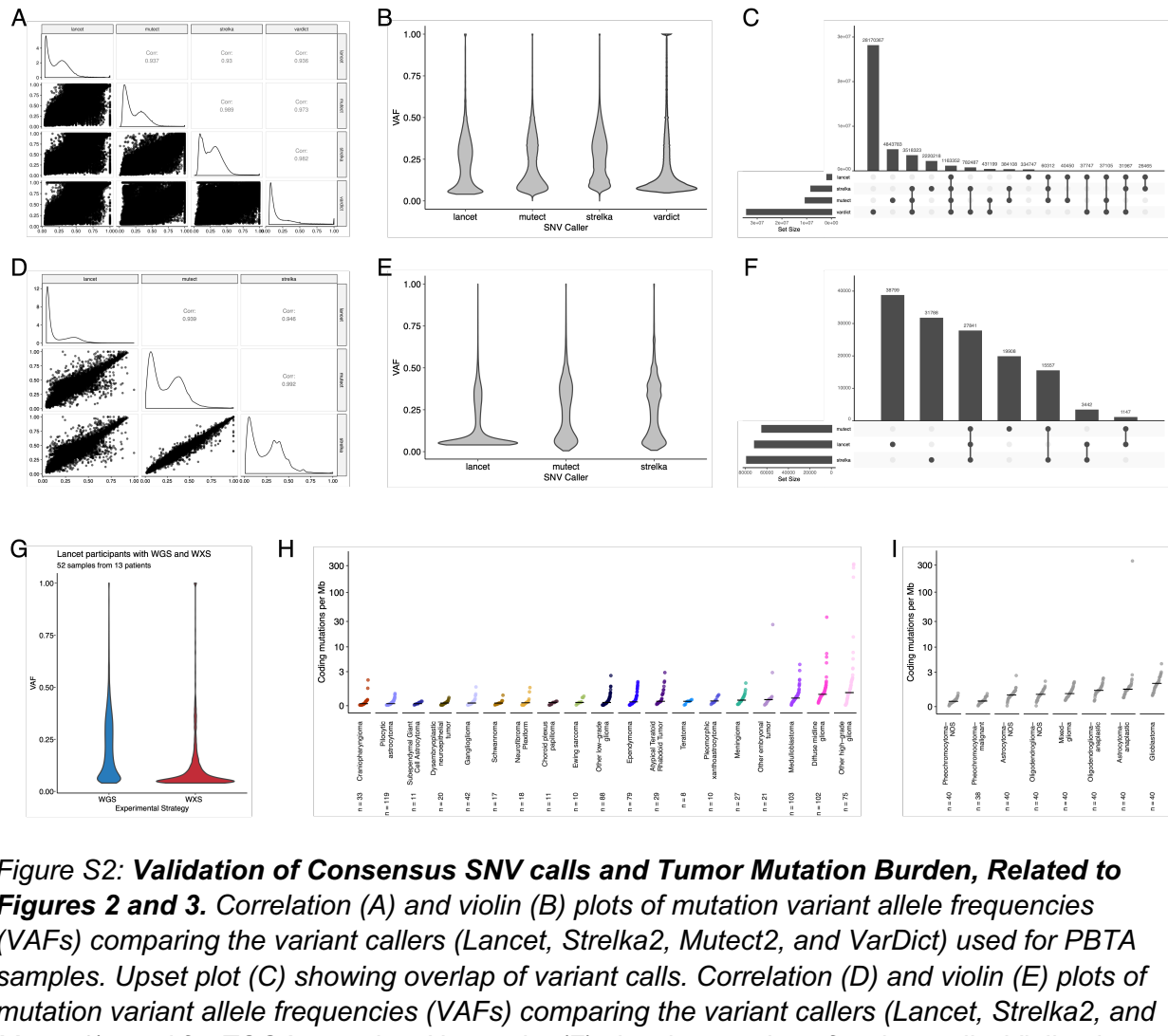
## Supplemental Information Titles and Legends



1554

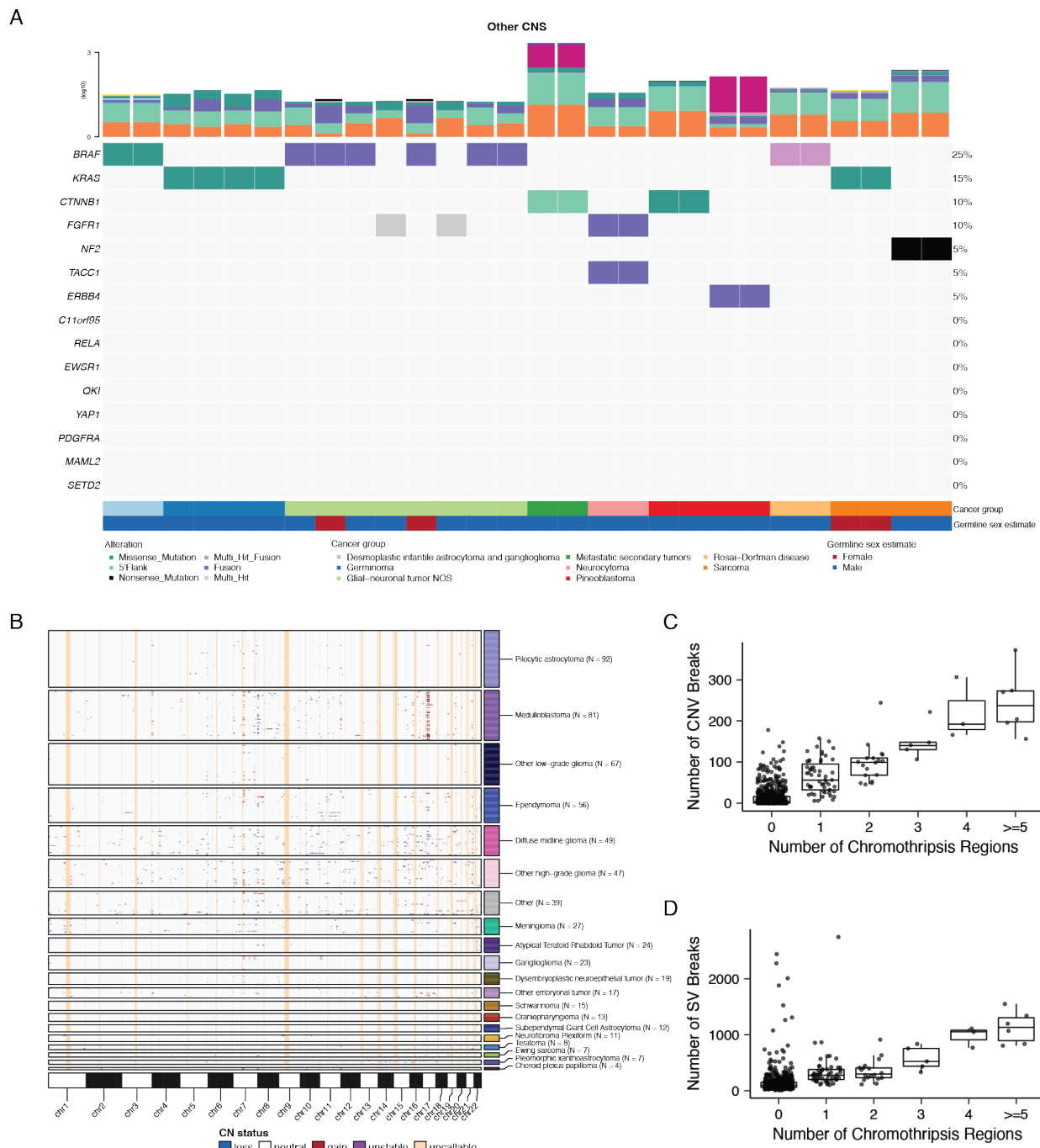
1555 **Figure S1: OpenPBTA Project Workflow, Related to Figure 1.** Biospecimens and data were  
1556 collected by CBTN and PNOC. Genomic sequencing and harmonization (orange boxes) were

1557 performed by the Kids First Data Resource Center (KFDRC). Analyses in the green boxes were  
1558 performed by contributors of the OpenPBTA project. Output files are denoted in blue. Figure  
1559 created with [BioRender.com](https://biorender.com).



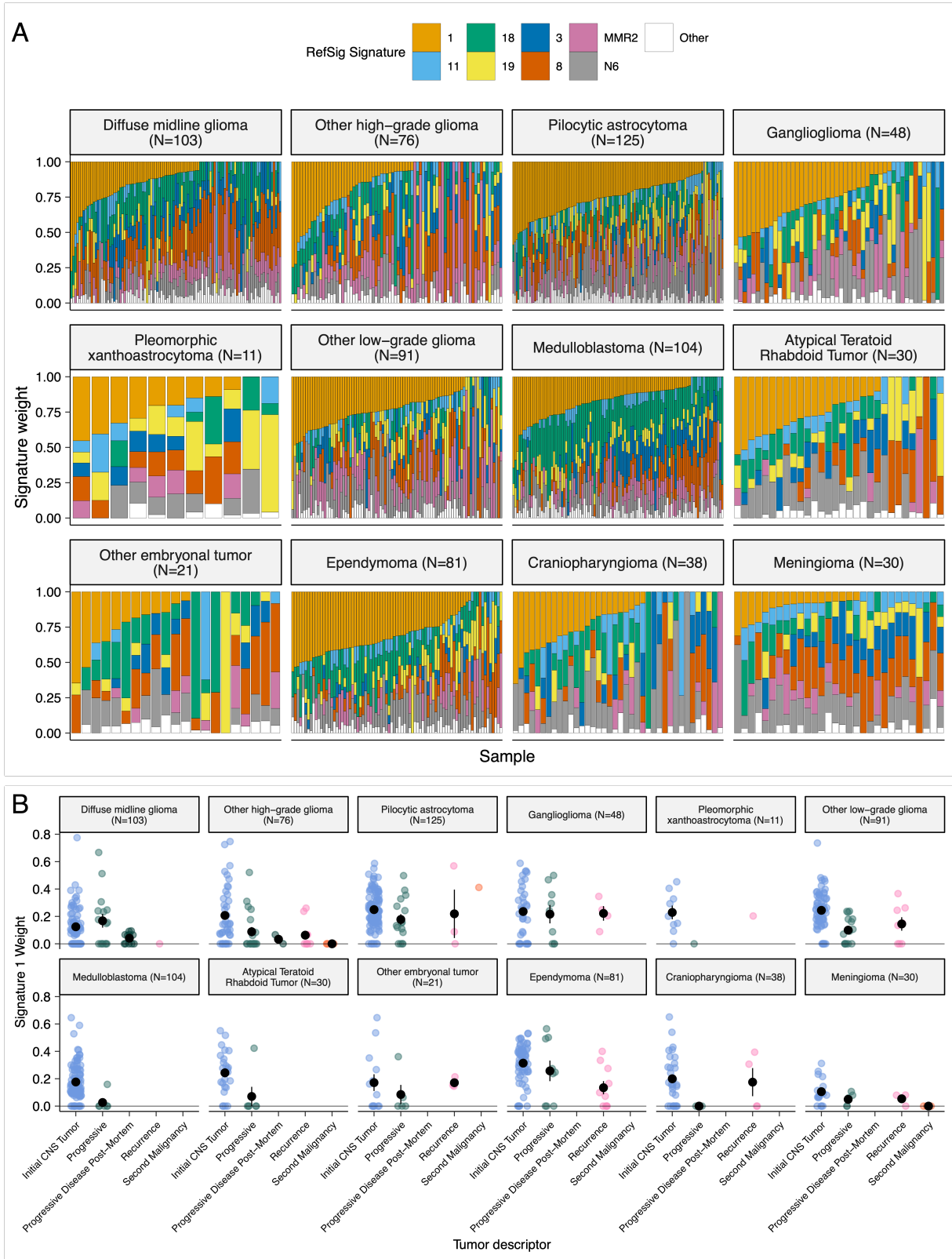
1560

1561 **Figure S2: Validation of Consensus SNV calls and Tumor Mutation Burden, Related to**  
1562 **Figures 2 and 3.** Correlation (A) and violin (B) plots of mutation variant allele frequencies  
1563 (VAFs) comparing the variant callers (Lancet, Strelka2, Mutect2, and VarDict) used for PBTA  
1564 samples. Upset plot (C) showing overlap of variant calls. Correlation (D) and violin (E) plots of  
1565 mutation variant allele frequencies (VAFs) comparing the variant callers (Lancet, Strelka2, and  
1566 Mutect2) used for TCGA samples. Upset plot (F) showing overlap of variant calls. Violin plots  
1567 (G) showing VAFs for Lancet calls performed on WGS and WXS from the same tumor (N = 52  
1568 samples from 13 patients). Cumulative distribution TMB plots for PBTA (H) and TCGA (I) tumors  
1569 using consensus SNV calls.

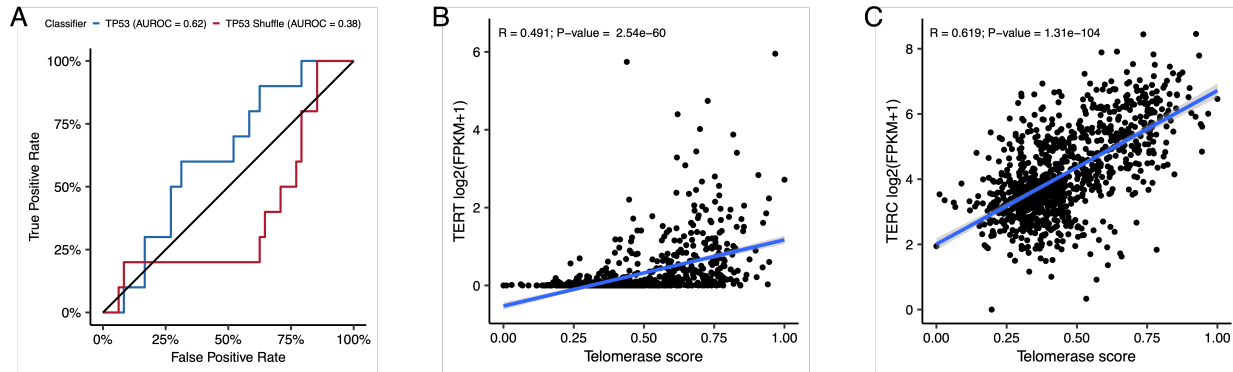


1571 **Figure S3: Genomic instability of pediatric brain tumors, Related to Figures 2 and 3. (A)**  
1572 *Oncoprint of canonical somatic gene mutations, CNVs, fusions, and TMB (top bar plot) for the*  
1573 *top 20 genes mutated across rare CNS tumors: desmoplastic infantile astrocytoma and*  
1574 *ganglioglioma (N = 2), germinoma (N = 4), glial-neuronal NOS (N = 8), metastatic secondary*  
1575 *tumors (N = 2), neurocytoma (N = 2), pineoblastoma (N = 4), Rosai-Dorfman disease (N = 2),*  
1576 *and sarcomas (N = 4). Patient sex (Germline sex estimate) and tumor histology (Cancer*  
1577 *Group) are displayed as annotations at the bottom of each plot. Only primary tumors with*  
1578 *mutations in the listed genes are shown. Multiple CNVs are denoted as a complex event. (B)*

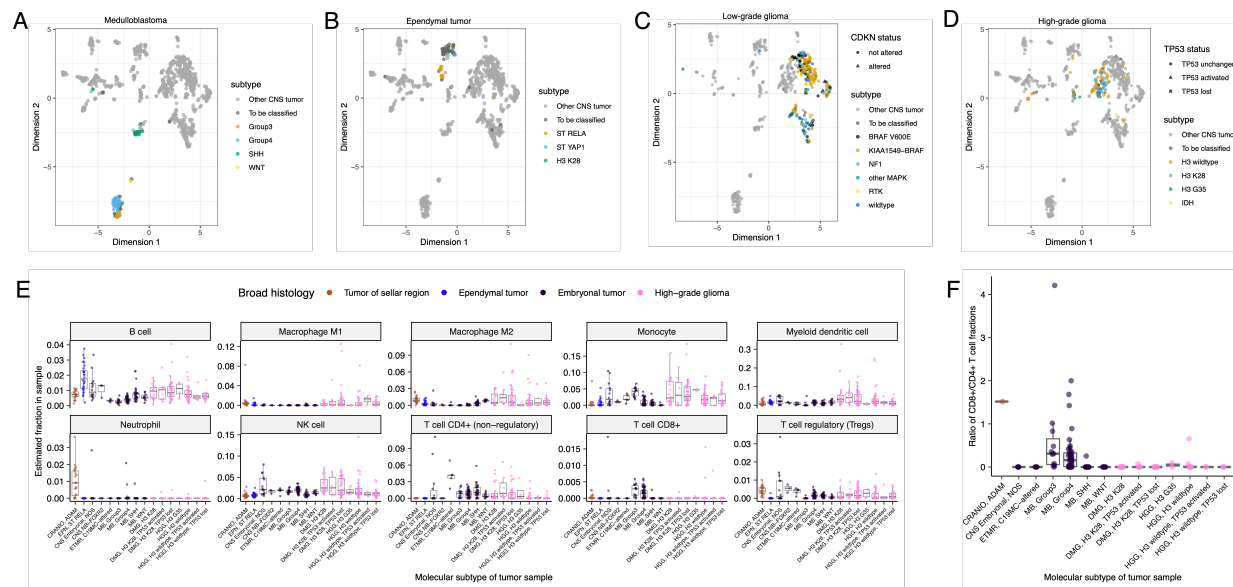
1579 *Genome-wide plot of CNV alterations by broad histology. Each row represents one sample. Box*  
1580 *and whisker plots of number of CNV breaks (C) or SV breaks (D) by number of chromothripsis*  
1581 *regions.*



1583 **Figure S4: Mutational signatures in pediatric brain tumors, Related to Figure 3. (A)**  
 1584 **Sample-specific RefSig signature weights across cancer groups ordered by decreasing**  
 1585 **Signature 1 exposure. (B) Proportion of Signature 1 plotted by phase of therapy for each cancer**  
 1586 **group.**



1587 **Figure S5: Quality control metrics for TP53 and EXTEND scores, Related to Figure 4. (A)**  
 1588 **Receiver Operating Characteristic for TP53 classifier run on FPKM of poly-A RNA-Seq samples.**  
 1589 **Correlation plots for telomerase scores (EXTEND) with RNA expression of TERT (B) and TERC**  
 1590 **(C).**



1592 **Figure S6: Subtype-specific clustering and immune cell fractions, Related to Figure 5.**  
 1593 **First two dimensions from UMAP of sample transcriptome data with points colored by**  
 1594 **molecular\_subtype for medulloblastoma (A), ependymoma (B), low-grade glioma**  
 1595 **(C), and high-grade glioma (D). (E) Box plots of quanTlseq estimates of immune cell fractions in**  
 1596 **histologies with more than one molecular subtype with  $N \geq 3$ . (F) Box plots of the ratio of**  
 1597 **immune cell fractions of CD8+ to CD4+ T cells in histologies with more than one molecular**  
 1598 **subtype with  $N \geq 3$ .**

1600 **Table S1. Related to Figure 1.** Table of specimens and associated metadata, clinical data, and  
1601 histological data utilized in the OpenPBTA project.

1602 **Table S2. Related to Figures 2 and 3.** Excel file with three sheets representing tables of TMB,  
1603 eight CNS mutational signatures, and chromothripsis events per sample, respectively.

1604 **Table S3. Related to Figures 4 and 5.** Excel file with three sheets representing tables of *TP53*  
1605 scores, telomerase EXTEND scores, and quanTIseq immune scores, respectively.

1606 **Table S4. Related to Figures 4 and 5.** Excel file with six sheets representing the survival  
1607 analyses performed for this manuscript. See **Star Methods** for details.

1608 **Table S5. Related to Figure 1.** Excel file with four sheets representing of all software and their  
1609 respective versions used for the OpenPBTA project, including the R packages in the OpenPBTA  
1610 Docker image, Python packages in the OpenPBTA Docker image, other command line tools in  
1611 the OpenPBTA Docker image, and all software used in the OpenPBTA workflows, respectively.  
1612 Note that all software in the OpenPBTA Docker image was utilized within the analysis  
1613 repository, but not all software was used for the final manuscript.

## 1614 **Consortia**

1615 The past and present members of the Children's Brain Tumor Network who contributed to the  
1616 generation of specimens and data are Adam C. Resnick, Alexa Plisiewicz, Allison M. Morgan,  
1617 Allison P. Heath, Alyssa Paul, Amanda Saratsis, Amy Smith, Ana Aguilar, Ana Guerreiro  
1618 Stücklin, Anastasia Arychnyna, Andrea Franson, Angela J. Waanders, Angela N. Viaene, Anita  
1619 Nirenberg, Anna Maria Buccoliero, Anna Yaffe, Anny Shai, Anthony Bet, Antoinette Price,  
1620 Arlene Luther, Ashley Plant, Augustine Eze, Bailey K. Farrow, Baoli Hu, Beth Frenkel, Bo  
1621 Zhang, Bobby Moulder, Bonnie Cole, Brian M. Ennis, Brian R. Rood, Brittany Lebert, Carina A.  
1622 Leonard, Carl Koschmann, Caroline Caudill, Caroline Drinkwater, Cassie N. Kline, Catherine  
1623 Sullivan, Chanel Keoni, Chiara Caporalini, Christine Bobick-Butcher, Christopher Mason,  
1624 Chunde Li, Claire Carter, Claudia MaduroCoronado, Clayton Wiley, Cynthia Wong, David E.  
1625 Kram, David Haussler, David Kram, David Pisapia, David Ziegler, Denise Morinigo, Derek  
1626 Hanson, Donald W. Parsons, Elizabeth Appert, Emily Drake, Emily Golbeck, Ena Agbodza, Eric  
1627 H. Raabe, Eric M. Jackson, Erin Alexander, Esteban Uceda, Eugene Hwang, Fausto Rodriguez,  
1628 Gabrielle S. Stone, Gary Kohanbash, Gavriella Silverman, George Rafidi, Gerald Grant, Gerri  
1629 Trooskin, Gilad Evrony, Graham Keyes, Hagop Boyajian, Holly B. Lindsay, Holly C. Beale, Ian  
1630 F. Pollack, James Johnston, James Palmer, Jane Minturn, Jared Pisapia, Jason E. Cain, Jason  
1631 R. Fangusaro, Javad Nazarian, Jeanette Haugh, Jeff Stevens, Jeffrey P. Greenfield, Jeffrey  
1632 Rubens, Jena V. Lilly, Jennifer L. Mason, Jessica B. Foster, Jim Olson, Jo Lynne Rokita,  
1633 Joanna J. Phillips, Jonathan Waller, Josh Rubin, Judy E. Palma, Justin McCroskey, Justine  
1634 Rizzo, Kaitlin Lehmann, Kamnaa Arya, Karlene Hall, Katherine Pehlivan, Kenneth Seidl,  
1635 Kimberly Diamond, Kristen Harnett, Kristina A. Cole, Krutika S. Gaonkar, Lamiya Tauhid, Laura  
1636 Prolo, Leah Holloway, Leslie Brosig, Lina Lopez, Lionel Chow, Madhuri Kambhampati, Mahdi  
1637 Sarmady, Margaret Nevins, Mari Groves, Mariarita Santi-Vicini, Marilyn M. Li, Marion Mateos,  
1638 Mateusz Koptyra, Matija Snuderl, Matthew Miller, Matthew Sklar, Matthew Wood, Meghan  
1639 Connors, Melissa Williams, Meredith Egan, Michael Fisher, Michael Koldobskiy, Michelle Monje,

1640 Migdalia Martinez, Miguel A. Brown, Mike Prados, Miriam Bornhorst, Mirko Scagnet, Mohamed  
1641 AbdelBaki, Monique Carrero-Tagle, Nadia Dahmane, Nalin Gupta, Nathan Young, Nicholas A.  
1642 Vitanza, Nicholas Tassone, Nicholas Van Kuren, Nicolas Gerber, Nithin D. Adappa, Nitin  
1643 Wadhwani, Noel Coleman, Obi Obayashi, Olena M. Vaske, Olivier Elemento, Oren Becher,  
1644 Philbert Oliveros, Phillip B. Storm, Pichai Raman, Prajwal Rajappa, Rintaro Hashizume, Rishi R.  
1645 Lulla, Robert Keating, Robert M. Lober, Ron Firestein, Sabine Mueller, Sameer Agnihotri,  
1646 Samuel G. Winebrake, Samuel Rivero-Hinojosa, Sarah Diane Black, Sarah Leary, Schuyler  
1647 Stoller, Shannon Robins, Sharon Gardner, Shelly Wang, Sherri Mayans, Sherry Tutson, Shida  
1648 Zhu, Sofie R. Salama, Sonia Partap, Sonika Dahiya, Sriram Venneti, Stacie Stapleton, Stephani  
1649 Campion, Stephanie Stefankiewicz, Stewart Goldman, Swetha Thambireddy, Tatiana S. Patton,  
1650 Teresa Hidalgo, Theo Nicolaides, Thinh Q. Nguyen, Thomas W. McLean, Tiffany Walker, Toba  
1651 Niazi, Tobey MacDonald, Valeria Lopez-Gil, Valerie Baubet, Whitney Rife, Xiao-Nan Li, Ximena  
1652 Cuellar, Yiran Guo, Yuankun Zhu, and Zeinab Helil.

1653 The past and present members of the Pacific Pediatric Neuro-Oncology Consortium who  
1654 contributed to the generation of specimens and data are Adam C. Resnick, Alicia Lenzen,  
1655 Alyssa Reddy, Amar Gajjar, Ana Guerreiro Stucklin, Anat Epstein, Andrea Franson, Angela  
1656 Waanders, Anne Bendel, Anu Banerjee, Ashley Margol, Ashley Plant, Brian Rood, Carl  
1657 Koschmann, Carol Bruggers, Caroline Hastings, Cassie N. Kline, Christina Coleman Abadi,  
1658 Christopher Tinkle, Corey Raffel, Dan Runco, Daniel Landi, Daphne Adele Haas-Kogan, David  
1659 Ashley, David Ziegler, Derek Hanson, Dong Anh Khuong Quang, Duane Mitchell, Elias Sayour,  
1660 Eric Jackson, Eric Raabe, Eugene Hwang, Fatema Malbari, Geoffrey McCowage, Girish Dhall,  
1661 Gregory Friedman, Hideho Okada, Ibrahim Qaddoumi, Iris Fried, Jae Cho, Jane Minturn, Jason  
1662 Blatt, Javad Nazarian, Jeffrey Rubens, Jena V. Lilly, Jennifer Elster, Jennifer L. Mason, Jessica  
1663 Schulte, Jonathan Schoenfeld, Josh Rubin, Karen Gauvain, Karen Wright, Katharine Offer,  
1664 Katie Metrock, Kellie Haworth, Ken Cohen, Kristina A. Cole, Lance Governale, Linda Stork,  
1665 Lindsay Kilburn, Lissa Baird, Maggie Skrypek, Marcia Leonard, Margaret Shatara, Margot  
1666 Lazow, Mariella Filbin, Maryam Fouladi, Matthew Miller, Megan Paul, Michael Fisher, Michael  
1667 Koldobskiy, Michael Prados, Michal Yalon Oren, Mimi Bandopadhyay, Miriam Bornhorst,  
1668 Mohamed AbdelBaki, Nalin Gupta, Nathan Robison, Nicholas Whipple, Nick Gottardo, Nicholas  
1669 A. Vitanza, Nicolas Gerber, Patricia Robertson, Payal Jain, Peter Sun, Priya Chan, Richard S  
1670 Lemons, Robert Wechsler-Reya, Roger Packer, Russ Geyer, Ryan Velasco, Sabine Mueller,  
1671 Sahaja Acharya, Sam Cheshier, Sarah Leary, Scott Coven, Sebastian M. Waszak, Sharon  
1672 Gardner, Sri Gururangan, Stewart Goldman, Susan Chi, Tab Cooney, Tatiana S. Patton,  
1673 Theodore Nicolaides, and Tom Belle Davidson.

## 1674 **References**

- 1675 1. Ostrom, Q.T., Cioffi, G., Gittleman, H., Patil, N., Waite, K., Kruchko, C., and Barnholtz-  
1676 Sloan, J.S. (2019). CBTRUS Statistical Report: Primary Brain and Other Central Nervous  
1677 System Tumors Diagnosed in the United States in 2012–2016. *Neuro-Oncology* 21, v1–v100.  
1678 [10.1093/neuonc/noz150](https://doi.org/10.1093/neuonc/noz150).
- 1679 2. Ostrom, Q.T., Gittleman, H., Xu, J., Kromer, C., Wolinsky, Y., Kruchko, C., and  
1680 Barnholtz-Sloan, J.S. (2016). CBTRUS Statistical Report: Primary Brain and Other Central

1681 1682 Nervous System Tumors Diagnosed in the United States in 2009–2013. *Neuro-Oncology* 18, v1–v75. [10.1093/neuonc/now207](https://doi.org/10.1093/neuonc/now207).

1683 3. Blank, P.M., Ostrom, Q.T., Rouse, C., Wolinsky, Y., Kruchko, C., Salcido, J., and Barnholtz-Sloan, J.S. (2015). Years of life lived with disease and years of potential life lost in children who die of cancer in the United States, 2009. *Cancer Med* 4, 608–619. [10.1002/cam4.410](https://doi.org/10.1002/cam4.410).

1687 1688 4. Oncology Center of Excellence, U.S. Food and Drug Administration (2022). [Pediatric Oncology Drug Approvals](#).

1689 1690 1691 5. Vable, A.M., Diehl, S.F., and Glymour, M.M. (2021). Code Review as a Simple Trick to Enhance Reproducibility, Accelerate Learning, and Improve the Quality of Your Team's Research. *American Journal of Epidemiology* 190, 2172–2177. [10.1093/aje/kwab092](https://doi.org/10.1093/aje/kwab092).

1692 1693 6. Parker, H. (2017). Opinionated analysis development. *PeerJ Preprints*, e3210v1. [10.7287/peerj.preprints.3210v1](https://doi.org/10.7287/peerj.preprints.3210v1).

1694 1695 1696 7. Beaulieu-Jones, B.K., and Greene, C.S. (2017). Reproducibility of computational workflows is automated using continuous analysis. *Nat Biotechnol* 35, 342–346. [10.1038/nbt.3780](https://doi.org/10.1038/nbt.3780).

1697 1698 8. Piwowar, H.A., Day, R.S., and Fridsma, D.B. (2007). Sharing Detailed Research Data Is Associated with Increased Citation Rate. *PLoS ONE* 2, e308. [10.1371/journal.pone.0000308](https://doi.org/10.1371/journal.pone.0000308).

1699 1700 1701 9. Cadwallader, L., Papin, J.A., Mac Gabhann, F., and Kirk, R. (2021). Collaborating with our community to increase code sharing. *PLoS Comput Biol* 17, e1008867. [10.1371/journal.pcbi.1008867](https://doi.org/10.1371/journal.pcbi.1008867).

1702 1703 1704 1705 10. Dang, M.T., Gonzalez, M.V., Gaonkar, K.S., Rathi, K.S., Young, P., Arif, S., Zhai, L., Alam, Z., Devalaraja, S., To, T.K.J., et al. (2021). Macrophages in SHH subgroup medulloblastoma display dynamic heterogeneity that varies with treatment modality. *Cell Reports* 34, 108917. [10.1016/j.celrep.2021.108917](https://doi.org/10.1016/j.celrep.2021.108917).

1706 1707 1708 1709 11. Foster, J.B., Griffin, C., Rokita, J.L., Stern, A., Brimley, C., Rathi, K., Lane, M.V., Buongervino, S.N., Smith, T., Madsen, P.J., et al. (2021). Development of GPC2-directed chimeric antigen receptors using mRNA for pediatric brain tumors. *bioRxiv*, 2021.07.06.451385. [10.1101/2021.07.06.451385](https://doi.org/10.1101/2021.07.06.451385).

1710 1711 1712 1713 12. Kline, C., Jain, P., Kilburn, L., Bonner, E.R., Gupta, N., Crawford, J.R., Banerjee, A., Packer, R.J., Villanueva-Meyer, J., Luks, T., et al. (2022). Upfront Biology-Guided Therapy in Diffuse Intrinsic Pontine Glioma: Therapeutic, Molecular, and Biomarker Outcomes from PNOC003. *Clinical Cancer Research*, OF1–OF14. [10.1158/1078-0432.ccr-22-0803](https://doi.org/10.1158/1078-0432.ccr-22-0803).

1714 1715 13. RACE Act Poised to Advance Pediatric Cancer Research (2020). *Cancer Discovery* 10, 1434–1434. [10.1158/2159-8290.cd-nb2020-081](https://doi.org/10.1158/2159-8290.cd-nb2020-081).

1716 14. Ijaz, H., Koptyra, M., Gaonkar, K.S., Rokita, J.L., Baubet, V.P., Tauhid, L., Zhu, Y.,  
1717 Brown, M., Lopez, G., Zhang, B., et al. (2019). Pediatric high-grade glioma resources from the  
1718 Children's Brain Tumor Tissue Consortium. *Neuro-Oncology* 22, 163–165.  
1719 [10.1093/neuonc/noz192](https://doi.org/10.1093/neuonc/noz192).

1720 15. Mueller, S., Jain, P., Liang, W.S., Kilburn, L., Kline, C., Gupta, N., Panditharatna, E.,  
1721 Magge, S.N., Zhang, B., Zhu, Y., et al. (2019). A pilot precision medicine trial for children with  
1722 diffuse intrinsic pontine glioma—PNOC003: A report from the Pacific Pediatric Neuro-Oncology  
1723 Consortium. *Int. J. Cancer*. [10.1002/ijc.32258](https://doi.org/10.1002/ijc.32258).

1724 16. Himmelstein, D.S., Rubinetti, V., Slochower, D.R., Hu, D., Malladi, V.S., Greene, C.S.,  
1725 and Gitter, A. (2019). Open collaborative writing with Manubot. *PLoS Comput Biol* 15,  
1726 e1007128. [10.1371/journal.pcbi.1007128](https://doi.org/10.1371/journal.pcbi.1007128).

1727 17. Merkel, D. (2014). [Docker: lightweight Linux containers for consistent development and deployment](#). *Linux Journal* 2014, 2:2.

1729 18. Boettiger, C., and Eddelbuettel, D. (2017). [An Introduction to Rocker: Docker Containers for R](#). arXiv:1710.03675 [cs].

1731 19. Kleihues, P., Louis, D.N., Scheithauer, B.W., Rorke, L.B., Reifenberger, G., Burger,  
1732 P.C., and Cavenee, W.K. (2002). The WHO classification of tumors of the nervous system. *J  
1733 Neuropathol Exp Neurol* 61, 215-25; discussion 226-9. [10.1093/jnen/61.3.215](https://doi.org/10.1093/jnen/61.3.215).

1734 20. Louis, D.N., Ohgaki, H., Wiestler, O.D., Cavenee, W.K., Burger, P.C., Jouvet, A.,  
1735 Scheithauer, B.W., and Kleihues, P. (2007). The 2007 WHO Classification of Tumours of the  
1736 Central Nervous System. *Acta Neuropathol* 114, 97–109. [10.1007/s00401-007-0243-4](https://doi.org/10.1007/s00401-007-0243-4).

1737 21. Louis, D.N., Perry, A., Reifenberger, G., von Deimling, A., Figarella-Branger, D.,  
1738 Cavenee, W.K., Ohgaki, H., Wiestler, O.D., Kleihues, P., and Ellison, D.W. (2016). The 2016  
1739 World Health Organization Classification of Tumors of the Central Nervous System: a summary.  
1740 *Acta Neuropathol* 131, 803–820. [10.1007/s00401-016-1545-1](https://doi.org/10.1007/s00401-016-1545-1).

1741 22. Louis, D.N., Perry, A., Wesseling, P., Brat, D.J., Cree, I.A., Figarella-Branger, D.,  
1742 Hawkins, C., Ng, H.K., Pfister, S.M., Reifenberger, G., et al. (2021). The 2021 WHO  
1743 Classification of Tumors of the Central Nervous System: a summary. *Neuro-Oncology* 23,  
1744 1231–1251. [10.1093/neuonc/noab106](https://doi.org/10.1093/neuonc/noab106).

1745 23. Ryall, S., Zapotocky, M., Fukuoka, K., Nobre, L., Guerreiro Stucklin, A., Bennett, J.,  
1746 Siddaway, R., Li, C., Pajovic, S., Arnoldo, A., et al. (2020). Integrated Molecular and Clinical  
1747 Analysis of 1,000 Pediatric Low-Grade Gliomas. *Cancer Cell* 37, 569–583.e5.  
1748 [10.1016/j.ccr.2020.03.011](https://doi.org/10.1016/j.ccr.2020.03.011).

1749 24. Campbell, B.B., Light, N., Fabrizio, D., Zatzman, M., Fuligni, F., de Borja, R., Davidson,  
1750 S., Edwards, M., Elvin, J.A., Hodel, K.P., et al. (2017). Comprehensive Analysis of  
1751 Hypermutation in Human Cancer. *Cell* 171, 1042–1056.e10. [10.1016/j.cell.2017.09.048](https://doi.org/10.1016/j.cell.2017.09.048).

1752 25. Ryall, S., Tabori, U., and Hawkins, C. (2020). Pediatric low-grade glioma in the era of  
1753 molecular diagnostics. *acta neuropathol commun* 8. [10.1186/s40478-020-00902-z](https://doi.org/10.1186/s40478-020-00902-z).

1754 26. Lambo, S., von Hoff, K., Korshunov, A., Pfister, S.M., and Kool, M. (2020). ETMR: a  
1755 tumor entity in its infancy. *Acta Neuropathol* 140, 249–266. [10.1007/s00401-020-02182-2](https://doi.org/10.1007/s00401-020-02182-2).

1756 27. Richardson, S., Hill, R.M., Kui, C., Lindsey, J.C., Grabovksa, Y., Keeling, C., Pease, L.,  
1757 Bashton, M., Crosier, S., Vinci, M., et al. (2021). Emergence and maintenance of actionable  
1758 genetic drivers at medulloblastoma relapse. *Neuro-Oncology* 24, 153–165.  
1759 [10.1093/neuonc/noab178](https://doi.org/10.1093/neuonc/noab178).

1760 28. Łastowska, M., Trubicka, J., Sobocińska, A., Wojtas, B., Niemira, M., Szałkowska, A.,  
1761 Krętowski, A., Karkucińska-Więckowska, A., Kaleta, M., Ejmont, M., et al. (2020). Molecular  
1762 identification of CNS NB-FOXR2, CNS EFT-CIC, CNS HGNET-MN1 and CNS HGNET-BCOR  
1763 pediatric brain tumors using tumor-specific signature genes. *acta neuropathol commun* 8.  
1764 [10.1186/s40478-020-00984-9](https://doi.org/10.1186/s40478-020-00984-9).

1765 29. Northcott, P.A., Buchhalter, I., Morrissey, A.S., Hovestadt, V., Weischenfeldt, J.,  
1766 Ehrenberger, T., Gröbner, S., Segura-Wang, M., Zichner, T., Rudneva, V.A., et al. (2017). The  
1767 whole-genome landscape of medulloblastoma subtypes. *Nature* 547, 311–317.  
1768 [10.1038/nature22973](https://doi.org/10.1038/nature22973).

1769 30. Mackay, A., Burford, A., Carvalho, D., Izquierdo, E., Fazal-Salom, J., Taylor, K.R.,  
1770 Bjerke, L., Clarke, M., Vinci, M., Nandhabalan, M., et al. (2017). Integrated Molecular Meta-  
1771 Analysis of 1,000 Pediatric High-Grade and Diffuse Intrinsic Pontine Glioma. *Cancer Cell* 32,  
1772 520–537.e5. [10.1016/j.ccr.2017.08.017](https://doi.org/10.1016/j.ccr.2017.08.017).

1773 31. Pratt, D., Quezado, M., Abdullaev, Z., Hawes, D., Yang, F., Garton, H.J.L., Judkins,  
1774 A.R., Mody, R., Chinnaiyan, A., Aldape, K., et al. (2020). Diffuse intrinsic pontine glioma-like  
1775 tumor with EZHIP expression and molecular features of PFA ependymoma. *acta neuropathol  
1776 commun* 8. [10.1186/s40478-020-00905-w](https://doi.org/10.1186/s40478-020-00905-w).

1777 32. Surrey, L.F., Jain, P., Zhang, B., Straka, J., Zhao, X., Harding, B.N., Resnick, A.C.,  
1778 Storm, P.B., Buccoliero, A.M., Genitori, L., et al. (2019). Genomic Analysis of Dysembryoplastic  
1779 Neuroepithelial Tumor Spectrum Reveals a Diversity of Molecular Alterations Dysregulating the  
1780 MAPK and PI3K/mTOR Pathways. *Journal of Neuropathology & Experimental Neurology*  
1781 78, 1100–1111. [10.1093/jnen/nlz101](https://doi.org/10.1093/jnen/nlz101).

1782 33. Pfaff, E., Remke, M., Sturm, D., Benner, A., Witt, H., Milde, T., von Bueren, A.O.,  
1783 Wittmann, A., Schöttler, A., Jorch, N., et al. (2010). *TP53* Mutation Is Frequently Associated  
1784 With *CTNNB1* Mutation or *MYCN* Amplification and Is Compatible With Long-Term Survival in  
1785 Medulloblastoma. *JCO* 28, 5188–5196. [10.1200/jco.2010.31.1670](https://doi.org/10.1200/jco.2010.31.1670).

1786 34. Lucas, C.-H.G., Gupta, R., Doo, P., Lee, J.C., Cadwell, C.R., Ramani, B., Hofmann,  
1787 J.W., Sloan, E.A., Kleinschmidt-DeMasters, B.K., Lee, H.S., et al. (2020). Comprehensive  
1788 analysis of diverse low-grade neuroepithelial tumors with FGFR1 alterations reveals a distinct

1789 molecular signature of rosette-forming glioneuronal tumor. *acta neuropathol commun* 8.  
1790 [10.1186/s40478-020-01027-z](https://doi.org/10.1186/s40478-020-01027-z).

1791 35. Wu, G., Diaz, A.K., Paugh, B.S., Rankin, S.L., Ju, B., Li, Y., Zhu, X., Qu, C., Chen, X.,  
1792 Zhang, J., et al. (2014). The genomic landscape of diffuse intrinsic pontine glioma and pediatric  
1793 non-brainstem high-grade glioma. *Nature Genetics* 46, 444–450. [10.1038/ng.2938](https://doi.org/10.1038/ng.2938).

1794 36. Degasperi, A., Amarante, T.D., Czarnecki, J., Shooter, S., Zou, X., Glodzik, D.,  
1795 Morganella, S., Nanda, A.S., Badja, C., Koh, G., et al. (2020). A practical framework and online  
1796 tool for mutational signature analyses show intertissue variation and driver dependencies. *Nat  
1797 Cancer* 1, 249–263. [10.1038/s43018-020-0027-5](https://doi.org/10.1038/s43018-020-0027-5).

1798 37. Wojciechowicz, K., Cantelli, E., Van Gerwen, B., Plug, M., Van Der Wal, A., Delzenne-  
1799 Goette, E., Song, J.-Y., De Vries, S., Dekker, M., and Riele, H.T. (2014). Temozolomide  
1800 Increases the Number of Mismatch Repair–Deficient Intestinal Crypts and Accelerates  
1801 Tumorigenesis in a Mouse Model of Lynch Syndrome. *Gastroenterology* 147, 1064–1072.e5.  
1802 [10.1053/j.gastro.2014.07.052](https://doi.org/10.1053/j.gastro.2014.07.052).

1803 38. Knijnenburg, T.A., Wang, L., Zimmermann, M.T., Chambwe, N., Gao, G.F., Cherniack,  
1804 A.D., Fan, H., Shen, H., Way, G.P., Greene, C.S., et al. (2018). Genomic and Molecular  
1805 Landscape of DNA Damage Repair Deficiency across The Cancer Genome Atlas. *Cell Reports*  
1806 23, 239–254.e6. [10.1016/j.celrep.2018.03.076](https://doi.org/10.1016/j.celrep.2018.03.076).

1807 39. Dittmer, D., Pati, S., Zambetti, G., Chu, S., Teresky, A.K., Moore, M., Finlay, C., and  
1808 Levine, A.J. (1993). Gain of function mutations in p53. *Nat Genet* 4, 42–46. [10.1038/ng0593-42](https://doi.org/10.1038/ng0593-42).

1809 40. Rokita, J.L., Rathi, K.S., Cardenas, M.F., Upton, K.A., Jayaseelan, J., Cross, K.L., Pfeil,  
1810 J., Egolf, L.E., Way, G.P., Farrel, A., et al. (2019). Genomic Profiling of Childhood Tumor  
1811 Patient-Derived Xenograft Models to Enable Rational Clinical Trial Design. *Cell Reports* 29,  
1812 1675–1689.e9. [10.1016/j.celrep.2019.09.071](https://doi.org/10.1016/j.celrep.2019.09.071).

1813 41. Noureen, N., Wu, S., Lv, Y., Yang, J., Alfred Yung, W.K., Gelfond, J., Wang, X., Koul, D.,  
1814 Ludlow, A., and Zheng, S. (2021). Integrated analysis of telomerase enzymatic activity unravels  
1815 an association with cancer stemness and proliferation. *Nat Commun* 12. [10.1038/s41467-020-20474-9](https://doi.org/10.1038/s41467-020-20474-9).

1817 42. Artandi, S.E., and DePinho, R.A. (2009). Telomeres and telomerase in cancer.  
1818 *Carcinogenesis* 31, 9–18. [10.1093/carcin/bgp268](https://doi.org/10.1093/carcin/bgp268).

1819 43. Ceja-Rangel, H.A., Sánchez-Suárez, P., Castellanos-Juárez, E., Peñaroja-Flores, R.,  
1820 Arenas-Aranda, D.J., Gariglio, P., and Benítez-Bribiesca, L. (2016). Shorter telomeres and high  
1821 telomerase activity correlate with a highly aggressive phenotype in breast cancer cell lines.  
1822 *Tumor Biol.* 37, 11917–11926. [10.1007/s13277-016-5045-7](https://doi.org/10.1007/s13277-016-5045-7).

1823 44. Oh, B.-K., Kim, H., Park, Y.N., Yoo, J.E., Choi, J., Kim, K.-S., Lee, J.J., and Park, C.  
1824 (2007). High telomerase activity and long telomeres in advanced hepatocellular carcinomas with  
1825 poor prognosis. *Lab Invest* 88, 144–152. [10.1038/labinvest.3700710](https://doi.org/10.1038/labinvest.3700710).

1826 45. Kulić, A., Plavetić, N.D., Gamulin, S., Jakić-Razumović, J., Vrbanec, D., and Sirotković-  
1827 Skerlev, M. (2016). Telomerase activity in breast cancer patients: association with poor  
1828 prognosis and more aggressive phenotype. *Med Oncol* 33. [10.1007/s12032-016-0736-x](https://doi.org/10.1007/s12032-016-0736-x).

1829 46. Wong, V.C.H., Morrison, A., Tabori, U., and Hawkins, C.E. (2010). Telomerase Inhibition  
1830 as a Novel Therapy for Pediatric Ependymoma. *Brain Pathology* 20, 780–786. [10.1111/j.1750-3639.2010.00372.x](https://doi.org/10.1111/j.1750-3639.2010.00372.x).

1832 47. Pich, O., Muños, F., Lolkema, M.P., Steeghs, N., Gonzalez-Perez, A., and Lopez-Bigas,  
1833 N. (2019). The mutational footprints of cancer therapies. *Nat Genet* 51, 1732–1740.  
1834 [10.1038/s41588-019-0525-5](https://doi.org/10.1038/s41588-019-0525-5).

1835 48. Aronson, M., Colas, C., Shuen, A., Hampel, H., Foulkes, W.D., Baris Feldman, H.,  
1836 Goldberg, Y., Muleris, M., Wolfe Schneider, K., McGee, R.B., et al. (2021). Diagnostic criteria  
1837 for constitutional mismatch repair deficiency (CMMRD): recommendations from the international  
1838 consensus working group. *J Med Genet* 59, 318–327. [10.1136/jmedgenet-2020-107627](https://doi.org/10.1136/jmedgenet-2020-107627).

1839 49. Lewis, P.W., Müller, M.M., Koletsky, M.S., Cordero, F., Lin, S., Banaszynski, L.A.,  
1840 Garcia, B.A., Muir, T.W., Becher, O.J., and Allis, C.D. (2013). Inhibition of PRC2 Activity by a  
1841 Gain-of-Function H3 Mutation Found in Pediatric Glioblastoma. *Science* 340, 857–861.  
1842 [10.1126/science.1232245](https://doi.org/10.1126/science.1232245).

1843 50. Hutter, S., Bolin, S., Weishaupt, H., and Swartling, F. (2017). Modeling and Targeting  
1844 MYC Genes in Childhood Brain Tumors. *Genes* 8, 107. [10.3390/genes8040107](https://doi.org/10.3390/genes8040107).

1845 51. Leone, G., Sears, R., Huang, E., Rempel, R., Nuckolls, F., Park, C.H., Giangrande, P.,  
1846 Wu, L., Saavedra, H.I., Field, S.J., et al. (2001). Myc requires distinct E2F activities to induce S  
1847 phase and apoptosis. *Mol Cell* 8, 105–13. [10.1016/s1097-2765\(01\)00275-1](https://doi.org/10.1016/s1097-2765(01)00275-1).

1848 52. Hannan, C.J., Lewis, D., O'Leary, C., Donofrio, C.A., Evans, D.G., Roncaroli, F., Brough,  
1849 D., King, A.T., Coope, D., and Pathmanaban, O.N. (2020). The inflammatory microenvironment  
1850 in vestibular schwannoma. *Neuro-Oncology Advances* 2. [10.1093/noajnl/vdaa023](https://doi.org/10.1093/noajnl/vdaa023).

1851 53. Petralia, F., Tignor, N., Reva, B., Koptyra, M., Chowdhury, S., Rykunov, D., Krek, A.,  
1852 Ma, W., Zhu, Y., Ji, J., et al. (2020). Integrated Proteogenomic Characterization across Major  
1853 Histological Types of Pediatric Brain Cancer. *Cell* 183, 1962–1985.e31.  
1854 [10.1016/j.cell.2020.10.044](https://doi.org/10.1016/j.cell.2020.10.044).

1855 54. Lin, G.L., Nagaraja, S., Filbin, M.G., Suvà, M.L., Vogel, H., and Monje, M. (2018). Non-  
1856 inflammatory tumor microenvironment of diffuse intrinsic pontine glioma. *acta neuropathol  
1857 commun* 6. [10.1186/s40478-018-0553-x](https://doi.org/10.1186/s40478-018-0553-x).

1858 55. Ross, J.L., Velazquez Vega, J., Plant, A., MacDonald, T.J., Becher, O.J., and  
1859 Hambardzumyan, D. (2021). Tumour immune landscape of paediatric high-grade gliomas. *Brain*  
1860 144, 2594–2609. [10.1093/brain/awab155](https://doi.org/10.1093/brain/awab155).

1861 56. Martin, A.M., Nirschl, C.J., Polanczyk, M.J., Bell, W.R., Nirschl, T.R., Harris-Bookman,  
1862 S., Phallen, J., Hicks, J., Martinez, D., Ogurtsova, A., et al. (2018). PD-L1 expression in

1863 1863 medulloblastoma: an evaluation by subgroup. *Oncotarget* 9, 19177–19191.

1864 [10.18632/oncotarget.24951](https://doi.org/10.18632/oncotarget.24951).

1865 1865 57. Bockmayr, M., Mohme, M., Klauschen, F., Winkler, B., Budczies, J., Rutkowski, S., and

1866 Schüller, U. (2018). Subgroup-specific immune and stromal microenvironment in

1867 medulloblastoma. *Oncolimmunology* 7, e1462430. [10.1080/2162402x.2018.1462430](https://doi.org/10.1080/2162402x.2018.1462430).

1868 1868 58. Duchemann, B., Naigeon, M., Auclin, E., Ferrara, R., Cassard, L., Jouniaux, J.-M.,

1869 Boselli, L., Grivel, J., Desnoyer, A., Danlos, F.-X., et al. (2022). CD8+ PD-1+ to CD4+PD-1+

1870 ratio (PERLS) is associated with prognosis of patients with advanced NSCLC treated with PD-

1871 (L)1 blockers. *J Immunother Cancer* 10, e004012. [10.1136/jitc-2021-004012](https://doi.org/10.1136/jitc-2021-004012).

1872 1872 59. Shindo, G., Endo, T., Onda, M., Goto, S., Miyamoto, Y., and Kaneko, T. (2013). Is the

1873 CD4/CD8 Ratio an Effective Indicator for Clinical Estimation of Adoptive Immunotherapy for

1874 Cancer Treatment? *JCT* 04, 1382–1390. [10.4236/jct.2013.48164](https://doi.org/10.4236/jct.2013.48164).

1875 1875 60. Gendoo, D.M.A., and Haibe-Kains, B. (2016). MM2S: personalized diagnosis of

1876 medulloblastoma patients and model systems. *Source Code Biol Med* 11. [10.1186/s13029-016-0053-y](https://doi.org/10.1186/s13029-016-0053-y).

1877 1877 61. Rathi, K.S., Arif, S., Koptyra, M., Naqvi, A.S., Taylor, D.M., Storm, P.B., Resnick, A.C.,

1878 Rokita, J.L., and Raman, P. (2020). A transcriptome-based classifier to determine molecular

1879 subtypes in medulloblastoma. *PLoS Comput Biol* 16, e1008263. [10.1371/journal.pcbi.1008263](https://doi.org/10.1371/journal.pcbi.1008263).

1880 1880 62. Yuza, K., Nagahashi, M., Watanabe, S., Takabe, K., and Wakai, T. (2017).

1881 Hypermutation and microsatellite instability in gastrointestinal cancers. *Oncotarget* 8, 112103–

1882 112115. [10.18632/oncotarget.22783](https://doi.org/10.18632/oncotarget.22783).

1883 1883 63. Bass, A.J., Thorsson, V., Shmulevich, I., Reynolds, S.M., Miller, M., Bernard, B., Hinoue,

1884 T., Laird, P.W., Curtis, C., Shen, H., et al. (2014). Comprehensive molecular characterization of

1885 gastric adenocarcinoma. *Nature* 513, 202–209. [10.1038/nature13480](https://doi.org/10.1038/nature13480).

1886 1886 64. Sharma, J., Bonfield, C.M., Singhal, A., Hukin, J., and Steinbok, P. (2015). Intracystic

1887 interferon- $\alpha$  treatment leads to neurotoxicity in craniopharyngioma: case report. *PED* 16, 301–

1888 304. [10.3171/2015.2.peds14656](https://doi.org/10.3171/2015.2.peds14656).

1889 1889 65. Mohammed, K.E.A., Mike, K.R.A., and Parkes, J. (2013). Unexpected brain atrophy

1890 following administration of intratumoral interferon alpha-2b for cystic craniopharyngioma: A case

1891 report. *IJCRI* 4, 719. [10.5348/ijcri-2013-12-419-cr-13](https://doi.org/10.5348/ijcri-2013-12-419-cr-13).

1892 1892 66. Coy, S., Rashid, R., Lin, J.-R., Du, Z., Donson, A.M., Hankinson, T.C., Foreman, N.K.,

1893 Manley, P.E., Kieran, M.W., Reardon, D.A., et al. (2018). Multiplexed immunofluorescence

1894 reveals potential PD-1/PD-L1 pathway vulnerabilities in craniopharyngioma. *Neuro-Oncology*

1895 20, 1101–1112. [10.1093/neuonc/noy035](https://doi.org/10.1093/neuonc/noy035).

1896 1896 67. Yuan, F., Cai, X., Zhu, J., Yuan, L., Wang, Y., Tang, C., Cong, Z., and Ma, C. (2021). A

1897 Novel Immune Classification for Predicting Immunotherapy Responsiveness in Patients With

1898 Adamantinomatous Craniopharyngioma. *Front Neurol* 12, 704130. [10.3389/fneur.2021.704130](https://doi.org/10.3389/fneur.2021.704130).

1900 68. Whelan, R., Prince, E., Gilani, A., and Hankinson, T. (2020). The Inflammatory Milieu of  
1901 Adamantinomatous Craniopharyngioma and Its Implications for Treatment. *J Clin Med* 9.  
1902 [10.3390/jcm9020519](https://doi.org/10.3390/jcm9020519).

1903 69. Apps, J.R., Carreno, G., Gonzalez-Meljum, J.M., Haston, S., Guiho, R., Cooper, J.E.,  
1904 Manshaei, S., Jani, N., Hölsken, A., Pettorini, B., et al. (2018). Tumour compartment  
1905 transcriptomics demonstrates the activation of inflammatory and odontogenic programmes in  
1906 human adamantinomatous craniopharyngioma and identifies the MAPK/ERK pathway as a  
1907 novel therapeutic target. *Acta Neuropathol* 135, 757–777. [10.1007/s00401-018-1830-2](https://doi.org/10.1007/s00401-018-1830-2).

1908 70. Grob, S., Mirsky, D.M., Donson, A.M., Dahl, N., Foreman, N.K., Hoffman, L.M.,  
1909 Hankinson, T.C., and Mulcahy Levy, J.M. (2019). Targeting IL-6 Is a Potential Treatment for  
1910 Primary Cystic Craniopharyngioma. *Front. Oncol.* 9. [10.3389/fonc.2019.00791](https://doi.org/10.3389/fonc.2019.00791).

1911 71. Gaonkar, K.S., Marini, F., Rathi, K.S., Jain, P., Zhu, Y., Chimicles, N.A., Brown, M.A.,  
1912 Naqvi, A.S., Zhang, B., Storm, P.B., et al. (2020). annoFuse: an R Package to annotate,  
1913 prioritize, and interactively explore putative oncogenic RNA fusions. *BMC Bioinformatics* 21.  
1914 [10.1186/s12859-020-03922-7](https://doi.org/10.1186/s12859-020-03922-7).

1915 72. University of California, San Francisco (2022). [A Pilot Trial Testing the Clinical Benefit of  
1916 Using Molecular Profiling to Determine an Individualized Treatment Plan in Children and Young  
1917 Adults With High Grade Glioma \(Excluding Diffuse Intrinsic Pontine Glioma\)](#) (clinicaltrials.gov).

1918 73. Open Pediatric Brain Tumor Atlas, C.B.T.N., Pediatric Neuro Oncology Consortium  
1919 (2022). Open Pediatric Brain Tumor Atlas. [10.24370/openppta](https://doi.org/10.24370/openppta).

1920 74. Li, H. (2013). [Aligning sequence reads, clone sequences and assembly contigs with  
1921 BWA-MEM](#). arXiv:1303.3997 [q-bio].

1922 75. DePristo, M.A., Banks, E., Poplin, R., Garimella, K.V., Maguire, J.R., Hartl, C.,  
1923 Philippakis, A.A., del Angel, G., Rivas, M.A., Hanna, M., et al. (2011). A framework for variation  
1924 discovery and genotyping using next-generation DNA sequencing data. *Nat Genet* 43, 491–498.  
1925 [10.1038/ng.806](https://doi.org/10.1038/ng.806).

1926 76. Faust, G.G., and Hall, I.M. (2014). SAMBLASTER: fast duplicate marking and structural  
1927 variant read extraction. *Bioinformatics* 30, 2503–2505. [10.1093/bioinformatics/btu314](https://doi.org/10.1093/bioinformatics/btu314).

1928 77. Tarasov, A., Vilella, A.J., Cuppen, E., Nijman, I.J., and Prins, P. (2015). Sambamba: fast  
1929 processing of NGS alignment formats. *Bioinformatics* 31, 2032–2034.  
1930 [10.1093/bioinformatics/btv098](https://doi.org/10.1093/bioinformatics/btv098).

1931 78. McKenna, A., Hanna, M., Banks, E., Sivachenko, A., Cibulskis, K., Kernytsky, A.,  
1932 Garimella, K., Altshuler, D., Gabriel, S., Daly, M., et al. (2010). The Genome Analysis Toolkit: A  
1933 MapReduce framework for analyzing next-generation DNA sequencing data. *Genome Res.* 20,  
1934 1297–1303. [10.1101/gr.107524.110](https://doi.org/10.1101/gr.107524.110).

1935 79. Poplin, R., Ruano-Rubio, V., DePristo, M.A., Fennell, T.J., Carneiro, M.O., Auwera,  
1936 G.A.V. der, Kling, D.E., Gauthier, L.D., Levy-Moonshine, A., Roazen, D., et al. (2018). Scaling

1937 accurate genetic variant discovery to tens of thousands of samples. bioRxiv, 201178.  
1938 [10.1101/201178](https://doi.org/10.1101/201178).

1939 80. Lee, S., Lee, S., Ouellette, S., Park, W.-Y., Lee, E.A., and Park, P.J. (2017).  
1940 NGSCheckMate: software for validating sample identity in next-generation sequencing studies  
1941 within and across data types. Nucleic Acids Research 45, e103–e103. [10.1093/nar/gkx193](https://doi.org/10.1093/nar/gkx193).

1942 81. DeLuca, D.S., Levin, J.Z., Sivachenko, A., Fennell, T., Nazaire, M.-D., Williams, C.,  
1943 Reich, M., Winckler, W., and Getz, G. (2012). RNA-SeQC: RNA-seq metrics for quality control  
1944 and process optimization. Bioinformatics 28, 1530–1532. [10.1093/bioinformatics/bts196](https://doi.org/10.1093/bioinformatics/bts196).

1945 82. Wang, K., Li, M., and Hakonarson, H. (2010). ANNOVAR: functional annotation of  
1946 genetic variants from high-throughput sequencing data. Nucleic Acids Research 38, e164–e164.  
1947 [10.1093/nar/gkq603](https://doi.org/10.1093/nar/gkq603).

1948 83. Landrum, M.J., Lee, J.M., Riley, G.R., Jang, W., Rubinstein, W.S., Church, D.M., and  
1949 Maglott, D.R. (2013). ClinVar: public archive of relationships among sequence variation and  
1950 human phenotype. Nucl. Acids Res. 42, D980–D985. [10.1093/nar/gkt1113](https://doi.org/10.1093/nar/gkt1113).

1951 84. Cingolani, P., Patel, V.M., Coon, M., Nguyen, T., Land, S.J., Ruden, D.M., and Lu, X.  
1952 (2012). Using *Drosophila melanogaster* as a Model for Genotoxic Chemical Mutational Studies  
1953 with a New Program, SnpSift. Front. Gene. 3. [10.3389/fgene.2012.00035](https://doi.org/10.3389/fgene.2012.00035).

1954 85. Kim, S., Scheffler, K., Halpern, A.L., Bekritsky, M.A., Noh, E., Källberg, M., Chen, X.,  
1955 Kim, Y., Beyer, D., Krusche, P., et al. (2018). Strelka2: fast and accurate calling of germline  
1956 and somatic variants. Nat Methods 15, 591–594. [10.1038/s41592-018-0051-x](https://doi.org/10.1038/s41592-018-0051-x).

1957 86. Benjamin, D., Sato, T., Cibulskis, K., Getz, G., Stewart, C., and Lichtenstein, L. (2019).  
1958 Calling Somatic SNVs and Indels with Mutect2. bioRxiv, 861054. [10.1101/861054](https://doi.org/10.1101/861054).

1959 87. Narzisi, G., Corvelo, A., Arora, K., Bergmann, E.A., Shah, M., Musunuri, R., Emde, A.-  
1960 K., Robine, N., Vacic, V., and Zody, M.C. (2018). Genome-wide somatic variant calling using  
1961 localized colored de Bruijn graphs. Commun Biol 1. [10.1038/s42003-018-0023-9](https://doi.org/10.1038/s42003-018-0023-9).

1962 88. Lai, Z., Markovets, A., Ahdesmaki, M., Chapman, B., Hofmann, O., McEwen, R.,  
1963 Johnson, J., Dougherty, B., Barrett, J.C., and Dry, J.R. (2016). VarDict: a novel and versatile  
1964 variant caller for next-generation sequencing in cancer research. Nucleic Acids Res 44, e108–  
1965 e108. [10.1093/nar/gkw227](https://doi.org/10.1093/nar/gkw227).

1966 89. Arora, K., Shah, M., Johnson, M., Sanghvi, R., Shelton, J., Nagulapalli, K., Oschwald,  
1967 D.M., Zody, M.C., Germer, S., Jobanputra, V., et al. (2019). Deep whole-genome sequencing of  
1968 3 cancer cell lines on 2 sequencing platforms. Sci Rep 9. [10.1038/s41598-019-55636-3](https://doi.org/10.1038/s41598-019-55636-3).

1969 90. McLaren, W., Gil, L., Hunt, S.E., Riat, H.S., Ritchie, G.R.S., Thormann, A., Flieck, P.,  
1970 and Cunningham, F. (2016). The Ensembl Variant Effect Predictor. Genome Biol 17.  
1971 [10.1186/s13059-016-0974-4](https://doi.org/10.1186/s13059-016-0974-4).

1972 91. Karczewski, K.J., Francioli, L.C., Tiao, G., Cummings, B.B., Alföldi, J., Wang, Q., Collins,  
1973 R.L., Laricchia, K.M., Ganna, A., Birnbaum, D.P., et al. (2020). The mutational constraint  
1974 spectrum quantified from variation in 141,456 humans. *Nature* 581, 434–443. [10.1038/s41586-020-2308-7](https://doi.org/10.1038/s41586-020-2308-7).

1976 92. Zvereva, M., Pisarev, E., Hosen, I., Kisil, O., Matskeplishvili, S., Kubareva, E., Kamalov,  
1977 D., Tivtikyan, A., Manel, A., Vian, E., et al. (2020). Activating Telomerase TERT Promoter  
1978 Mutations and Their Application for the Detection of Bladder Cancer. *IJMS* 21, 6034.  
1979 [10.3390/ijms21176034](https://doi.org/10.3390/ijms21176034).

1980 93. Boeva, V., Popova, T., Bleakley, K., Chiche, P., Cappo, J., Schleiermacher, G.,  
1981 Janoueix-Lerosey, I., Delattre, O., and Barillot, E. (2011). Control-FREEC: a tool for assessing  
1982 copy number and allelic content using next-generation sequencing data. *Bioinformatics* 28,  
1983 423–425. [10.1093/bioinformatics/btr670](https://doi.org/10.1093/bioinformatics/btr670).

1984 94. Boeva, V., Zinovyev, A., Bleakley, K., Vert, J.-P., Janoueix-Lerosey, I., Delattre, O., and  
1985 Barillot, E. (2010). Control-free calling of copy number alterations in deep-sequencing data  
1986 using GC-content normalization. *Bioinformatics* 27, 268–269. [10.1093/bioinformatics/btq635](https://doi.org/10.1093/bioinformatics/btq635).

1987 95. Talevich, E., Shain, A.H., Botton, T., and Bastian, B.C. (2016). CNVkit: Genome-Wide  
1988 Copy Number Detection and Visualization from Targeted DNA Sequencing. *PLoS Comput Biol*  
1989 12, e1004873. [10.1371/journal.pcbi.1004873](https://doi.org/10.1371/journal.pcbi.1004873).

1990 96. Oesper, L., Satas, G., and Raphael, B.J. (2014). Quantifying tumor heterogeneity in  
1991 whole-genome and whole-exome sequencing data. *Bioinformatics* 30, 3532–3540.  
1992 [10.1093/bioinformatics/btu651](https://doi.org/10.1093/bioinformatics/btu651).

1993 97. Mermel, C.H., Schumacher, S.E., Hill, B., Meyerson, M.L., Beroukhim, R., and Getz, G.  
1994 (2011). GISTIC2.0 facilitates sensitive and confident localization of the targets of focal somatic  
1995 copy-number alteration in human cancers. *Genome Biol* 12. [10.1186/gb-2011-12-4-r41](https://doi.org/10.1186/gb-2011-12-4-r41).

1996 98. Chen, X., Schulz-Trieglaff, O., Shaw, R., Barnes, B., Schlesinger, F., Källberg, M., Cox,  
1997 A.J., Kruglyak, S., and Saunders, C.T. (2015). Manta: rapid detection of structural variants and  
1998 indels for germline and cancer sequencing applications. *Bioinformatics* 32, 1220–1222.  
1999 [10.1093/bioinformatics/btv710](https://doi.org/10.1093/bioinformatics/btv710).

2000 99. Geoffroy, V., Hererger, Y., Kress, A., Stoetzel, C., Piton, A., Dollfus, H., and Muller, J.  
2001 (2018). AnnotSV: an integrated tool for structural variations annotation. *Bioinformatics* 34,  
2002 3572–3574. [10.1093/bioinformatics/bty304](https://doi.org/10.1093/bioinformatics/bty304).

2003 100. Dobin, A., Davis, C.A., Schlesinger, F., Drenkow, J., Zaleski, C., Jha, S., Batut, P.,  
2004 Chaisson, M., and Gingeras, T.R. (2012). STAR: ultrafast universal RNA-seq aligner.  
2005 *Bioinformatics* 29, 15–21. [10.1093/bioinformatics/bts635](https://doi.org/10.1093/bioinformatics/bts635).

2006 101. Li, B., and Dewey, C.N. (2011). RSEM: accurate transcript quantification from RNA-Seq  
2007 data with or without a reference genome. *BMC Bioinformatics* 12. [10.1186/1471-2105-12-323](https://doi.org/10.1186/1471-2105-12-323).

2008 102. Uhrig, S., Ellermann, J., Walther, T., Burkhardt, P., Fröhlich, M., Hutter, B., Toprak, U.H.,  
2009 Neumann, O., Stenzinger, A., Scholl, C., et al. (2021). Accurate and efficient detection of gene  
2010 fusions from RNA sequencing data. *Genome Res.* 31, 448–460. [10.1101/gr.257246.119](https://doi.org/10.1101/gr.257246.119).

2011 103. Haas, B.J., Dobin, A., Stransky, N., Li, B., Yang, X., Tickle, T., Bankapur, A., Ganote, C.,  
2012 Doak, T.G., Pochet, N., et al. (2017). STAR-Fusion: Fast and Accurate Fusion Transcript  
2013 Detection from RNA-Seq. *bioRxiv*, 120295. [10.1101/120295](https://doi.org/10.1101/120295).

2014 104. Mayakonda, A., Lin, D.-C., Assenov, Y., Plass, C., and Koeffler, H.P. (2018). Maftools:  
2015 efficient and comprehensive analysis of somatic variants in cancer. *Genome Res.* 28, 1747–  
2016 1756. [10.1101/gr.239244.118](https://doi.org/10.1101/gr.239244.118).

2017 105. Quinlan, A.R., and Hall, I.M. (2010). BEDTools: a flexible suite of utilities for comparing  
2018 genomic features. *Bioinformatics* 26, 841–842. [10.1093/bioinformatics/btq033](https://doi.org/10.1093/bioinformatics/btq033).

2019 106. Meyer, L.R., Zweig, A.S., Hinrichs, A.S., Karolchik, D., Kuhn, R.M., Wong, M., Sloan,  
2020 C.A., Rosenbloom, K.R., Roe, G., Rhead, B., et al. (2012). The UCSC Genome Browser  
2021 database: extensions and updates 2013. *Nucleic Acids Research* 41, D64–D69.  
2022 [10.1093/nar/gks1048](https://doi.org/10.1093/nar/gks1048).

2023 107. Lawrence, M., Huber, W., Pagès, H., Aboyoun, P., Carlson, M., Gentleman, R., Morgan,  
2024 M.T., and Carey, V.J. (2013). Software for Computing and Annotating Genomic Ranges. *PLoS  
2025 Comput Biol* 9, e1003118. [10.1371/journal.pcbi.1003118](https://doi.org/10.1371/journal.pcbi.1003118).

2026 108. Gu, Z., Eils, R., and Schlesner, M. (2016). Complex heatmaps reveal patterns and  
2027 correlations in multidimensional genomic data. *Bioinformatics* 32, 2847–2849.  
2028 [10.1093/bioinformatics/btw313](https://doi.org/10.1093/bioinformatics/btw313).

2029 109. Cortés-Ciriano, I., Lee, J.J.-K., Xi, R., Jain, D., Jung, Y.L., Yang, L., Gordenin, D.,  
2030 Klimczak, L.J., Zhang, C.-Z., Pellman, D.S., et al. (2020). Comprehensive analysis of  
2031 chromothripsis in 2,658 human cancers using whole-genome sequencing. *Nat Genet* 52, 331–  
2032 341. [10.1038/s41588-019-0576-7](https://doi.org/10.1038/s41588-019-0576-7).

2033 110. Sturm, G., Finotello, F., Petitprez, F., Zhang, J.D., Baumbach, J., Fridman, W.H., List,  
2034 M., and Aneichyk, T. (2019). Comprehensive evaluation of transcriptome-based cell-type  
2035 quantification methods for immuno-oncology. *Bioinformatics* 35, i436–i445.  
2036 [10.1093/bioinformatics/btz363](https://doi.org/10.1093/bioinformatics/btz363).

2037 111. Finotello, F., Mayer, C., Plattner, C., Laschober, G., Rieder, D., Hackl, H., Krogsdam, A.,  
2038 Loncova, Z., Posch, W., Wilflingseder, D., et al. (2019). Molecular and pharmacological  
2039 modulators of the tumor immune contexture revealed by deconvolution of RNA-seq data.  
2040 *Genome Med* 11. [10.1186/s13073-019-0638-6](https://doi.org/10.1186/s13073-019-0638-6).

2041 112. Hänelmann, S., Castelo, R., and Guinney, J. (2013). GSVA: gene set variation analysis  
2042 for microarray and RNA-Seq data. *BMC Bioinformatics* 14. [10.1186/1471-2105-14-7](https://doi.org/10.1186/1471-2105-14-7).

2043 113. Liberzon, A., Birger, C., Thorvaldsdóttir, H., Ghandi, M., Mesirov, Jill P., and Tamayo, P.  
2044 (2015). The Molecular Signatures Database Hallmark Gene Set Collection. *Cell Systems* 1,  
2045 417–425. [10.1016/j.cels.2015.12.004](https://doi.org/10.1016/j.cels.2015.12.004).

2046 114. McInnes, L., Healy, J., and Melville, J. (2020). [UMAP: Uniform Manifold Approximation and Projection for Dimension Reduction](#). arXiv:1802.03426 [cs, stat].

2048 115. Lambert, S.A., Jolma, A., Campitelli, L.F., Das, P.K., Yin, Y., Albu, M., Chen, X., Taipale,  
2049 J., Hughes, T.R., and Weirauch, M.T. (2018). The Human Transcription Factors. *Cell* 172, 650–  
2050 665. [10.1016/j.cell.2018.01.029](https://doi.org/10.1016/j.cell.2018.01.029).

2051 116. Ramkissoon, L.A., Horowitz, P.M., Craig, J.M., Ramkissoon, S.H., Rich, B.E.,  
2052 Schumacher, S.E., McKenna, A., Lawrence, M.S., Bergthold, G., Brastianos, P.K., et al. (2013).  
2053 Genomic analysis of diffuse pediatric low-grade gliomas identifies recurrent oncogenic  
2054 truncating rearrangements in the transcription factor *MYBL1*. *Proc. Natl. Acad. Sci. U.S.A.* 110,  
2055 8188–8193. [10.1073/pnas.1300252110](https://doi.org/10.1073/pnas.1300252110).

2056 117. Northcott, P.A., Shih, D.J.H., Peacock, J., Garzia, L., Sorana Morrissy, A., Zichner, T.,  
2057 Stütz, A.M., Korshunov, A., Reimand, J., Schumacher, S.E., et al. (2012). Subgroup-specific  
2058 structural variation across 1,000 medulloblastoma genomes. *Nature* 488, 49–56.  
2059 [10.1038/nature11327](https://doi.org/10.1038/nature11327).

2060 118. Sturm, D., Orr, Brent A., Toprak, Umut H., Hovestadt, V., Jones, David T.W., Capper, D.,  
2061 Sill, M., Buchhalter, I., Northcott, Paul A., Leis, I., et al. (2016). New Brain Tumor Entities  
2062 Emerge from Molecular Classification of CNS-PNETs. *Cell* 164, 1060–1072.  
2063 [10.1016/j.cell.2016.01.015](https://doi.org/10.1016/j.cell.2016.01.015).

2064 119. Kleinman, C.L., Gerges, N., Papillon-Cavanagh, S., Sin-Chan, P., Pramatarova, A.,  
2065 Quang, D.-A.K., Adoue, V., Busche, S., Caron, M., Djambazian, H., et al. (2013). Fusion of  
2066 TTYH1 with the C19MC microRNA cluster drives expression of a brain-specific DNMT3B  
2067 isoform in the embryonal brain tumor ETMR. *Nat Genet* 46, 39–44. [10.1038/ng.2849](https://doi.org/10.1038/ng.2849).

2068 120. Valentijn, L.J., Koster, J., Zwijnenburg, D.A., Hasselt, N.E., van Sluis, P., Volckmann, R.,  
2069 van Noesel, M.M., George, R.E., Tytgat, G.A.M., Molenaar, J.J., et al. (2015). TERT  
2070 rearrangements are frequent in neuroblastoma and identify aggressive tumors. *Nat Genet* 47,  
2071 1411–1414. [10.1038/ng.3438](https://doi.org/10.1038/ng.3438).

2072 121. Cobrinik, D., Ostrovnaya, I., Hassimi, M., Tickoo, S.K., Cheung, I.Y., and Cheung, N.-  
2073 K.V. (2013). Recurrent pre-existing and acquired DNA copy number alterations, including focal  
2074 *TERT* gains, in neuroblastoma central nervous system metastases. *Genes Chromosomes  
2075 Cancer* 52, 1150–1166. [10.1002/gcc.22110](https://doi.org/10.1002/gcc.22110).

2076 122. Karlsson, J., Lilljebjörn, H., Holmquist Mengelbier, L., Valind, A., Rissler, M., Øra, I.,  
2077 Fioretos, T., and Gisselsson, D. (2015). Activation of human telomerase reverse transcriptase  
2078 through gene fusion in clear cell sarcoma of the kidney. *Cancer Letters* 357, 498–501.  
2079 [10.1016/j.canlet.2014.11.057](https://doi.org/10.1016/j.canlet.2014.11.057).

2080 123. Karsy, M., Guan, J., Cohen, A.L., Jensen, R.L., and Colman, H. (2017). New Molecular  
2081 Considerations for Glioma: IDH, ATRX, BRAF, TERT, H3 K27M. *Curr Neurol Neurosci Rep* 17.  
2082 [10.1007/s11910-017-0722-5](https://doi.org/10.1007/s11910-017-0722-5).

2083 124. Bandopadhyay, P., Ramkissoon, L.A., Jain, P., Bergthold, G., Wala, J., Zeid, R.,  
2084 Schumacher, S.E., Urbanski, L., O'Rourke, R., Gibson, W.J., et al. (2016). MYB-QKI  
2085 rearrangements in angiocentric glioma drive tumorigenicity through a tripartite mechanism. *Nat Genet* 48, 273–282. [10.1038/ng.3500](https://doi.org/10.1038/ng.3500).

2087 125. Johann, P.D., Erkek, S., Zapatka, M., Kerl, K., Buchhalter, I., Hovestadt, V., Jones,  
2088 D.T.W., Sturm, D., Hermann, C., Segura Wang, M., et al. (2016). Atypical Teratoid/Rhabdoid  
2089 Tumors Are Comprised of Three Epigenetic Subgroups with Distinct Enhancer Landscapes.  
2090 *Cancer Cell* 29, 379–393. [10.1016/j.ccr.2016.02.001](https://doi.org/10.1016/j.ccr.2016.02.001).

2091 126. Mong, E.F., Yang, Y., Akat, K.M., Canfield, J., VanWye, J., Lockhart, J., Tsibris, J.C.M.,  
2092 Schatz, F., Lockwood, C.J., Tuschl, T., et al. (2020). Chromosome 19 microRNA cluster  
2093 enhances cell reprogramming by inhibiting epithelial-to-mesenchymal transition. *Sci Rep* 10.  
2094 [10.1038/s41598-020-59812-8](https://doi.org/10.1038/s41598-020-59812-8).

2095 127. Ryall, S., Guzman, M., Elbabaa, S.K., Luu, B., Mack, S.C., Zapotocky, M., Taylor, M.D.,  
2096 Hawkins, C., and Ramaswamy, V. (2017). H3 K27M mutations are extremely rare in posterior  
2097 fossa group A ependymoma. *Childs Nerv Syst* 33, 1047–1051. [10.1007/s00381-017-3481-3](https://doi.org/10.1007/s00381-017-3481-3).

2098 128. Pajtler, Kristian W., Witt, H., Sill, M., Jones, David T.W., Hovestadt, V., Kratochwil, F.,  
2099 Wani, K., Tatevossian, R., Punchihewa, C., Johann, P., et al. (2015). Molecular Classification of  
2100 Ependymal Tumors across All CNS Compartments, Histopathological Grades, and Age Groups.  
2101 *Cancer Cell* 27, 728–743. [10.1016/j.ccr.2015.04.002](https://doi.org/10.1016/j.ccr.2015.04.002).

2102 129. Parker, M., Mohankumar, K.M., Punchihewa, C., Weinlich, R., Dalton, J.D., Li, Y., Lee,  
2103 R., Tatevossian, R.G., Phoenix, T.N., Thiruvenkatam, R., et al. (2014). C11orf95–RELA fusions  
2104 drive oncogenic NF-κB signalling in ependymoma. *Nature* 506, 451–455. [10.1038/nature13109](https://doi.org/10.1038/nature13109).

2105 130. Bi, W.L., Greenwald, N.F., Abedalthagafi, M., Wala, J., Gibson, W.J., Agarwalla, P.K.,  
2106 Horowitz, P., Schumacher, S.E., Esaulova, E., Mei, Y., et al. (2017). Genomic landscape of  
2107 high-grade meningiomas. *npj Genomic Med* 2. [10.1038/s41525-017-0014-7](https://doi.org/10.1038/s41525-017-0014-7).

2108 131. Youngblood, M.W., Duran, D., Montejo, J.D., Li, C., Omay, S.B., Özduman, K., Sheth,  
2109 A.H., Zhao, A.Y., Tyrtova, E., Miyagishima, D.F., et al. (2020). Correlations between genomic  
2110 subgroup and clinical features in a cohort of more than 3000 meningiomas. *Journal of*  
2111 *Neurosurgery* 133, 1345–1354. [10.3171/2019.8.jns191266](https://doi.org/10.3171/2019.8.jns191266).

2112 132. Qaddoumi, I., Orisme, W., Wen, J., Santiago, T., Gupta, K., Dalton, J.D., Tang, B.,  
2113 Haupfear, K., Punchihewa, C., Easton, J., et al. (2016). Genetic alterations in uncommon low-  
2114 grade neuroepithelial tumors: BRAF, FGFR1, and MYB mutations occur at high frequency and  
2115 align with morphology. *Acta Neuropathol* 131, 833–845. [10.1007/s00401-016-1539-z](https://doi.org/10.1007/s00401-016-1539-z).

2116 133. Thomas, C., Soschinski, P., Zwaig, M., Oikonomopoulos, S., Okonechnikov, K., Pajtler,  
2117 K.W., Sill, M., Schweizer, L., Koch, A., Neumann, J., et al. (2020). The genetic landscape of

2118 choroid plexus tumors in children and adults. *Neuro-Oncology* 23, 650–660.  
2119 [10.1093/neuonc/noaa267](https://doi.org/10.1093/neuonc/noaa267).

2120 134. Sekine, S., Shibata, T., Kokubu, A., Morishita, Y., Noguchi, M., Nakanishi, Y., Sakamoto, M., and Hirohashi, S. (2002). Craniopharyngiomas of adamantinomatous type harbor beta-catenin gene mutations. *Am J Pathol* 161, 1997–2001. [10.1016/s0002-9440\(10\)64477-x](https://doi.org/10.1016/s0002-9440(10)64477-x).

2123 135. Krooks, J., Minkov, M., and Weatherall, A.G. (2018). Langerhans cell histiocytosis in children. *Journal of the American Academy of Dermatology* 78, 1035–1044.  
2125 [10.1016/j.jaad.2017.05.059](https://doi.org/10.1016/j.jaad.2017.05.059).

2126 136. Antin, C., Tauziède-Espriat, A., Debily, M.-A., Castel, D., Grill, J., Pagès, M., Ayrault, O., Chrétien, F., Gareton, A., Andreuolo, F., et al. (2020). EZHIP is a specific diagnostic biomarker for posterior fossa ependymomas, group PFA and diffuse midline gliomas H3-WT with EZHIP overexpression. *acta neuropathol commun* 8. [10.1186/s40478-020-01056-8](https://doi.org/10.1186/s40478-020-01056-8).

2130 137. Rosenthal, R., McGranahan, N., Herrero, J., Taylor, B.S., and Swanton, C. (2016). deconstructSigs: delineating mutational processes in single tumors distinguishes DNA repair deficiencies and patterns of carcinoma evolution. *Genome Biol* 17. [10.1186/s13059-016-0893-4](https://doi.org/10.1186/s13059-016-0893-4).

2133 138. Burel-Vandenbos, F., Pierron, G., Thomas, C., Reynaud, S., Gregoire, V., Duhil de Benaze, G., Croze, S., Chivoret, N., Honavar, M., Figarella-Branger, D., et al. (2020). A polyphenotypic malignant paediatric brain tumour presenting a *MN1-PATZ1* fusion, no epigenetic similarities with CNS High-Grade Neuroepithelial Tumour with *MN1* Alteration (CNS HGNET-MN1) and related to *PATZ1*-fused sarcomas. *Neuropathol Appl Neurobiol* 46, 506–509.  
2138 [10.1111/nan.12626](https://doi.org/10.1111/nan.12626).

2139 139. Kram, D.E., Henderson, J.J., Baig, M., Chakraborty, D., Gardner, M.A., Biswas, S., and Khatua, S. (2018). Embryonal Tumors of the Central Nervous System in Children: The Era of Targeted Therapeutics. *Bioengineering (Basel)* 5. [10.3390/bioengineering5040078](https://doi.org/10.3390/bioengineering5040078).

2142 140. Rao, S., Rajeswarie, R.T., Chickabasaviah Yasha, T., Nandeesh, B.N., Arivazhagan, A., and Santosh, V. (2017). LIN28A, a sensitive immunohistochemical marker for Embryonal Tumor with Multilayered Rosettes (ETMR), is also positive in a subset of Atypical Teratoid/Rhabdoid Tumor (AT/RT). *Childs Nerv Syst* 33, 1953–1959. [10.1007/s00381-017-3551-6](https://doi.org/10.1007/s00381-017-3551-6).

2146 141. PDQ® Pediatric Treatment Editorial Board [Childhood Medulloblastoma and Other Central Nervous System Embryonal Tumors Treatment \(PDQ®\): Health Professional Version](#). In PDQ Cancer Information Summaries (National Cancer Institute).

2149 142. Miele, E., De Vito, R., Ciolfi, A., Pedace, L., Russo, I., De Pasquale, M.D., Di Giannatale, A., Crocoli, A., Angelis, B.D., Tartaglia, M., et al. (2020). DNA Methylation Profiling for Diagnosing Undifferentiated Sarcoma with Capicua Transcriptional Receptor (CIC) Alterations. *IJMS* 21, 1818. [10.3390/ijms21051818](https://doi.org/10.3390/ijms21051818).

2153 143. Korshunov, A., Ryzhova, M., Jones, D.T.W., Northcott, P.A., van Sluis, P., Volckmann, R., Koster, J., Versteeg, R., Cowdrey, C., Perry, A., et al. (2012). LIN28A immunoreactivity is a

2155 potent diagnostic marker of embryonal tumor with multilayered rosettes (ETMR). *Acta*  
2156 *Neuropathol* 124, 875–881. [10.1007/s00401-012-1068-3](https://doi.org/10.1007/s00401-012-1068-3).

2157 144. Rustagi, N., Hampton, O.A., Li, J., Xi, L., Gibbs, R.A., Plon, S.E., Kimmel, M., and  
2158 Wheeler, D.A. (2016). ITD assembler: an algorithm for internal tandem duplication discovery  
2159 from short-read sequencing data. *BMC Bioinformatics* 17. [10.1186/s12859-016-1031-8](https://doi.org/10.1186/s12859-016-1031-8).

2160 145. Mohila, C.A., Rauch, R.A., and Adesina, A.M. (2016). Central Neurocytoma and  
2161 Extraventricular Neurocytoma. In *Atlas of Pediatric Brain Tumors* (Springer International  
2162 Publishing), pp. 195–199. [10.1007/978-3-319-33432-5\\_20](https://doi.org/10.1007/978-3-319-33432-5_20).

2163 146. Crotty, T.B., Scheithauer, B.W., Young, W.F., Davis, D.H., Shaw, E.G., Miller, G.M., and  
2164 Burger, P.C. (1995). Papillary craniopharyngioma: a clinicopathological study of 48 cases.  
2165 *Journal of Neurosurgery* 83, 206–214. [10.3171/jns.1995.83.2.0206](https://doi.org/10.3171/jns.1995.83.2.0206).

2166 147. Bunin, G.R., Surawicz, T.S., Witman, P.A., Preston-Martin, S., Davis, F., and Bruner,  
2167 J.M. (1998). The descriptive epidemiology of craniopharyngioma. *Journal of Neurosurgery* 89,  
2168 547–551. [10.3171/jns.1998.89.4.0547](https://doi.org/10.3171/jns.1998.89.4.0547).

2169 148. Chang, M.T., Bhattarai, T.S., Schram, A.M., Bielski, C.M., Donoghue, M.T.A., Jonsson,  
2170 P., Chakravarty, D., Phillips, S., Kandoth, C., Penson, A., et al. (2018). Accelerating Discovery  
2171 of Functional Mutant Alleles in Cancer. *Cancer Discovery* 8, 174–183. [10.1158/2159-8290.cd-17-0321](https://doi.org/10.1158/2159-8290.cd-17-0321).

2173 149. Chang, M.T., Asthana, S., Gao, S.P., Lee, B.H., Chapman, J.S., Kandoth, C., Gao, J.,  
2174 Soccia, N.D., Solit, D.B., Olshen, A.B., et al. (2015). Identifying recurrent mutations in cancer  
2175 reveals widespread lineage diversity and mutational specificity. *Nat Biotechnol* 34, 155–163.  
2176 [10.1038/nbt.3391](https://doi.org/10.1038/nbt.3391).

2177 150. Harms, K.L., and Chen, X. (2006). The functional domains in p53 family proteins exhibit  
2178 both common and distinct properties. *Cell Death Differ* 13, 890–897. [10.1038/sj.cdd.4401904](https://doi.org/10.1038/sj.cdd.4401904).

2179 151. Guha, T., and Malkin, D. (2017). Inherited *TP53* Mutations and the Li–Fraumeni  
2180 Syndrome. *Cold Spring Harb Perspect Med* 7, a026187. [10.1101/cshperspect.a026187](https://doi.org/10.1101/cshperspect.a026187).

2181 152. Li, H., Handsaker, B., Wysoker, A., Fennell, T., Ruan, J., Homer, N., Marth, G.,  
2182 Abecasis, G., Durbin, R. (2009). The Sequence Alignment/Map format and SAMtools.  
2183 *Bioinformatics* 25, 2078–9. [10.1093/bioinformatics/btp352](https://doi.org/10.1093/bioinformatics/btp352).

2184 153. Kaplan, E.L., and Meier, P. (1958). Nonparametric Estimation from Incomplete  
2185 Observations. *Journal of the American Statistical Association* 53, 457–481. [10.2307/2281868](https://doi.org/10.2307/2281868).

2186 154. Mantel, N. (1966). [Evaluation of survival data and two new rank order statistics arising in its consideration](#). *Cancer Chemother Rep* 50, 163–70.

2188 155. Cox, D.R. (1972). Regression Models and Life-Tables. *Journal of the Royal Statistical  
2189 Society: Series B (Methodological)* 34, 187–202. [10.1111/j.2517-6161.1972.tb00899.x](https://doi.org/10.1111/j.2517-6161.1972.tb00899.x).

2190 156. Rokita, J.L., and Brown, M. (2022). d3b-center/OpenPBTA-workflows: Release v1.0.4  
2191 (Zenodo) [10.5281/zenodo.6968175](https://doi.org/10.5281/zenodo.6968175).

2192 157. Taroni, J., Savonen, C., Krutika Gaonkar, Stephanie, Chante Bethell, Rokita, J.L.,  
2193 Shapiro, J., Greene, C., Yuankun Zhu, Komal Rathi, et al. (2022). AlexsLemonade/OpenPBTA-  
2194 analysis: Initial Submission (Zenodo) [10.5281/zenodo.7044567](https://doi.org/10.5281/zenodo.7044567).